

From the Institut für Experimentelle Tumorforschung
(Director: Prof. Dr. rer. nat. Susanne Sebens)
at the University Medical Center Schleswig-Holstein, Campus Kiel
at Kiel University

**TUMOR VACCINATION: CHITOSAN NANOPARTICLES AS ANTIGEN
VEHICLES TO PROMOTE TUMOR-DIRECTED T CELL RESPONSES**

Dissertation
to acquire the doctoral degree (Dr. med.)
at the Faculty of Medicine
at Kiel University

presented by
Frederik Walter
from **Offenburg**

Kiel **2022**

1st Reviewer: Prof. Dr. Susanne Sebens

2nd Reviewer: Prof. Dr. Claus-Christian Glüer

Date of oral examination: 29.03.2022

Approved for printing, Kiel, 04.11.2021

Signed: Prof. Dr. Susanne Sebens

(Chairperson of the Examination Committee)

- to my family -

Table of Contents

I. List of abbreviations	VI
II. List of figures	IX
1. Introduction	1
1.1 Cancer and its relevance in today's medicine	1
1.1.1 Epidemiology and status quo	1
1.1.2 Established therapeutic strategies and more recent developments	2
1.2 Immunoediting in tumor development	3
1.3 Immunotherapy	6
1.3.1 Theoretic background and current clinical relevance	6
1.3.2 Chances, limitations and obstacles	7
1.4 Tumor vaccination	8
1.4.1 Concept and goal of tumor vaccination	8
1.4.2 The role of dendritic cells in tumor vaccinations	9
1.4.3 Different vaccination approaches and their stage of development	10
1.4.3.1 Tumor vaccines in the context of personalized medicine	10
1.4.3.2 Oncolytic viruses	11
1.4.3.3 <i>In situ</i> vaccines	12
1.4.3.4 Antigen presenting cell based strategies	12
1.4.3.5 Peptide and nucleic acid based strategies	13
1.4.4 The usage of nanoparticles for improving tumor vaccines	13
1.4.4.1 How nanoparticles can enhance the effect of tumor vaccines	13
1.4.4.2 The subgroup of polymeric nanoparticles	14
1.4.4.3 Chitosan, its characteristics and resulting opportunities	15
1.5 Aim of this study	16

2. Materials	17
2.1 Laboratory devices	17
2.2 Consumables	19
2.3 Kit Systems	21
2.4 Software	21
2.5 Chemicals, reagents and buffers	22
2.5.1 Chemicals and reagents.....	22
2.5.2 Buffers.....	23
2.6 Peptides and chitosan nanoparticles	24
2.6.1 Peptides.....	24
2.6.2 Chitosan nanoparticles.....	24
2.7 Animals	25
2.8 Cell biological material	25
2.8.1 Cell lines.....	25
2.8.2 Human primary cells.....	26
2.8.3 Growth factors and cytokines.....	26
2.8.4 Cell culture media.....	27
2.9 Molecular biological material	28
2.9.1 Human primers.....	28
2.9.2 Mouse primers.....	29
2.10 Antibodies	30
2.10.1 Anti-human antibodies.....	30
2.10.2 Anti-mouse antibodies.....	32
3. Methods	34
3.1. Cell biological methods	34
3.1.1 Cell lines.....	34
3.1.2 Cell thawing and freezing.....	34

3.1.3 Cell culture.....	34
3.1.4 Cell Counting	35
3.1.5 Generation of stimulation solution with chitosan nanoparticles	36
3.1.6 Isolation of human monocytes.....	36
3.1.7 <i>In vitro</i> generation of polarized human macrophages and dendritic cells	39
3.1.8 Harvesting of <i>in vitro</i> generated human macrophages.....	39
3.1.9. Isolation of CD8 ⁺ T cells obtained from OT-1 mice.....	40
3.1.10 Coculture of CD8 ⁺ T cells with antigen-pulsed DC2.4 cells and assessment of T cell activation markers.....	41
3.1.11 Coculturing PancOVA/Panc02 cells with CD8 ⁺ T cells and subsequent killing assay	41
3.2 Immunobiological methods	42
3.2.1 Flow cytometry.....	42
3.2.2 ImageStream	44
3.2.3 NYONE [®] cell imaging	44
3.2.4 Imaging with the Lionheart™ FX Automated Microscope.....	45
3.2.5 Caspase 3/7 activity assay	46
3.3 Molecular biological methods	46
3.3.1 Isolation of nucleic acids	46
3.3.2 Reverse transcription	47
3.3.3. Quantitative real-time polymerase chain reaction	48
3.4 Statistical analysis.....	49
3.5 Ethics statement	49
4. Results	50
4.1 Large chitosan nanoparticles (90/20 and 90/50) but not small ones (90/10) considerably impair viability and morphology of human primary monocytic cells.....	50
4.2 Antigen-loaded chitosan nanoparticles are taken up by human and murine dendritic cells	53

4.3 Antigen-loaded 90/10 chitosan nanoparticles barely affect viability and morphology of human dendritic cells.....	55
4.4 Stimulation with chitosan nanoparticles causes phenotypic changes in human and in murine dendritic cells.....	57
4.4.1 Surface marker expression in human dendritic cells is barely affected by treatment with chitosan nanoparticles.....	57
4.4.2 RNA analysis of human dendritic cells shows significant proinflammatory phenotypic changes after stimulation with antigen-loaded chitosan nanoparticles.....	59
4.4.3 Murine dendritic cells exhibit a more proinflammatory phenotype after stimulation with antigen-loaded chitosan nanoparticles	61
4.5 MHC-I mediated presentation of SIINFEKL can hardly be detected after treatment of DC2.4 cells with 90/10 OVA chitosan nanoparticles.....	62
4.6 90/10 OVA stimulation of DC2.4 cells leads to modest but detectable activation of CD8⁺ T cells after coculturing DC2.4 cells and CD8⁺ T cells.....	63
4.7 Treatment of DC2.4 cells with 90/10 SIINFEKL leads to pronounced MHC-I mediated SIINFEKL presentation	64
4.8 Antigen presentation of DC2.4 cells stimulated with 90/10 SIINFEKL chitosan nanoparticles causes activation of SIINFEKL-specific CD8⁺ T cells.....	66
4.8.1 After coculture with 90/10 SIINFEKL treated DC2.4 cells, CD8 ⁺ T cells expand and upregulate expression of CD25 and CD69.....	66
4.8.2 CD8 ⁺ T cell survival can be improved by increasing mIL-2 concentration.....	68
4.9 CD8⁺ T cells cocultured with 90/10 SIINFEKL stimulated DC2.4 cells efficiently kill SIINFEKL expressing PancOVA cells	71
5. Discussion.....	73
5.1 Size of chitosan nanoparticles impacts cellular viability and morphology of human dendritic cells	73
5.2 Antigen-loaded 90/10 chitosan nanoparticles are efficiently taken up by dendritic cells with some particles remaining tightly attached to the outer cell membrane	74
5.3 SIINFEKL encapsulated in chitosan nanoparticles is liberated and presented by dendritic cells via MHC-I	76

5.4 Stimulation with antigen-loaded chitosan nanoparticles promotes a proinflammatory phenotype in human and murine dendritic cells	78
5.5 Stimulation with 90/10 SIINFEKL chitosan nanoparticles leads to DC2.4 cell-mediated activation of cocultured CD8 ⁺ T cells	80
5.6 CD8 ⁺ T cells activated by coculture with 90/10 SIINFEKL chitosan nanoparticle pre-stimulated DC2.4 cells efficiently kill SIINFEKL expressing tumor cells	81
6. Summary	83
7. Supplementary data	85
8. Bibliography	89
9. Appendix	100
9.1 Eidesstattliche Erklärung	100
9.2 Publications and poster presentations	101
9.3 Acknowledgements	102
9.4 Curriculum vitae	103

I. List of abbreviations

°C	Degree Celsius
g	Force of gravity
γ-PGA	γ-glutamic acid
μ	Micro
m	Milli
n	Nano
AF	Alexa Fluor
ALL	Acute lymphoblastic leukemia
ANOVA	Analysis of variance
APC	Allophycocyanine
APC	Antigen presenting cell
BCL-2	B cell lymphoma-2
BF	Brightfield
BSA	Bovine serum albumin
BV510	Brilliant Violet 510
CAR	Chimeric antigen receptor
CCE	Counterflow centrifugation elutriation
CD	Cluster of differentiation
cDNA	Complementary deoxyribonucleic acid
CNP	Chitosan nanoparticle
Ct	Cycle threshold
CTL	Cytotoxic T lymphocyte
CTLA-4 (CD152)	Cytotoxic T-lymphocyte-associated protein 4
Cy7	Cyanine 7
DC	Dendritic cell
DMSO	Dimethyl sulfoxide
DNA	Deoxyribonucleic acid
DNTP	Deoxynucleoside triphosphate

EDTA	Ethylenediaminetetraacetic acid
FACS	Fluorescence-activated cell sorting; flow cytometry
Fc	Fragment crystallizable
FcR	Fragment crystallizable receptor
FCS	Fetal calf serum
FDA	U.S. Food and Drug Administration
FL	Fluorescence
FI	Fluorescence intensity
FITC	Fluorescein isothiocyanate
FSC	Forward scatter
fw	Forward
G418	Geneticin
GM-CSF	Granulocyte macrophage-colony stimulating factor
h	Hour(s)
hDC	Human dendritic cell
HEPES	4-(2-hydroxyethyl)-1-piperazineethanesulfonic acid
HER-2	Human epidermal growth factor receptor 2
HLA	Human leucocyte antigen
Ig	Immunoglobulin
IFNγ	Interferon gamma
IL	Interleukin
ISX	ImageStream XMark II
L-Gln	L-Glutamine
LRS	Lymphocyte retaining system
MΦ	Macrophages
M-CSF	Macrophage colony-stimulating growth factor
MFI	Median fluorescence intensity
MHC	Major histocompatibility complex
NEAA	Non-essential amino acids
NiM	Nano-in-microparticle
NK cells	Natural killer cells

NP	Nanoparticle
OVA	Ovalbumin
PDAC	Pancreatic ductal adenocarcinoma
PBMCs	Peripheral blood mononuclear cells
PBS	Phosphate-buffered saline
PD-1/PD-L1 (CD279)	Programmed cell death protein (ligand-) 1
PE	Phycoerythrin
Pen/Strep	Penicillin/streptomycin
PFA	Paraformaldehyde
PI	Propidium iodide
PLGA	Poly lactic-co-glycolic acid
poly I:C	Polyinosinic:polycytidylic acid
qPCR	Quantitative real-time polymerase chain reaction
RBC	Red blood cell/erythrocyte
RNA	Ribonucleic acid
rpm	Rounds per minute
RPMI	Roswell Park memorial institute
RT	Room temperature
rv	Reverse
s.e.m	Standard errors of the mean
SEM	Scanning electron microscope
SSC	Side scatter
SIINFEKL	Ovalbumin 257-264
TAA	Tumor-associated antigen
TGF- β1	Transforming growth factor beta 1
Th	T helper
TLR	Toll-like receptor
TNA	Tumor neoantigen
TNF-α	Tumor necrosis factor-alpha
TSA	Tumor-specific antigen
VEGF	Vascular endothelial growth factor

II. List of figures

Figure 1	The Cancer-Immunity cycle.
Figure 2	Cancer immunoediting and its three phases.
Figure 3/I	The role of dendritic cells in the initiation of immune responses.
Figure 3/II	Intracellular pathways of cross-presentation.
Figure 4	Strategies for and composition of tumor vaccines.
Figure 5	Chitosan, the chemical structure (I) and resulting form of chitosan nanoparticles (II).
Figure 6	Schematic illustration of cellular separation achieved by Pan-coll-supported density gradient centrifugation
Figure 7	Two representative dot plots of different cell fractions after counterflow centrifugation elutriation.
Figure 8	Illustration of the generation of differently polarized macrophages and dendritic cells.
Figure 9	Schematic overview of the CD8 ⁺ T cell related working steps and the performed coculture assays.
Figure 10	Scheme of a flow cytometer.
Figure 11	Treatment with large chitosan nanoparticles alters morphology and cellular confluence of human dendritic cells, M1- and M2-like macrophages.
Figure 12	Caspase 3/7 activity level increases after stimulation of human primary monocytic cells with chitosan nanoparticles, in particular with large ones
Figure 13	In human dendritic cells, propidium iodide intensity is higher and cell confluence lower, the bigger the diameter of added chitosan nanoparticles.

Figure 14	Stimulation with FITC-conjugated chitosan nanoparticles loaded with SIINFEKL or OVA leads to similar percentages of FITC-positive dendritic cells.
Figure 15	Internalization of ovalbumin-loaded FITC-conjugated chitosan nanoparticles in murine and human DCs is confirmed by ImageStream analyses.
Figure 16	Antigen-loaded 90/10 chitosan nanoparticles do not impair the viability of human dendritic cells.
Figure 17	90/10 chitosan nanoparticles, with or without an encapsulated antigen hardly cause changes in CD80, CD86, HLA-DR and PD-L1 expression on human dendritic cells.
Figure 18	Human dendritic cells exhibit a more proinflammatory phenotype after stimulation with antigen-loaded chitosan nanoparticles.
Figure 19	Murine DC2.4 cells display a more proinflammatory phenotype after stimulation with chitosan nanoparticles.
Figure 20	DC2.4 cells hardly present SIINFEKL via MHC-I after treatment with 90/10 OVA chitosan nanoparticles.
Figure 21	Treatment of DC2.4 cells with 90/10 OVA chitosan nanoparticles leads to activation of CD8 ⁺ T cells.
Figure 22	After stimulation with 90/10 SIINFEKL chitosan nanoparticles, DC2.4 cells present SIINFEKL via MHC-I.
Figure 23	Coculture of CD8 ⁺ T cells with DC2.4 cells stimulated with 90/10 SIINFEKL chitosan nanoparticles leads to enhanced T cell expansion and clustering.
Figure 24	CD8 ⁺ T cells cocultured with 90/10 SIINFEKL chitosan nanoparticle-stimulated DC2.4 cells exhibit elevated expression of activation markers CD25 and CD69
Figure 25	Stimulation of CD8 ⁺ T cells with 150 ng/ml mL-2 improves cell survival.

Figure 26	After increasing mIL-2 concentration, CD8 ⁺ T cells cocultured with 90/10 SIINFEKL chitosan nanoparticle-treated DC2.4 cells show CD25 and CD69 positivity.
Figure 27	90/10 SIINFEKL chitosan nanoparticle-stimulated DC2.4 cells activate CD8 ⁺ T cells being enabled to efficiently kill Pan-cOVA cells.
Supplementary figure 1	Prior to coculture of differently treated DC2.4 cells and CD8 ⁺ T cells, MHC-I mediated presentation of SIINFEKL on DC2.4 cells can be confirmed in cells treated with 90/10 SIINFEKL chitosan nanoparticles or soluble SIINFEKL.
Supplementary figure 2	Stimulation with 90/10 OVA or 90/10 SIINFEKL chitosan nanoparticles for 24 hours does not negatively impact morphology or confluence of human dendritic cells.
Supplementary figure 3	Stimulation of DC2.4 cells with soluble OVA peptide does not lead to increased 25-D1.16 antibody binding.
Supplementary figure 4	Treatment of DC2.4 cells with increased amount of 90/10 SIINFEKL chitosan nanoparticles only leads to slight increase of H-2K ^b mediated SIINFEKL presentation.

1. Introduction

1.1 Cancer and its relevance in today's medicine

1.1.1 Epidemiology and status quo

The prevention and therapeutic management of cancer is one of the most pressing issues for modern medicine and healthcare systems worldwide to solve. Even though the average survival of cancer patients has remarkably improved over the last decades, resulting in a 5-year survival rate of over 50% in most cases and entities (1), a lot of work remains to be done to improve the patients' prognoses. A growing number of cancer related publications per year and a rising economic burden are indicators outlining the huge impact of cancer on the society as a whole (2). In spite of all the efforts that were made, there do still exist barely treatable tumor entities tied to concerningly poor prognosis. Prominent examples are pancreatic ductal adenocarcinoma (PDAC) where late detection and low resectability rates lead to high mortality (3) or non-small cell lung carcinoma where established therapeutic regimens often cannot satisfyingly prolong survival (4) particularly in a metastasized situation which is present in many, even in many newly diagnosed patients (5). The urgent need for new and improved cancer therapy is not only justified by cancer's relatively high mortality but also by its significant incidence. As of now, even distinct cancer entities belong to the top ten causes of death, particularly in middle- and high-income countries (6,7). All cancers taken together are second placed on this list in western countries right behind cardiovascular diseases (8,9). An ongoing discussion is being held about whether cancer will continue being one of the most relevant causes of death or the trend of a rising will reverse. There exist predictions proposing that the aging population is going to lead to an increasing incidence of cancer over the next years (10), even though not all entities are assumed to be affected equally by this development (11). While some hope to beat or at least control cancer within the next decades (12), other projections are more skeptical but still acknowledge that different treatment strategies have the potential to influence the cancer-related mortality in a positive way (11). Indeed, a look into the past shows that there has been made striking progress in cancer treatment with arguably one of the most outstanding developments being the development of the tyrosine kinase

inhibitor Imatinib around the turn of the millennium (13). Since then, the prognosis of patients with chronic myeloid leukemia has drastically improved (14) which is why Imatinib is a good example to fundamentally display how new therapeutic approaches can lead to immediate progress in the treatment of cancer. Unfortunately, not all malignancies can be treated the same way and with comparable success which is why despite all the research a lot of cancers are classified as incurable at the time of their diagnosis. One example for this situation is PDAC where in more than half of cases, the primary tumor has already disseminated before being detected (15). The resulting condition is tied to a poor prognosis because local therapies such as surgeries cannot provide complete cure to a then systemic illness. Clearly, the goal must be to not let situations like these develop. A large percentage of cancers is preventable by, e.g. the avoidance of tobacco or alcohol (16) pointing out that everyone's lifestyle can contribute to cancer prevention. A different aspect of prevention is surveillance and screening. Meanwhile, screening for colorectal or cervical carcinoma is highly established and accepted even though potential overdiagnosis must always be considered when evaluating new or re-evaluating existing screening methods (17). However, despite of large analyses and new methods even in the relatively new and far-reaching field of chemoprevention (18), it is as of now inevitable that some cancers can only be diagnosed at a later stage and had already been progressing systemically until detection. Therefore, therapeutic approaches have to be optimized and new concepts must be developed for those patients, who cannot be successfully treated with the current therapeutic regimens.

1.1.2 Established therapeutic strategies and more recent developments

Therapy of cancer was and is still largely dominated by comparatively traditional methods often referred to as the three pillars of tumor treatment: Surgery, radiotherapy and chemotherapy. Even though these are established therapeutic principles, progress has not spared these methods. Compared to decades ago, surgery can now be performed with less harm and less radical- and invasiveness for the patients, e.g. in breast cancer (19), improving post-interventional quality of life. Furthermore, metastatic surgery is becoming more and more widespread, for example in colorectal cancer with liver metastases (20). Radiotherapy offers new developments like stereotactic radiosurgery where small tumors, especially those located in the head can be attacked very precisely with high-dose radiation (21). As for chemotherapy, new

substances and protocols are constantly being evaluated. A big step in expanding the therapeutic repertoire was the addition of targeted therapies and immunotherapy to the list of methods to effectively cure cancer. Targeted therapies make use of molecular structures in and on tumor cells that are often linked directly to the so-called hallmarks of cancer and are therefore mostly either specific for cancer cells or markedly overexpressed on malignant cells in relation to benign cells (22,23). A prominent drug of this class is Bevacizumab, an antibody blocking the Vascular Endothelial Growth Factor (VEGF). VEGF is often overexpressed in tumors (24) because of its importance for angiogenesis. Immunotherapy basically has the goal to enhance the immune response against cancer cells through mechanisms such as inhibition of negative immune regulation caused by the cancer cells. New therapeutics have successfully been tested and are therefore approved for numerous cancer entities (25). However, as mentioned before (**1.1.1**) currently available therapies still fail to significantly improve the prognosis of many cancer patients. As a consequence, a better understanding of cancer's biology for instance regarding the role of the immune system in tumor development is required.

1.2 Immunoediting in tumor development

The basis for immunotherapeutic drugs has been set decades ago when researchers started hypothesizing about the relevance of the interplay between cancer and the immune system (26). During the last years, the interactions have been clarified and models, such as the Cancer-Immunity Cycle, have been proposed. This model describes the required steps leading from the release of cancer antigens from dead tumor cells to the eventual killing of malignant cells through cytotoxic T cells (CTL) (27) (**Figure 1**). The cycle outlines how immune cells and cancer cells interact on a single cell basis. However, in the present clinical situation, the cancer cells' heterogeneity, meaning that a tumor contains a plethora of unequally differentiated cells, must be taken into consideration. The 'Three Es' of immunoediting elimination, equilibrium and escape outline how heterogeneity can ultimately contribute to tumor survival by describing the changes occurring in the cellular interplay (28) (**Figure 2**). First, in the elimination phase, the production and liberation of proinflammatory cytokines due to infection or damage of tissues induces a strong, local immune response. This initiates the recruitment of various effector cells of the innate immune system such as macrophages (M Φ) or also dendritic cells (DCs) towards the altered or malignant cells. Subsequent killing of these cells induces the

liberation, processing and eventual presentation of antigens, such as tumor associated antigens (TAAs) by antigen presenting cells (APCs). This allows the recruitment of antigen specific T lymphocytes. Therefore, the elimination phase can be described as a complex process, in which innate and adaptive immune system work together to successfully destroy transformed cells (29).

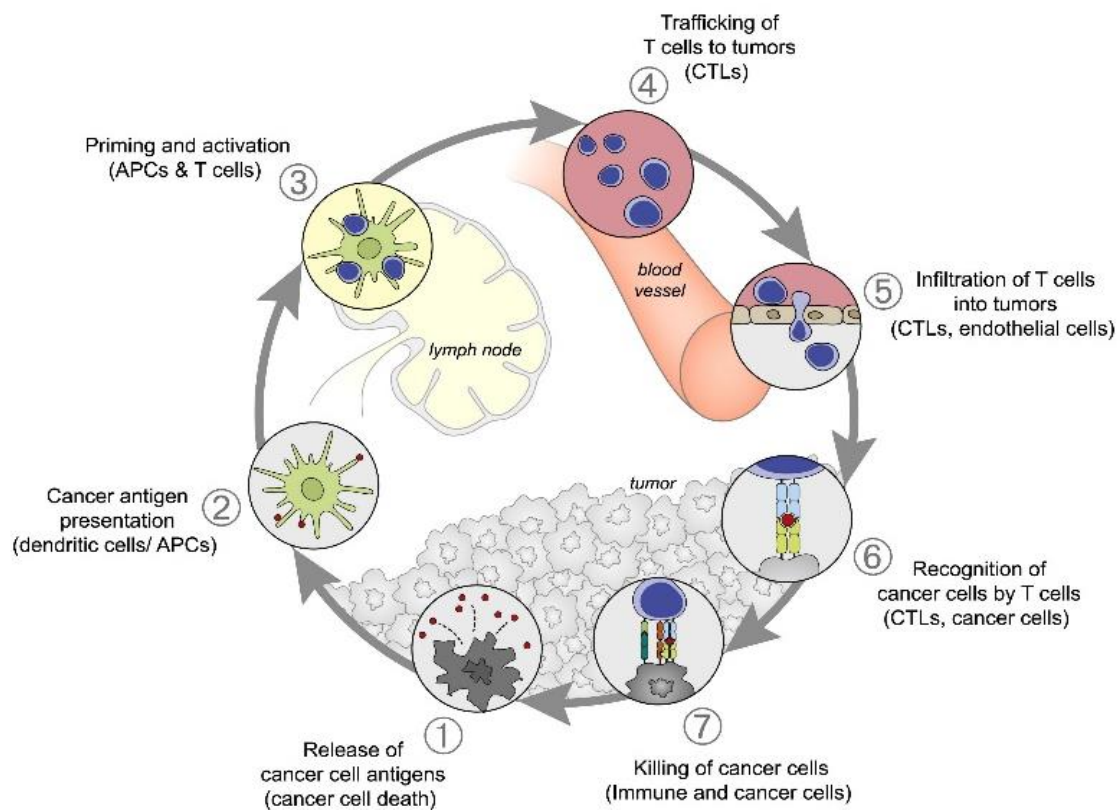


Figure 1: The Cancer-Immunity cycle. Figure taken from (27). An illustration of the different processes and the involved cells that altogether compose an immune reaction against cancer cells. A release of TAAs triggers an immune response leading to killing of malignant cells that fundamentals on cancer antigen presentation on APCs such as DCs. Abbreviations: CTL: cytotoxic T cell, APC: antigen presenting cell, TAA: tumor associated antigen

However, the killing might not affect all cells to the same extent due to arising or pre-existing heterogeneous intratumoral differentiations that can ultimately lead to cell survival. This survival of parts of the transformed cells characterizes the following equilibrium phase. Here, the tumoral lesion enters a dormant stage controlled by the immune system. It is a state of variable length in which the transformed cell population undergoes multiple genetic and epigenetic changes (28). Various cytokines like the interleukins (IL) -12 and -23 (30), and signaling pathways influence the further development as well as the microenvironment's cellular composition (31) or the interferon- γ (IFN γ) and tumor necrosis factor (TNF) receptor 1 promoting activity of TAA specific T helper (Th) 1 cells (32,33). The equilibrium phase may be followed by an escape phase in which the tumor cells elude the control of the immune system. The fatal consequence for patients is the outgrowth of the tumor mass resulting in clinically apparent cancer. Many mechanisms seem to promote this fatal transition. A loss of immunogenicity due to reduced antigen expression, the eventual predominance of cells that do not present strong antigens, or a loss of major histocompatibility complexes (MHC) type 1, are known mechanisms contributing to tumor progress (34) (**Figure 2**). Furthermore, the expression of the regulating molecules Cytotoxic T-Lymphocyte-Associated Protein 4 (CTLA-4) and Programmed Cell Death Protein 1/ Programmed Death Ligand-1 (PD1/PD-L1) as well as the overexpression of B-cell Lymphoma-2 (BCL-2) are central factors in immune escape (34). Moreover, cytokines in the tumor microenvironment seem to play a role in tumor escape, particularly the production and presence of the antiinflammatory cytokines IL-10 and tumor growth factor β (TGF- β) (35). All in all, it has been revealed that the interplay between malignant cells and the immune system is crucial for the development and progress of cancer. Therefore, drugs have been and are being designed to intervene in this process in order to improve the overall survival of cancer patients by supporting the patients' immune system in the fight against malignant cells (36).

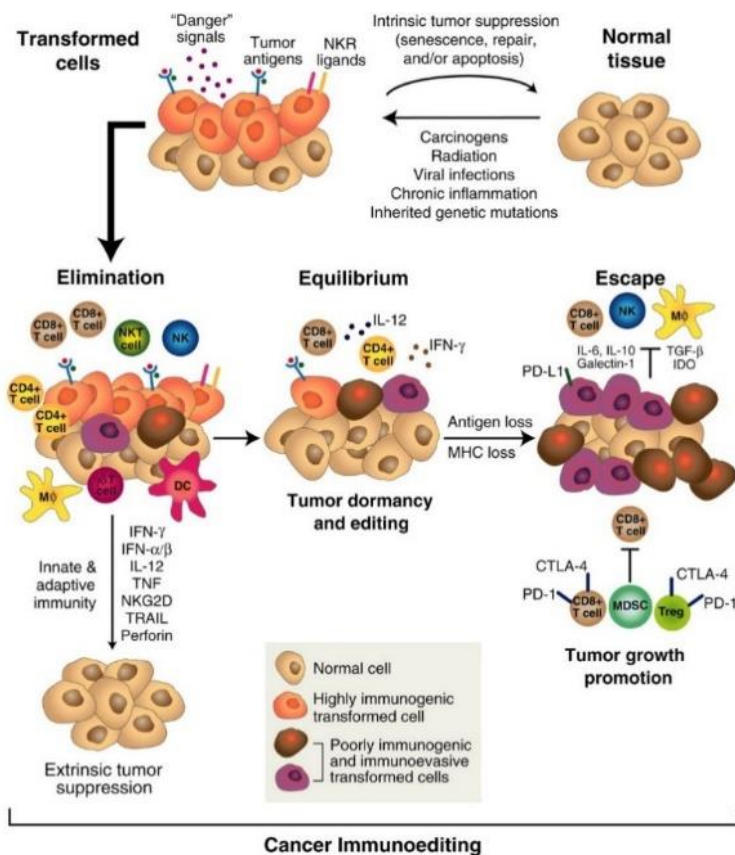


Figure 2: Cancer immunoediting and its three phases. Figure taken from (34), cancer immunoediting can be divided into three distinct phases that are referred to as the ‘three Es’: Elimination, equilibrium and escape. The figure outlines the occurring changes in immunological response and the tumor cell mass during the process of immunoediting.

1.3 Immunotherapy

1.3.1 Theoretic background and current clinical relevance

Immunotherapies have been tested during the last 20 years and are meanwhile getting approved for the treatment of a growing number of malignant entities (37). Besides newer approaches like tumor vaccination and older concepts like the administration of cytokines such as IL-2 for therapy of metastasized melanoma (38), the most popular and broadly used forms of immunotherapy are monoclonal antibodies targeting the immune checkpoint inhibitors CTLA-4 or PD-1/PD-L1 pathways as well as therapy with chimeric antigen receptor (CAR) T cells. In an oncological context, CTLA-4 and PD-1/PD-L1, can be described as inhibitors of tumor-directed immune response via negative regulation of T cell activation. CTLA-4 is a costimulatory molecule, expressed by cytotoxic T cells. Its binding to cluster of differentiation (CD) 80 or CD86 on APCs leads to inhibitory signaling in cytotoxic T cells (39–41). The exact signal

cascade behind this process is yet to be explained in total, but it is known that in large parts CTLA-4 acts antithetically to CD28. Both bind to the B7 molecules CD80 and CD86 expressed on APCs but have oppositional effects on the CTLs with CD28 initiating an activating signal cascade. PD-L1 is often overexpressed in tumor tissues by tumor cells and APCs and its binding (42) to PD-1 also leads to decreased T cell activity and proliferation (39). Thus, blocking CTLA-4 or the PD-1/PD-L1 axis leads to overcoming the inhibitory function and is promoting anti-tumor immunity. With the introduction of immune checkpoint inhibitors, the translation of this valuable knowledge to clinical usage has been completed and has significantly improved the prognosis of patients suffering from several cancer entities, e.g. melanoma. An even newer approach to stimulate the immune system against malignant cells is the therapy with CAR T cells. Here, the patient's own T cells get modified *in vitro* so that they express a chimeric antigen receptor – the CAR. The binding of this CAR to the corresponding antigen that is found on malignant cells leads to subsequent killing of the cancer cells. The variety of available CARs is growing from only targeting CD19 (43) to a multitude of different targetable antigens which broadens the possible spectrum of indications, particularly in hematological neoplasms where CAR T cells have already shown promising results (44). Immune checkpoint inhibition and CAR T cell therapy are two examples that stand out from immunotherapeutic concepts and approaches because they are already established as beneficial for the patients. The long list of approvals by the U.S. Food and Drug Administration (FDA) over the last years highlight the dynamics and progress that was made (25). In some cases, these therapies are even considered first line therapeutics (45). Recent estimations assume that more than 40% of cancer patients are formally eligible for receiving treatment with checkpoint inhibitors regarding the current spectrum of indications (46).

1.3.2 Chances, limitations and obstacles

The rather new concept of immunotherapy is not free of problems that are usually occurring when using more traditional therapeutic regimens. Efficacy cannot be reliably predicted and shows considerable interindividual variability while adverse effects can always develop and cause severe difficulties. Still, even though statistical meta-analysis discovered that, as of 2018, only 13% of all cancer patients respond to immune checkpoint inhibitors (46), groundbreaking trials have shown significant benefit in less roughly defined populations. Checkpoint

inhibitors like the CTLA-4 targeting antibody Ipilimumab in the case of metastasized malignant melanomas and CAR T cells – e.g. for CD19⁺ relapsed or refractory B-cell acute lymphoblastic leukemia (ALL) – have proven their superiority compared to other regimens in their respective pivotal trials (47,48). It must be considered that long-time cure could still not be reached very often with these substances, keeping in mind that patients with particularly fatal prognoses have been treated and assessed in most of these trials. Side effects are usually related to an overactivation of the immune system. However, compared to established treatment regimens, immunotherapy seems to go along with a favorable side effect profile, regarding the amount and the severity of the occurring adverse effects (49). This represents a very important point since a common oncological problem is that therapies have to be stopped or administered in reduced dosages because the patients' overall condition does not allow continuing the regular regimen. Yet, as mentioned previously (46) by far not all cancer entities (e.g. PDAC) respond to the present immunotherapies which creates an urgent need for further innovation. Indeed, many different treatment approaches are continuously being evaluated among them the concept of tumor vaccination.

1.4 Tumor vaccination

1.4.1 Concept and goal of tumor vaccination

There are two ways in which vaccines can be utilized in an oncological context. Preventive vaccines against viruses such as the hepatitis B virus and the human papilloma virus contribute to a lower incidence of hepatocellular (50) and cervix carcinoma (51) that are often related to previous infections with the respective viruses. On the other hand, therapeutic tumor vaccines aim to restore the body's ability to produce specific and powerful effector cells which in a next step attack and destroy already present malignant cells. A key for the concept lies in the fact that cancer cells usually exhibit a different antigen pattern than non-neoplastic cells. Thus, these differing antigens - TAAs and tumor-specific antigens (TSA) - represent potential therapeutic targets (52). In theory, tumor cells will sooner or later get in contact with APCs that recognize the abnormal antigens and subsequently induce a T cell response after processing and presenting the phagocytosed TAAs and TSAs (27). However, cancer cells manipulate their microenvironment, leading to decreased immune effects on the tumor and eventually to survival or outgrowth of the malignancies (34). Potentially, therapeutic tumor vaccinations can

act as counterbalance against these tumor-mediated effects therefore enabling the immune system of the patients to effectively attack and kill the malignant cells.

1.4.2 The role of dendritic cells in tumor vaccinations

Crucial for the concept of tumor vaccination are DCs, a cell type building a bridge between the innate and the adaptive immune system (53–55). DCs can ubiquitously be found in tissues where they reside until they detect a pathogen or potentially also a malignantly transformed cell. Consequently, DCs as well as other APCs like macrophages initiate phagocytosis of the abnormal cells or pathogens. In the next step, DCs migrate to nearby lying lymph nodes where they present the processed antigens, internalized from the phagocytosed compounds, to T cells (**Figure 3/I**). DCs are described as professional APCs due to their capabilities of presenting antigens particularly efficient and of cross-presenting phagocytosed exogenous antigens (53) (**Figure 3/II**). The latter mechanism bases on distinct, separate, intracellular pathways and enables DCs to present exogenous antigens not only via MHC-II but also via MHC-I (56–58). In the following, CD8⁺ T cells get activated and the secretion of proinflammatory cytokines by DCs supports the progress of the initiated immune reaction. The presence of DCs in many tumors as well as their ability to internalize antigens not only from dying or dead cells but also from viable tumor cells in a process called ‘nibbling’ ensures a constant ability of presenting and cross-presenting antigens which is the fundamental first step of immune reaction (59,60). DCs are pivotal in the generation of antigen-specific CD8⁺ cells with an impaired function of DCs correlating with lower CTL responses and in conclusion, to decreased strength of immune responses (61). Thus, the function DCs as relevant players in the immuno-oncological anti-tumor response must be considered when designing tumor vaccines.

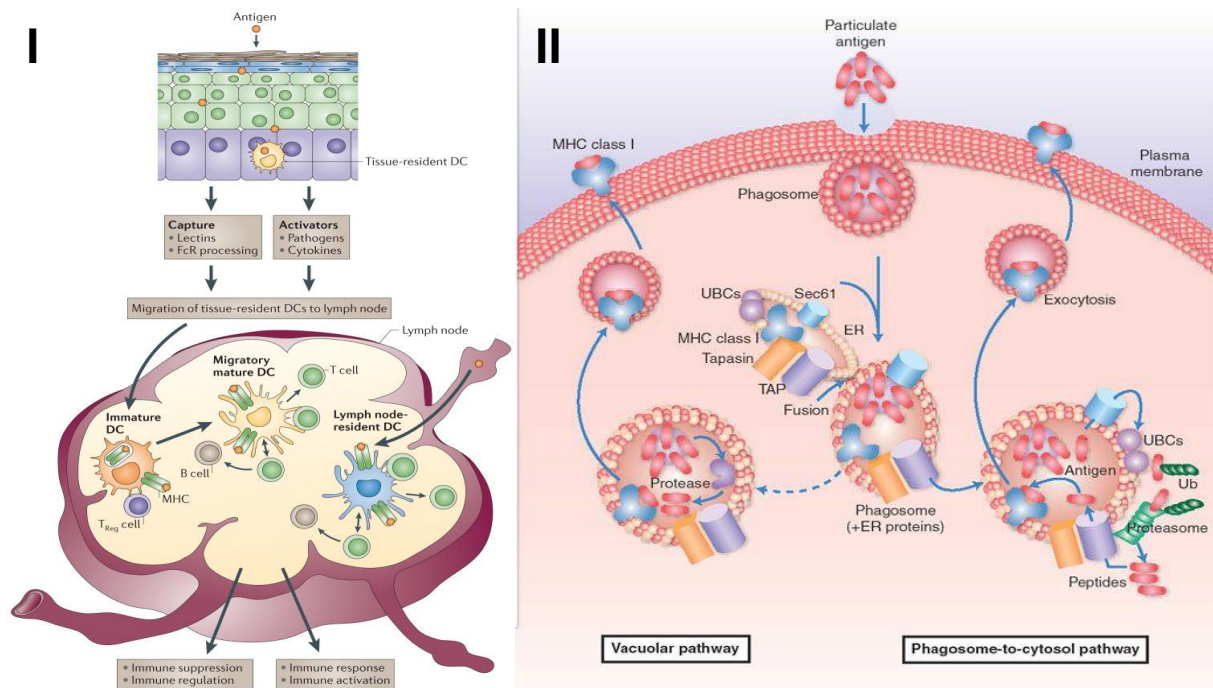


Figure 3/I: The role of dendritic cells in the initiation of immune responses. Figure taken from (53). Dendritic cells set off an immune response by presenting previously phagocytosed and processed antigens to T cells in nearby lying lymph nodes. The scheme describes antigen-presentation, migration and maturation of tissue-resident DCs.

Figure 3/II: Intracellular pathways of cross-presentation. Figure taken from (56). Dendritic cells can present exogenous antigens via MHC-I through a process called ‘cross-presentation’. The figure illustrates differing intracellular pathways by which the exogenous antigen gets transported through the compartments eventually ending up being presented via MHC-I on the cellular membrane.

1.4.3 Different vaccination approaches and their stage of development

1.4.3.1 Tumor vaccines in the context of personalized medicine

Therapeutic tumor vaccination is a strategy that comprises a variety of different approaches (**Figure 4**). As with other therapeutic concepts in oncology such as chemotherapy or targeted therapy with monoclonal antibodies, it is key to find targetable characteristics that are as specific and as restricted to tumor cells as possible. A central role is played by antigens that are either tumor-associated like gp100 and thus overexpressed on tumor cells - in the case of gp100 e.g. on melanoma cells - or tumor-specific, where a highly specific and characteristic mutation leads to the generation of a unique antigen (52,62). These TSAs, also called tumor neoantigens (TNAs) (63,64), are ideal for developing unique, individual vaccines for personalized treatment. In xenograft tumor models, it was demonstrated that enriched T cells,

primed to highly specific, patient-derived neoantigens, can drastically inhibit tumor growth (65). Even though clinical translation of such a highly precise vaccine model has not yet been completed, this is an encouraging result. Above all, these therapies would have to be customized to each individual patient according to individual tumor profiles thus presenting a further step towards the realization of personalized precision medicine.

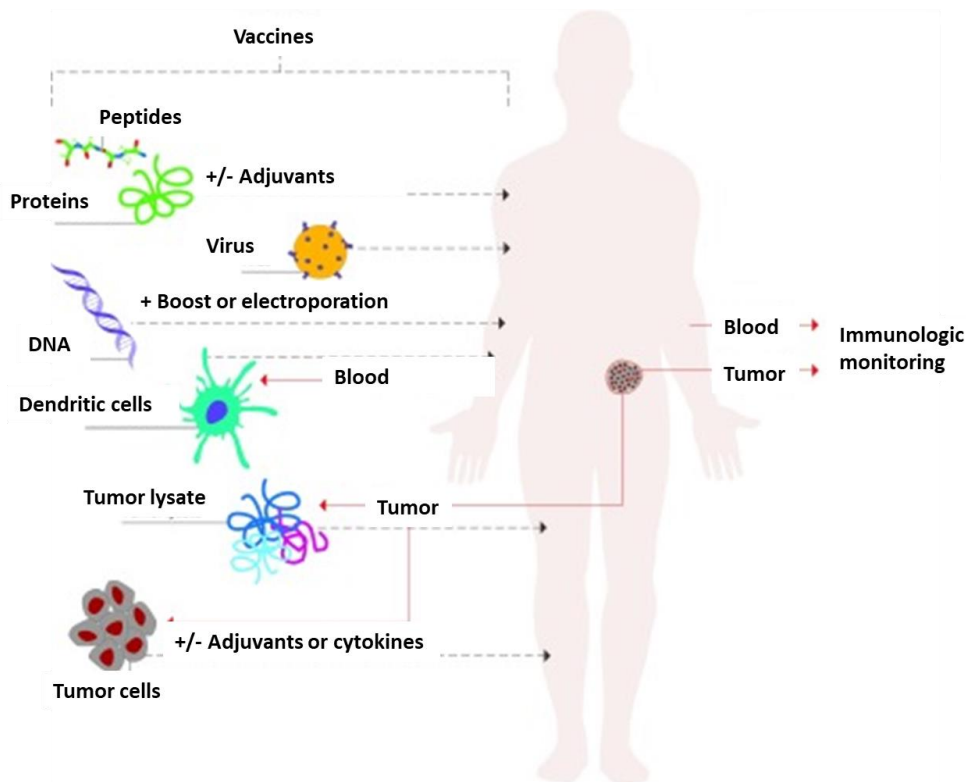


Figure 4: Strategies for and composition of tumor vaccines. Figure modified according to (62). An overview of the potential approaches of tumor vaccination. Most proposed and tested vaccines do not contain only an immunogenic compound but are boosted with adjuvants in order to enhance the vaccines' efficacy.

1.4.3.2 Oncolytic viruses

A less personalized approach is therapy based on usage of oncolytic viruses. After injection, and selective virus replication in tumor cells (66), anti-tumor effects unfold: The immediate consequence of intratumoral virus replication is cell death, followed by enhanced virus-mediated presentation of tumor-associated and tumor-specific antigens that can lead to systemic, favorable immune responses (67). In a randomized, multicenter Phase III trial (OPTiM), intratumoral injection of the FDA-approved drug Talimogene Laherparepvec, an oncolytic herpes simplex virus showed beneficial effects for patients with unresectable melanoma (68,69).

More recently, a Phase II study in patients with advanced melanoma suggested that Talmogene Laherparepvec might be a useful addition to the established therapy regimen with the CTLA-4 blocker Ipilimumab, a CTLA-4 (70) suggesting synergetic effects between different kinds of immunotherapy.

1.4.3.3 *In situ* vaccines

In situ vaccines get administered at the tumor site generating systemic, so-called 'abscopal effects'. These develop because the vaccines neutralize tumor-mediated effects on its surrounding microenvironment (**see chapter 1.2**) and induce tumor antigen-release by boosting cell death (71,72). In a study by Hammerich *et. al.*, radiotherapy, that is an *in situ* vaccine itself (73), was combined with the toll-like receptor (TLR) 3 agonist poly-ICLC and fms-like tyrosine kinase 3 ligand that plays an important role in the development of DCs (74,75). In a small sample size of eleven patients with indolent B cell lymphoma, *in situ* vaccination was able to induce tumor regression while being tolerated well. In this context, the role of DCs was demonstrated and it was stated that intratumoral, cross-presenting DCs are essential for the generation of a potent immune response (75).

1.4.3.4 Antigen presenting cell based strategies

As pointed out, APCs and particularly DCs (**see chapter 1.4.2**) are key players in the process of every immune response. Besides CAR-T Cells (**see chapter 1.3.1**), there exist other forms of autologous cell immunotherapy, where a cell product named Sipuleucel-T, containing T, B, natural killer cells (NKs) and DCs, is utilized (76). In the IMPACT trial, a significant benefit in overall survival of patients with metastatic castration-resistant prostate cancer was detected, leading to FDA approval for this indication in 2010 (77). A multitude of trials, mostly in Phase I or II that test DC-only vaccines have recently been and are currently being conducted (78). In one trial, autologous, TNA-specific DCs have been re-transplanted into patients with advanced melanoma which has not shown considerable side effects while the number of TNA-specific CD8⁺ T cells was elevated, indicating a tumor-specific immune response (79). Furthermore, absence of severe side effects as well as good outcomes in terms of reaching partial and complete responses were reported in another trial where a DC vaccine together with Ipilimumab was administered to patients suffering from pretreated advanced melanoma (80).

1.4.3.5 Peptide and nucleic acid based strategies

In contrast to the mentioned APC-based strategies, all immune reaction related steps occur *in vivo* with the systemic administration of tumor-derived, immunogenic peptides or nucleic acids causing APC and T cell activation. In a phase I trial orchestrated by Tiriveedhi *et al.*, a deoxyribonucleic acid (DNA) vaccine against breast cancer has not led to concerning adverse effects and the results suggest that beneficial effects on progression free survival could exist (81). In comparison, peptide based vaccines are much more common and are also tested in more clinical settings. For instance a gp100 vaccine was evaluated by Schwartzentruher *et al.* in a randomized phase III study in patients with advanced melanoma (82). Some early phase clinical trials with Neli pepimut/E75 based vaccines as well as with other human Epidermal Growth Factor Receptor 2 (HER-2) derived peptides have shown potential to improve treatment strategies for breast cancers even with only low levels of HER-2 expression (83,84). Here, Granulocyte-Macrophage Colony Stimulating Factor (GM-CSF) was administered as an adjuvant to enhance the potency of the generated immune response. TLR agonists like Imiquimod or polyinosinic:polycytidylic acid (poly I:C) (TLR3), other proinflammatory cytokines like Interferon α or also Montanide ISA-51 that was used in the presented melanoma study (82) are further examples for adjuvants. An obstacle for peptide vaccines is the human leucocyte antigen (HLA) restriction, meaning that a peptide vaccine is only useful in patients with matching HLA alleles (62). Since clinical outcomes are not yet satisfying enough, advanced concepts such as multi-epitope vaccines, combinations with other therapeutics, and personalized peptide vaccinations are being evaluated (63).

1.4.4 The usage of nanoparticles for improving tumor vaccines

1.4.4.1 How nanoparticles can enhance the effect of tumor vaccines

Another strategy to improve the therapeutic effects of peptide or nucleic acid based DC targeting vaccines is the usage of delivery systems such as liposomes (85,86), virus-like particles (87) and nanoparticles (NPs). These delivery systems are implemented to improve the potency of tumor vaccines by ensuring a more effective, coordinated uptake of the encapsulated compounds as well as providing additional adjuvant effects and promoting cross-presentation (88). For this purpose, it is crucial that the administered vaccine effectively reaches DCs and

subsequently gets taken up by them. This initial step can be problematic. Short peptides, suitable for inducing immune responses (89) are defenseless against proteolytic enzymes. Due to their size and biochemical properties they are not predestined to be taken up and processed by DCs as effectively as it could be possible if they were encapsulated into a nanoparticle structure (90,91). The mere internalization of nanoparticles by APCs has previously been described, for example through using fluorochrome-conjugated (90) or partly photoluminescent nanoparticles (92). Importantly, it was shown that nanoparticles with encapsulated antigens can lead to stronger immune reactions than the soluble antigen alone, indicating a more effective uptake. In this regard, it is central to note that the mere particles without encapsulated antigens have not led to relevant effects (93). Yet, it must be considered that the beneficial effects of nanoparticles cannot be generalized. Different structural origins, shapes and sizes of nanoparticles lead to individual outcomes and imply distinct advantages and disadvantages. Taking these variables into account, most research are using NPs of sizes between 10 and 200 nm in diameter (94).

1.4.4.2 The subgroup of polymeric nanoparticles

The material from which nanoparticles are produced can be very diverse as well. In the context of tumor vaccines, many research groups work with polymers like γ -glutamic acid (γ -PGA), poly lactic-co-glycolic acid (PLGA), chitosan or others (95). It has been demonstrated that DCs are able to internalize these polymers efficiently, *in vitro* as well as *in vivo*, leading to noteworthy immune responses driven by the encapsulated antigen and enhanced by adjuvant effects of the nanoparticle-composing structure (96). A profound insight in how polymer based nanoparticles can increase the potency of immune responses was provided by Luo et al.. In *in vitro* and mouse models, ovalbumin (OVA)-loaded PC7A-NPs were superior compared to soluble OVA in terms of inducing an immune response that was objectified by e.g. IFN γ secretion of CD8⁺ cells, MHC-I mediated antigen presentation and inhibited tumor growth. Remarkably, these results were obtained with a vaccine without adjuvant (97). Given the situation that peptide based vaccines often do not reach the desired effectivity even when applied with adjuvants, this result underlines the potential of polymeric NPs in tumor vaccine approaches. On the other hand, nanoparticles can also provide advantages regarding the delivery of adjuvants. While poly I:C, a ligand of TLR3, has a short half-life when injected nakedly (98), encapsulation

in nanoparticles can prevent poly I:C from degradation by nucleases. Han *et al.* took advantage of the adjuvant effect of poly I:C to enhance the immune reaction generated by CNPs that were loaded with varying peptides. Moreover, in this study, stronger immune responses *in vitro* and prolonged survival of tumor bearing mice *in vivo* were recorded when CNPs (OVA + poly I:C) were administered in comparison with mere OVA (99).

1.4.4.3 Chitosan, its characteristics and resulting opportunities

Chitosan is a biopolymer generated through deacetylation of chitin (100) that is already utilized for non-medical purposes for example in cosmetics or the production of wine (101) (**Figure 5(I) for chemical composition**). Certain biochemical properties of chitosan have also led to its experimental application in medical fields, more precisely as basis for generating nanoparticles, hydrogels or wound dressings (102). One of chitosan's biochemical characteristics is the existence of positively charged amino groups that support the internalization of CNPs in cells, most notably into immune cells of the nasal mucosa (102). Furthermore, chitosan is highly biocompatible and biodegradable (103,104). The resulting low overall toxicity is supported by the described long-lasting usage in everyday products (101). Moreover, chitosan is inexpensive and easy to synthesize. Altogether, these characteristics highlight the potential suitability of chitosan as carrier substance for drug delivery (105). For instance, CNPs have provided a more targeted doxorubicin delivery in mouse models resulting in elevated drug concentrations and increased toxicity towards tumor cells (106). Ideally, usage of such carrier nanoparticles could allow dose reductions without causing a loss of efficacy which, given the adverse effects of drugs in general and cytostatic drugs in particular, would benefit the patients. In regard to employment of CNPs for tumor vaccines, the immunostimulatory effect of chitosan plays a large role since adjuvants are needed in order to generate a more potent immune response (107,108). Moreover, due to its mucoadhesive properties, that can be explained by the interaction of chitosan's positively charged amino groups with negatively charged sialic acid in the mucus (104), chitosan based vaccines could be an option for not only parenteral but also mucosal vaccination. In this simple procedure that takes advantage of the pronounced immunologically active tissue in the respiratory tract (109), the vaccine gets administered intranasally in form of a spray. Chitosan could be a particularly suitable carrier substance since it facilitates transepithelial antigen transport by affecting epithelial tight junctions

(110). Importantly, the induction of immune responses upon intranasal vaccination with CNPs, temporarily incorporated in a mannitol matrix (**Figure 5(II)**) for easier usage has already been recorded in mice (111).

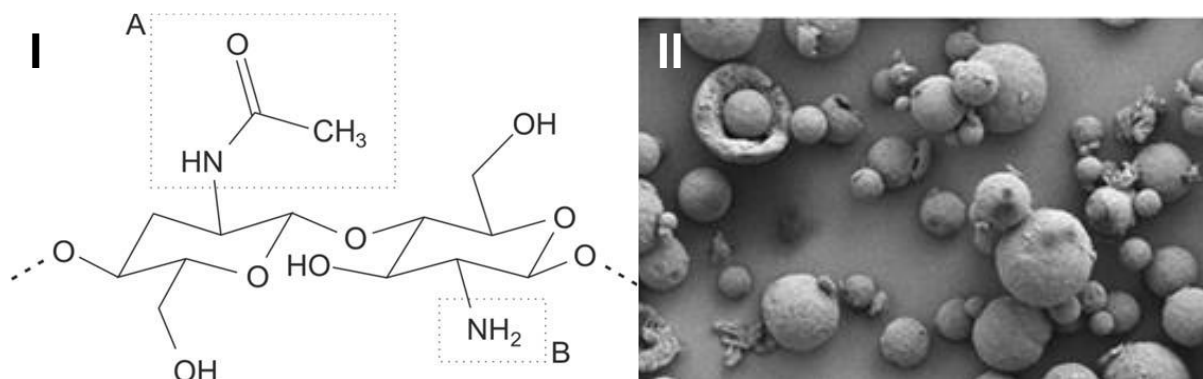


Figure 5: Chitosan, the chemical structure (I) and resulting form of chitosan nanoparticles (II). Figure taken from (112). The chemical composition of the polysaccharide chitosan (left) and scanning electron microscope (SEM) pictures of chitosan nanoparticles embedded in a mannitol matrix thus forming a nano-in-microparticle structure (right).

1.5 Aim of this study

As of today, cancer is the 2nd most common cause of death worldwide (8). The resulting, enormous relevance of cancer has led to extensive research and improvements in their comprehension and therapy (1,14,25,45). Tumor vaccines are regarded as promising immunotherapeutic options with a great potential to be introduced into clinical usage since encouraging results have already been registered in preclinical trials (95,97,99). However, further analyses are needed in order to identify the most effective vaccination strategies. The utilization of nanoparticles as carrier vehicles is believed to improve the efficacy of tumor vaccines. Chitosan offers plenty of favorable properties and the chitosan-based NP formulation used in this study features characteristics that allow mucosal vaccination via intranasal administration (104,111,112) Thus, this study aims to investigate whether these CNPs are a suitable antigen delivery system that is able to induce a potent antigen-specific immune response. For this purpose, we assessed the role of CNP size with respect to uptake in and survival of APCs and characterized the phenotype of human and murine DCs after CNP stimulation. Furthermore, we assessed whether antigens, encapsulated in CNPs get presented efficiently by DCs via MHC-I and whether this presentation is adequate to induce activation and functional activity of antigen-specific CD8⁺ T cells.

2. Materials

2.1 Laboratory devices

<u>Device</u>	<u>Manufacturer</u>
<u>Centrifuges</u>	
Avanti J-20 XP	Beckmann Coulter GmbH, Krefeld, DE
Centrifuge 5804 R	Eppendorf AG, Hamburg, DE
HERAEUS Fresco 17	Thermo Scientific, Schwerte, DE
HERAEUS Multifuge X1	Thermo Scientific, Schwerte, DE
HERAEUS Pico 17	Thermo Scientific, Schwerte, DE
Rotina 420 R	Andreas Hettich GmbH, Tuttlingen, DE
Sprout® mini centrifuge	Heathrow Scientific, Vernon Hills, US
<u>Incubators/shakers</u>	
BBD 6220 CO2 incubator	Thermo Scientific, Schwerte, DE
GyroTwister 3D shaker	Labnet, Woodbridge, US
HERA Cell 240 incubator	Thermo Scientific, Schwerte, DE
Medingen W 12 water bath	Preiss-Daimler, Wilsdruff, DE
QBA1 block heater	Grant Instruments, Shepreth, UK
Stuart SRT9 tube roller	Bibby Scientific Ltd. Stone, UK
WTC ED-53 incubator	Binder, Tuttlingen, DE
<u>Measuring devices</u>	
Amnis ImageStream XMark II flow cytometer (ISX)	Merck Millipore, Darmstadt, DE
FACScalibur flow cytometer	Becton Dickinson, Heidelberg, DE
Infinite® 200PRO microplate reader	Tecan, Crailsheim, DE
LightCycler 480 II	Roche, Basel, CH
Lionheart™ FX Automated Microscope	BioTek, Winooski, US

LSRFortessa flow cytometer	Becton Dickinson, Heidelberg, DE
NanoQuant plate	Tecan, Crailsheim, DE
Neubauer counting chamber	Marienfeld Superior GmbH, Lauda-Koenigshofen, DE
NYONE® cell imager	Synentec GmbH, Elmshorn, DE
pH 7110 pH-meter	InoLab, Weilheim, DE
<u>Microscopes</u>	
AE2000	Motic, Wetzlar, DE
Axiovert 25	Carl Zeiss AG, Jena, DE
EVOS XL Core Cell Imaging System	AMG, Bothell, US
<u>Others</u>	
Arpege LN2 container	KGW-Isotherm, Karlsruhe, DE
CS autoclave	Matachana GmbH, Selmsdorf, DE
Freezer (4°C)	Liebherr, Ochsenhausen, DE
Fridge (-20°C)	Liebherr, Ochsenhausen, DE
HERAfreeze basic freezer (-80°C)	Thermo Scientific, Schwerte, DE
JE-5.0 Elutriator Rotor	Beckmann Coulter GmbH, Krefeld, DE
Laboport vacuum pump	KNF Neuberger, Freiburg, DE
Masterflex® L/S® tubing pump	Cole Parner Instruments, Kehl, DE
MC6 laboratory cabinet	Waldner GmbH, Wangen, DE
MR Hei-Mix S magnetic stirrer	Heidoph Instruments, Schwabach, DE
PluriPlex magnetic roller	PluriSelect, Freiburg, DE
Scotsman AF103 ice flaker	Hubbard Systems, Ipswich, UK
Sunrise remote control	Tecan, Crailsheim, DE
Sonicator Sonopuls	Bandelin, Berlin, DE
Vacuum pump	VWR, Radnor, US
VORTEX Genius 3 vortex shaker	IKA-Werke, Staufen, DE

<u>Pipettes</u>	
Finnpipette™ F1 0.2-2 µl	Thermo Scientific, Schwerte, DE
Finnpipette™ F1 1-10 µl	Thermo Scientific, Schwerte, DE
Finnpipette™ F1 2-20 µl	Thermo Scientific, Schwerte, DE
Finnpipette™ F1 10-100 µl	Thermo Scientific, Schwerte, DE
Finnpipette™ F1 20-200 µl	Thermo Scientific, Schwerte, DE
Finnpipette™ F1 100-1000 µl	Thermo Scientific, Schwerte, DE
Finnpipette™ Multichannel 5-50 µl	Thermo Scientific, Schwerte, DE
Finnpipette™ Multichannel 20-200 µl	Thermo Scientific, Schwerte, DE
Pipetboy® acu	Integra Biosciences, Fernwald, DE
Pipetus®	Hirschmann Laborgeräte, Eberstadt, DE
Ripette® multistep dispenser	Ritter, Schwabmuenchen, DE

<u>Sterile benches</u>	
HERA Safe	Thermo Scientific, Schwerte, DE
HERA Safe KS	Thermo Scientific, Schwerte, DE
HERAEUS LaminAir HB 2448	Thermo Scientific, Schwerte, DE

<u>Scales</u>	
Precisa BJ 2100D	Precisa Gravimetrics AG, Dietikon, CH
Precisa XB120A	Precisa Gravimetrics AG, Dietikon, CH

2.2 Consumables

<u>Consumable</u>	<u>Manufacturer</u>
0.1-10 µl, 10-200 µl, 100-1000 µl pipette tubes	Sarstedt, Nümbrecht, DE
0.05 ml, 1.25 ml, 5.0 ml Ritips®	Ritter, Schwabmuenchen, DE
0.5 ml, 1.5 ml, 2 ml Safe Seal tubes	Sarstedt, Nümbrecht, DE

15 ml, 50 ml centrifuge tubes/falcon tubes	Sarstedt, Nümbrecht, DE
5 ml, 10 ml, 25 ml serological pipettes	Sarstedt, Nümbrecht, DE
12-well plates flat bottom	Sarstedt, Nümbrecht, DE
18 mm coverslips	Menzel, Braunschweig, DE
25 cm² cell culture flasks	Sarstedt, Nümbrecht, DE
75 cm² cell culture flasks	Sarstedt, Nümbrecht, DE
96-well plates flat bottom	Sarstedt, Nümbrecht, DE
96-well plates round bottom	Sarstedt, Nümbrecht, DE
96-well plates conic bottom	Nerbe plus GmbH, Winsen, DE
Cell scraper 25 cm	Sarstedt, Nümbrecht, DE
CryoPure tubes, 1.8 ml	Sarstedt, Nümbrecht, DE
LightCycler 480 Sealing foil	Roche, Basel, CH
LightCycler 480 96 well multiwell plate	Roche, Basel, CH
FACS tubes 500 µl	Sarstedt, Nümbrecht, DE
FACS tubes 5 ml	Sarstedt, Nümbrecht, DE
Micro-Touch nitrile examination gloves	Ansell GmbH, München, DE
Parafilm M sealing film	Brand GmbH, Wertheim, DE
Pasteur pipettes ISO 7712	Glaswarenfabrik Kerl Hecht GmbH, Sondheim/Roehn, DE
Scalpel	Feather, Osaka, JP
SuperFrost object slide 76x26mm	Menzel, Braunschweig, DE
Syringe 10 ml	Sarstedt, Nümbrecht, DE
Thermanox Plastic coverslips 15 mm	Thermo Scientific, Schwerte, DE
Transfer pipettes 3.5 ml	Sarstedt, Nümbrecht, DE
Vue Life culture bag 32-C	Saint-Gobain, Courbevoie, FR

2.3 Kit Systems

<u>Kit</u>	<u>Manufacturer</u>
CaspaseGlo® 3/7 Assay	Promega, Mannheim DE
MojoSort™ Kit	Biolegend, Fell, DE
MycoAlert™ Mycoplasma detection kit	Lonza Group, Basel, CH
peqGOLD Total ribonucleic acid (RNA) kit	PeqLab, Erlangen, DE
RevertAid First Strand cDNA Synthesis kit	Thermo Scientific, Schwerte, DE

2.4 Software

<u>Software</u>	<u>Manufacturer</u>
FACScalibur CellQuest	BD Biosciences, San Jose, US
FlowJo 10.1r3	FlowJo, LCC, Ashland, US
i-control™ Microplate Reader Software	Tecan, Crailsheim, DE
LightCycler 480 Software	Roche, Basel, CH
Lionheart™ FX Automated Microscope analysis software 'Gen5'	BioTek, Winooski, US
Microsoft Office 2016	Microsoft Corporation, Redmond, US
SigmaPlot 12.5	Systat Software Inc., Chicago, US
Weasel v3.0	The Walter and Eliza Hall Institute of medical research, Victoria, US
Zotero	Center for History and New Media at the George Mason University, Fairfax, US

2.5 Chemicals, reagents and buffers

2.5.1 Chemicals and reagents

<u>Chemical/reagent</u>	<u>Manufacturer</u>
2-Mercaptoethanol	Sigma-Aldrich, St. Louis, US
Accutase® solution	EMD Millipore Corporation, Temecula, California, US
Acetone	Th. Geyer GmbH, Renningen, DE
Aqua ad iniectabilia	B. Braun AG, Melsungen, DE
Bovine serum albumin (BSA), fraction V	Biomol, Hamburg, DE
Dimethyl sulfoxide (DMSO)	Th. Geyer GmbH, Renningen, DE
Ethanol, 99.8 % denaturated	Th. Geyer GmbH, Renningen, DE
Ethanol, absolute	Th. Geyer GmbH, Renningen, DE
Ethylendiamintetraacetic acid (EDTA)	Carl Roth GmbH, Karlsruhe, DE
FACSflow sheath fluid	BD Biosciences, San Jose, US
Fragment crystallizable receptor (FcR) blocking reagent human	Miltenyi Biotech GmbH, Bergisch Gladbach, DE
FcR blocking reagent mouse	Miltenyi Biotech GmbH, Bergisch Gladbach, DE
Fetal calf serum (FCS)	PAN-Biotech, Aidenbach, DE
Fixation/permeabilization concentrate	eBioscience, Frankfurt, DE
Fixation/permeabilization diluent	eBioscience, Frankfurt, DE
Geneticin (G418) sulphate	Merck Millipore, Darmstadt, DE
HEPES buffer 1 M	PAN Biotech, Aidenbach, DE
L-Glutamine (L-GLN)	PAA, Pasching, AT
LightCycler 480 SYBR Green I Master	Roche, Basel, CH
Minimum essential medium non-essential amino acids (MEM NEAA)	Thermo Scientific, Schwerte, DE
Pancoll human, 1.077 g/l	Pan-Biotech GmbH, Aidenbach, DE
Paraformaldehyde (PFA) 4.5 %	BUEFA Chemikalien GmbH, Hude, DE

Penicillin-Streptomycin (Pen/Strep)	PAA, Pasching, AT
Phosphate-buffered saline (PBS)	Merck millipore, Darmstadt, DE
Propium Iodide (PI)	Life technologies, Darmstadt, DE
Roswell Park Memorial Institute (RPMI) 1640 medium	Biochrom, Berlin, DE
Sodium pyruvate	Biochrom, Berlin, DE
Solution 555	Beckmann Coulter GmbH, Krefeld, DE
Triton X-100	Sigma-Aldrich, St. Louis, US
Trypan blue solution Fluka 0.4 %	Sigma-Aldrich, St. Louis, US
Trypsin-EDTA	PAA, Pasching, AT

2.5.2 Buffers

<u>Buffer</u>	<u>Composition</u>
<u>Counterflow centrifugation elutriation</u>	
Elutriation buffer	0.1 % (v/v) FCS in PBS 10 mM EDTA PBS pH 7.4
Erythrocyte lysis buffer	1x Ammonium Chloride Potassium 155 mM Ammonium Chloride 10 mM Potassium bicarbonate 0.1 mM EDTA
<u>Flow cytometry (FACS)</u>	
Fixation solution	1 % (v/v) PFA in MACS buffer
Fixation/permeabilization solution	25 % (v/v) Fixation/permeabilization Concentrate in Fixation/permeabilization diluent
MACS buffer	0.5 % BSA 2 mM EDTA

	in PBS (pH 7.2)
Perm washing buffer	10 % (v/v) permeabilization buffer (10x) in ddH ₂ O

2.6 Peptides and chitosan nanoparticles

2.6.1 Peptides

<u>Peptide</u>	<u>Manufacturer</u>
Ovalbumin	Sigma-Aldrich, St. Louis, US
SIINFEKL (OVA 257-264)	Invivogen, Toulouse, FR

2.6.2 Chitosan nanoparticles

All chitosan nanoparticles were produced by the working group led by Professor Scherließ, Kiel, Germany

<u>Nanoparticle type</u>	<u>z-average/diameter</u>	<u>Polydispersity index</u>
90/10 (with and without fluorescein isothiocyanate (FITC)-conjugation)	220 nm	<0.17
90/20 (with and without FITC-conjugation)	384 nm	0.22
90/50 (with and without FITC-conjugation)	706 nm	0.39
90/10 OVA (with and without FITC-conjugation)	201 nm	0.14
90/20 OVA (with and without FITC-conjugation)	321 nm	0.15
90/10 SIINFEKL	211 nm	0.15

2.7 Animals

<u>Animal</u>	<u>Information</u>	<u>Provider</u>
OT-1 mice (C57BL/6)	OT-1 – short for OVA-specific, class I-restricted TCR transgenic – mice are harboring CD8 ⁺ T cells with a transgenic T cell receptor that specifically recognizes OVA 257-264 (amino acid sequence SIINFEKL) presented in the context of H-2K ^b (113) .	Charles River, Wilmington, US

2.8 Cell biological material

2.8.1 Cell lines

<u>Cell line</u>	<u>Information</u>	<u>Reference</u>
DC2.4 Murine dendritic cells	Immortalized murine dendritic cells. Created by transducing bone marrow isolates of C57BL/6 mice with retroviral vectors encoding for GM-CSF, myc and raf. These cells were kindly donated by Professor Dr. Scherließ, Kiel, DE.	(114)

Panc02	Murine PDAC cells derived	(115)
Murine PDAC cells	from 3-methyl-cholanthrene treated C57BL/6 mice.	
	These cells were kindly donated by Dr. Bauer, Marburg, DE.	
PancOVA	Panc02 cells, transfected	(116,117)
Murine PDAC cells (Panc02), expressing OVA.	with the gene encoding for OVA.	
	These cells were kindly donated by Dr. Bauer, Marburg, DE.	

2.8.2 Human primary cells

Human primary cells were isolated from thrombocyte-depleted leukocyte retaining systems (LRS).

Leukocyte retaining systems	UKSH blood donation center Citti-Park, Kiel, DE
------------------------------------	---

2.8.3 Growth factors and cytokines

GM-CSF, human recombinant	Biolegend, Fell, DE
Interleukin-2, murine recombinant	Biolegend, Fell, DE
Interleukin-4, human recombinant	Biolegend, Fell, DE
M-CSF, human recombinant	Biolegend, Fell, DE

2.8.4 Cell culture media

Cell culture media	Composition
DC 2.4 cell culture	DC 2.4 Medium RPMI 1640 (w/o Glutamine) 10 % (v/v) FCS, 1 % (v/v) L-Gln, 1 % (v/v) Pen/Strep, 1 % NEAA
Human DC culture	Human DC Medium RPMI 1640 (w/o Glutamine) 10% (v/v) FCS, 1 % (v/v) L-Gln, 1 % (v/v) Pen/Strep supplemented with: 800 U/ml GM-CSF 250 U/ml IL-4
Macrophage culture GM-CSF stimulation for generation of M1-macrophages <u>or</u> M-CSF stimulation for generation of M2-macrophages	Macrophage medium RPMI 1640 (w/o Glutamine) 10 % (v/v) FCS, 1 % (v/v) L-Gln, 1 % (v/v) Pen/Strep supplemented with: 50 ng/ml GM-CSF (M1) or 50 ng/ml M-CSF (M2)
OT1 mice derived CD8⁺ T cell culture	T cell medium RPMI 1640 (w/o Glutamine) 10 % (v/v) FCS, 3 % (v/v) HEPES, 2 % (v/v) sodium pyruvate, 2 % (v/v) Pen/Strep
Murine pancreatic cell culture (Panc02, PancOVA)	Panc Medium RPMI 1640 (w/o Glutamine) 10 % (v/v) FCS, 1 % (v/v) L-Gln, 1 % (v/v) Pen/Strep supplemented with: 0,5 mg/ml G418 sulphate in first passages

2.9 Molecular biological material

2.9.1 Human primers

<u>Gene</u>	<u>Sequence</u> <u>Fw – forward</u> <u>Rv – reverse</u>	<u>Annealing °C</u>	<u>Manufacturer</u>
GAPDH	Fw-TCCATGACAACCTTTGGTATCGTGG Rv-GACGCCTGCTTCACCACCTTCT	58	Eurofins, Hamburg, DE
IL-1β	Fw-AGTGCTCCTTCCAGGACCTGGA Rv-CACTCTCCAGCTGTAGAGTGG	58	Eurofins, Hamburg, DE
IL-6	Fw-ATGCAATAACCACCCCTGAC Rv-GAGGTGCCCATGCTACATTT	58	Realtime Primers, Elkins Park, US
IL-10	Fw-AAGCCTGACCACGCTTTCTA Rv-ATGAAGTGGTTGGGGAATGA	58	Realtime Primers, Elkins Park, US
TNF-α	Fw-TCCTTCAGACACCCTCAACC Rv-AGGCCCCAGTTTGAATTCTT	58	Eurofins, Hamburg, DE
TGF-β1	Fw-CGTGGAGCTGTACCAGAAATA Rv-TCCGGTGACATCAAAAGATAA	58	Eurofins, Hamburg, DE

2.9.2 Mouse primers

<u>Gene</u>	<u>Sequence</u>	<u>Annealing °C</u>	<u>Manufacturer</u>
GAPDH	Fw-TCCATGACAACCTTTGGTATCGTGG Rv-GACGCCTGCTTCACCACCTTCT	58	Eurofins, Hamburg, DE
mIL-1β	Fw-ATCCTCTGTGACTCATGGGAT Rv-GATCCACACTCTCCAGCTGCA	55	Biometra, Göttingen, DE
mIL-6	Fw-TAGTCCTTCTACCCCAATTTCC Rv-TTGGTCCTTAGCCACTCCTTC	58	Eurofins, Hamburg, DE
mIL-10	Fw-AGTGGAGCAGGTGAAGAGTG Rv-TTCGGAGAGAGGTACAAACG	58	Realtime Primers, Elkins Park, US
mTNF-α	Fw-CCCACTCTGACCCCTTACT Rv-TTTGAGTCCTTGATGGTGGT	58	Eurofins, Hamburg, DE
mTGF-β1	Fw-GCTGAACCAAGGAGACGGAA Rv-AGAAGTTGGCATGGTAGCCC	58	Eurofins, Hamburg, DE

2.10 Antibodies

2.10.1 Anti-human antibodies

<u>Specificity-Conju- gate (Clone)</u>	<u>Host (Isotype)</u>	<u>Stock in µg/ml</u> <u>Application</u> <u>(Dilution)</u>	<u>Manufacturer</u>
Anti-human isotype controls			
IgG2b-Fluorescein isothiocyanate (FITC) (MPC-11)	Mouse (IgG2b)	200 FACS (1:40)	Biolegend, Fell, DE
IgG1-Allophycocya- nine (APC) (MOPC- 21)	Mouse (IgG2b)	200 FACS (1:16.6)	Biolegend, Fell, DE
IgG1-Phycoerythrin (PE) (MOPC-21)	Mouse (IgG1)	200 FACS (1:10 and 1:20)	Biolegend, Fell, DE
IgG1-FITC (MOPC-21)	Mouse (IgG1)	500 FACS (1:150)	Biolegend, Fell, DE
IgG2a-PE (MOPC-173)	Mouse (IgG2a)	200 FACS (1:50)	Biolegend, Fell, DE
IgG1-PeCyanine 7 (Cy7) (MOPC-21)	Mouse (IgG1)	200 FACS (1:10)	Biolegend, Fell, DE

Anti-human primary antibodies

<u>Specificity-Conju- gate (Clone)</u>	<u>Host (Isotype)</u>	<u>Stock in µg/ml</u> <u>Application</u> <u>(Dilution)</u>	<u>Manufacturer</u>
CD1a-PE (HI149)	Mouse (IgG1)	200 FACS (1:10)	Biolegend, Fell, DE
CD11c-APC (S-HCL-3)	----	100 ISX (1:10)	Biolegend, Fell, DE
CD14-PE (M5E2)	Mouse (IgG1)	200 FACS (1:50)	Biolegend, Fell, DE
CD16-PE (3G8)	Mouse (IgG1)	100 FACS (1:50)	Biolegend, Fell, DE
CD80-APC (2D10)	Mouse (IgG1)	200 FACS (1:16.6)	Biolegend, Fell, DE
CD83-FITC (HB15e)	Mouse (IgG1)	200 FACS (1:20)	Biolegend, Fell, DE
CD86-Alexa Fluor (AF) 488 (IT2.2)	Mouse (IgG2b)	400 FACS (1:16.6)	Biolegend, Fell, DE
CD163-PE (REA812)	Human (igG1)	50 FACS (1:20)	Miltenyi Biotech GmbH, Bergisch Gla- dbach, DE
CD206-FITC (15-2)	Mouse (IgG1)	200 FACS (1:50)	Biolegend, Fell, DE
E-Cadherin-AF647 (67A4)	----	200 ISX (1:40)	Biolegend, Fell, DE
HLA-DR-FITC (L243)	Mouse (IgG2a)	200 FACS (1:40)	Biolegend, Fell, DE
PD-L1-PeCy7 (MIH1)	Mouse (IgG1)	200 FACS (1:10)	BD Biosciences, San Jose, US

2.10.2 Anti-mouse antibodies

Anti-mouse isotype controls

<u>Specificity-Conju- gate (Clone)</u>	<u>Host (Isotype)</u>	<u>Stock in µg/ml</u> <u>Application</u> <u>(Dilution)</u>	<u>Manufacturer</u>
IgG1-APC (G0114F7)	Rat (IgG1)	200 FACS (1:20)	Biolegend, Fell, DE
IgG2a-FITC (RTK2758)	Rat (IgG2a)	500 FACS (1:40; 1:50)	Biolegend, Fell, DE
IgG-PE (HTK888)	Armenian Hamster (IgG)	200 FACS (1:20)	Biolegend, Fell, DE
IgG2b-FITC (RTK4530)	Rat (IgG2b)	500 FACS (1:40)	Biolegend, Fell, DE
IgG2a-Brilliant vio- let 510 (BV510) (RTK2758)	Rat (IgG2a)	100 FACS (1:20)	Biolegend, Fell, DE
IgG2a-PeCy7 (RTK2758)	Rat (IgG2a)	200 FACS (1:40)	Biolegend, Fell, DE
IgG2b-APC (RTK4530)	Rat (IgG2b)	200 FACS (1:5)	Biolegend, Fell, DE

Anti-mouse primary antibodies

<u>Specificity-Conju- gate (Clone)</u>	<u>Host (Isotype)</u>	<u>Stock in µg/ml</u> <u>Application</u> <u>(Dilution)</u>	<u>Manufacturer</u>
CD4-BV510 (RM4-5)	Rat (IgG2a)	80 FACS (1:16)	Biolegend, Fell, DE
CD8a-PeCy7 (53-6.7)	Rat (IgG2a)	200 FACS (1:40)	Biolegend, Fell, DE
CD11c-PE (HL3)	Hamster (IgG ₁ , λ2)	200 ISX (1:5 and 1:10)	BD Biosciences, San Jose, US
CD25-APC (PC61)	Rat (IgG1)	200 FACS (1:20)	Biolegend, Fell, DE
CD40-PeCy7 (3/23)	Rat (IgG2a)	200 FACS (1:5)	Biolegend, Fell, DE
CD44-FITC (IM7)	Rat (IgG2b)	500 FACS (1:40)	Biolegend, Fell, DE
CD62L-FITC (MEL-14)	Rat (IgG2a)	500 FACS (1:40)	Biolegend, Fell, DE
CD69-PE (H1.2F3)	Armenian Hamster (IgG9)	200 FACS (1:20)	Biolegend, Fell, DE
CD80-PE (16-10A1)	Armenian Hamster (IgG)	200 FACS (1:20)	Biolegend, Fell, DE
CD86-FITC (GL-1)	Rat (IgG2a)	500 FACS (1:50)	Biolegend, Fell, DE
H-2K^b bound to SI- INFEKL-PE (25-D1.16)	Mouse (IgG1)	200 FACS (1:20)	Biolegend, Fell, DE

3. Methods

3.1. Cell biological methods

3.1.1 Cell lines

In order to characterize CNP uptake efficiency as well as antigen presentation and effects of CNPs on DCs, the cell line DC2.4 was used. These immortalized murine DC cell line derived from C57BL/6 mice have previously shown to be able to efficiently present exogenous antigens on MHC I (114), thus being a suitable *in vitro* model for investigating the effects of CNPs on DCs. Panc02 and PancOVA cells have been generated from a 3-methyl-cholanthrene induced murine PDAC. The expression of ovalbumin on PancOVA cells allowed us to investigate the efficacy of CNP induced CD8⁺ T cell responses, while Panc02 cells were used as negative control.

3.1.2 Cell thawing and freezing

Initially, cells frozen in liquid nitrogen were thawed by carefully resuspending them in 10 ml prewarmed cell medium, transferring them into 50 ml tubes and centrifuging them for 5 minutes at 300 g. This procedure was repeated once more before seeding the cells in 10 ml medium into 75 cm² cell culture flasks. On the following day, cell medium was renewed. Cells reaching a confluence of at least 80% could be stored long-term in liquid nitrogen by resuspending them in 1 ml FCS supplemented with 10% (v/v) DMSO after detachment and subsequent centrifugation at 300 g. The cells were transferred into a cryo tube and eventually stored in an isopropanol containing cryo box for the first 24 hours at - 80°C before being moved permanently into a liquid nitrogen container at - 180°C.

3.1.3 Cell culture

All cell lines were cultivated in 75 cm² cell culture flasks, filled with 10 ml of the respective cell culture medium. The cells were incubated at 37°C with 5% CO₂ and 85% relative humidity. All cell culture related working steps were executed under sterile conditions, tests for detecting potential mycoplasma contamination were performed in regular intervals. DC2.4 cells, Panc02 cells as well as PancOVA cells were split twice a week in a 1:4 or 1:5 ratio upon reaching at

least 80% density in their respective cell flasks. When cells have reached sufficient density to be split Panc02 and PancOVA cells were first incubated in 5 ml prewarmed Trypsin/EDTA for 5 minutes at 37°C to ensure proper detachment from the flask ground. The serine protease trypsin operates by cleaving peptide bonds on the C-terminal site of either lysine or arginine thus breaking up adhesion bonds. EDTA is a chelator binding Ca^{2+} that is also obligate for cellular adhesion. DC2.4 cells were detached with 5 ml Accutase® solution under the same conditions as described for the other cell lines. Accutase® is a mix of various proteolytic and collagenolytic enzymes, providing a particularly gentle cell detachment. In both cases, 5 ml prewarmed cell medium were added after a few minutes, when the cells were fully detached to stop the proteolytic reaction. Then, cells were transferred into a 50 ml tube and centrifuged for 5 minutes at 300 g. After removing the supernatants and resuspending the cells in 10 ml of their respective cell medium, cells were split in the desired ratio and transferred into new 75 cm² cell culture flasks. For subsequent experiments, cells were seeded into flat-bottom 12-well plates at a defined number per well.

3.1.4 Cell Counting

When precise determination of cell number was required, centrifuged cells were resuspended in a determined volume of cell medium. Then, 10 µl of this suspension were filled into a Neubauer counting chamber. Cells were immediately counted under the light microscope, extrapolating the resulting cell count with the aid of the following formulas:

1. ***Cells/ml = Cells averagely counted in one big square x 10⁴***
2. ***Total cell number = Cells/ml x volume of cell suspension (in ml)***

If a very high, thus uncountable number of cells had been expected in advance, 1:10 dilution was executed by diluting 100 µl cell suspension with 900 µl cell medium. Ten µl of the resulting suspension were again filled into the Neubauer chamber and the calculated total cell number was multiplied with the dilution factor 10. Optionally, trypan blue staining was performed in a 1:10 ratio before counting the cells. Hereby, the number of dead cells was determined by dyeing them blue. In contrast, viable cells with undamaged membranes remain colorless because in these cases, trypan blue cannot enter the cytosol.

3.1.5 Generation of stimulation solution with chitosan nanoparticles

CNPs of standardized sizes were produced through ionic gelation by the working group of Professor Scherließ from the Pharmaceutic Institute of Kiel University according to established protocols (112,118). Both, FITC-conjugated and unconjugated particles decreased marginally in size after encapsulation of OVA and SIINFEKL (OVA 257-264) peptides. Until the CNP powder got in contact with liquids, the nanoparticles were embedded in a mannitol matrix thus forming a nano-in-microparticle structure (NiM). After seeding in flat-bottom 12-well plates, cells were stimulated with CNPs after adherence to the cell culture flasks was verified. First, the nano-in-microparticle powder was resuspended in cell medium. After contact with liquids such as cell medium, the mannitol dissolved, the actual CNPs were therefore liberated. Stimulation of cells was executed by adding 100 µl of the CNP suspension to every well, each containing 1 ml cell medium resulting in a concentration of roughly 100 µg CNPs per ml cell medium.

3.1.6 Isolation of human monocytes

For *in vitro* generation of both macrophages and DCs, monocytes were isolated from thrombocyte-depleted lymphocyte retaining systems (LRS) in a first step. These LRS were delivered from the local blood donation station where it was ensured that only blood from healthy donors came to use. Informed consent was obtained from the donors. The content of one LRS was filled into a 75 cm² cell culture flask then PBS was added until a final volume of 140 ml was reached. In a total of four 50 ml tubes, 35 ml of this suspension were carefully layered onto 15 ml of prepared Pancoll separation solution. These tubes were centrifuged for 25 minutes at 350 g with particular importance on ensuring slow acceleration and deceleration. The effect of this density gradient centrifugation was enhanced by Pancoll solution that contains polysucrose molecules improving erythrocyte aggregation at the bottom of the tube leading to the development of the following cell layers during the centrifugation (**Figure 6**) based on the cells' unequal density.

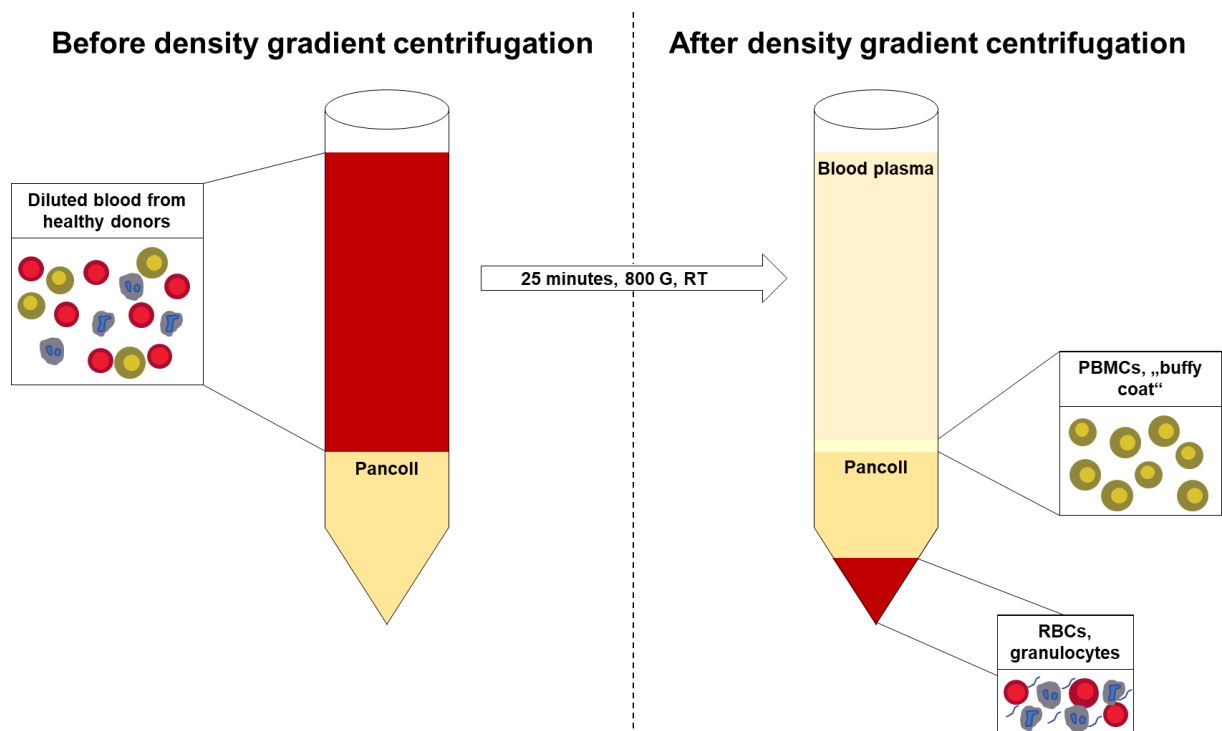


Figure 6: Schematic illustration of cellular separation achieved by Pancoll-supported density gradient centrifugation. After 25 minutes of centrifugation at 350 g erythrocytes (RBCs) and granulocytes aggregate on the tube's bottom while a 'buffy coat' containing PBMCs appears as a thin, white layer right above the pancoll solution. The process is facilitated by polysucrose molecules in Pancoll that contribute to the fixation of RBCs and granulocytes in the cone of the tube.

The supernatant was then aspirated while the so-called 'buffy coat' with lymphocytes and monocytes was collected and transferred to a fresh 50 ml tube, pooling two buffy coats per tube. Next, the cells were washed twice with 20 ml of ice-cold elutriation buffer. Each washing step was followed by centrifugation at 4°C and 300 g for 10 and 7 minutes, respectively. If too many erythrocytes remained in the tube, a brief erythrocyte lysis for 5 minutes was performed in between, that was then followed by an additional centrifugation for 10 minutes under the same conditions. Subsequently, the cells were resuspended in elutriation buffer obtaining 5×10^8 cells per 50 ml and counted with a Neubauer counting chamber before proceeding with counterflow centrifugation elutriation (CCE). CCE is an established method for providing gentle cell separation based on differing cellular sedimentation potential. The cell suspension was pumped into the chamber of a JE-5.0 elutriation rotor while the elutriation centrifuge was already running, thereby containing the cells in the chamber because of the developed centrifugal forces. After the chamber was fully loaded with all utilized peripheral blood

mononuclear cells (PBMC), a constant liquid flow through the pump and a complex tube system was maintained, thus creating a force acting against the centrifugal force generated by the elutriator. The flowrate was slowly being augmented, the balance of power between pump force and centrifugal force was therefore altered. This resulted into pushing more and more cells through the chamber's exit into another tube system where cells could eventually be collected from. More precisely, after extensive washing of the whole system, cells were loaded as soon as the centrifuge obtained a stable rotational speed at 2305 g and 4°C with the pump maintaining a consisting flowrate of 26 ml/min. After PBMC loading was completed, cold elutriation buffer was continuously pumped through the system with the flowrate being augmented up to 41 ml/min during the process. Step by step, cell fractions were collected in 50 ml tubes. At the end, the centrifuge was stopped with the pump still being set at a flowrate of 41 ml/min, hence pushing practically all the remaining cells out of the chamber into 50 ml tubes. Immediately, samples of every fraction were taken and checked for monocyte purity with flow cytometry analyses using the forward and side scatters to validly distinguish monocytes from the smaller and less granulated lymphocytes (**Figure 7**). Monocyte purity of > 90% was required for further use of the respective fractions.

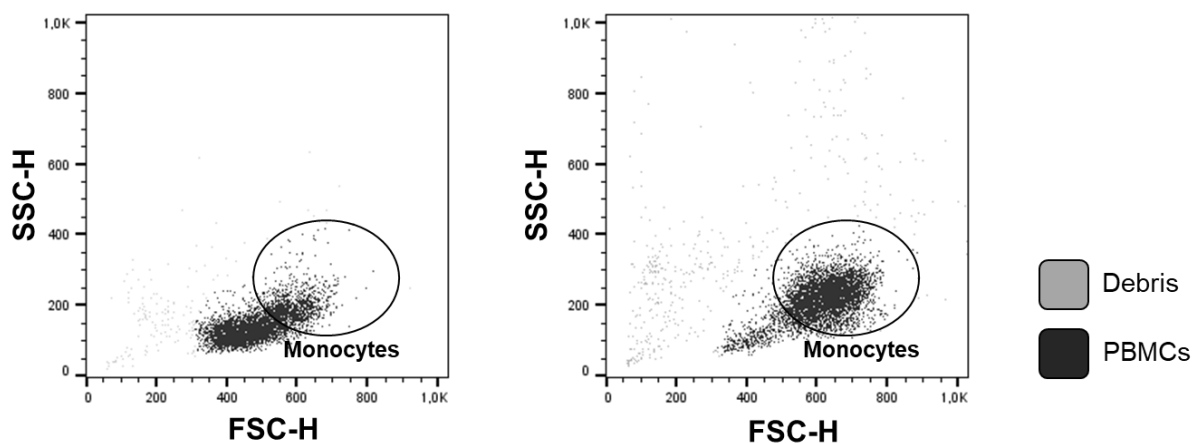


Figure 7: Two representative dot plots of different cell fractions after counterflow centrifugation elutriation. While lymphocytes are the predominant population in the fraction depicted on the left, monocytes account for more than 90% of cells (debris excluded) of the fraction analyzed on the right making this fraction suitable for generation of DCs or macrophages. Thus, CCE provides a reliable method of excluding the smaller, less granulated lymphocytes from the cell suspension from which macrophages and dendritic cells were generated afterwards.

3.1.7 *In vitro* generation of polarized human macrophages and dendritic cells

Macrophages can exhibit a large variety of phenotypes. A model for roughly differentiating those different types of macrophages in *in vitro* studies is the distinction between M1-like and M2-like macrophages (119). In order to generate these two differently polarized macrophage subtypes, the previously isolated fractions containing monocytes with a purity of at least 90% (**see chapter 3.1.6**) were centrifuged at 4°C and 350 g for 10 minutes and pooled thereafter. Then, cells were resuspended in macrophage medium, supplemented with either 10% (v/v) FCS for M1-like macrophages or 1% (v/v) FCS for M2-like macrophages. After counting the monocytes, they were distributed in 50 ml tubes containing between 15 and 20 x 10⁶ cells per tube. Cell culture medium was added up to a volume of 27 ml. For ensuring proper differentiation, 50 ng/ml GM-CSF (for M1-like polarization) or M-CSF (for M2-like polarization) were supplemented according to differentiation strategies that had already been in use in the working group (120,121) as well as elsewhere (122). The content of the tubes was eventually filled into Vue Life culture bags that were incubated for 7 days at 37°C with 5 % CO₂ and 85 % relative humidity (**Figure 8**). For generation of DCs, monocytes were centrifuged and pooled as outlined above and then resuspended in DC culture medium, also supplemented with 10% (v/v) FCS to eventually obtain 1 x 10⁶ cells per ml in a 50 ml tube. This suspension was subsequently seeded into flat-bottom 12-well plates resulting in a concentration of 1 x 10⁶ cells/1 ml/ well. After verified adherence of monocytes, cells were stimulated with 250 U/ml IL-4 and 800 U/ml GM-CSF. This stimulation was repeated after 48 hours, cell differentiation was completed on day 5 (**Figure 8**).

3.1.8 Harvesting of *in vitro* generated human macrophages

After 7 days of differentiation culture, macrophages were harvested and seeded into flat-bottom 12-well plates. For this purpose, the cell-filled Vue Life culture bags were stored on ice for at least 30 minutes. Then, cells were mechanically detached, the culture bags were rinsed with 20 ml PBS to support full detachment. Cells from one bag were transferred into a 50 ml tube and centrifuged for 10 minutes at 300 g. After separately pooling M1-like and M2-like macrophages from the culture bags, cells were gently resuspended in 10 ml of their respective cell medium before a second centrifugation this time with 150 g was performed. Supernatants were afterwards aspirated, macrophages were counted and seeded in the desired density.

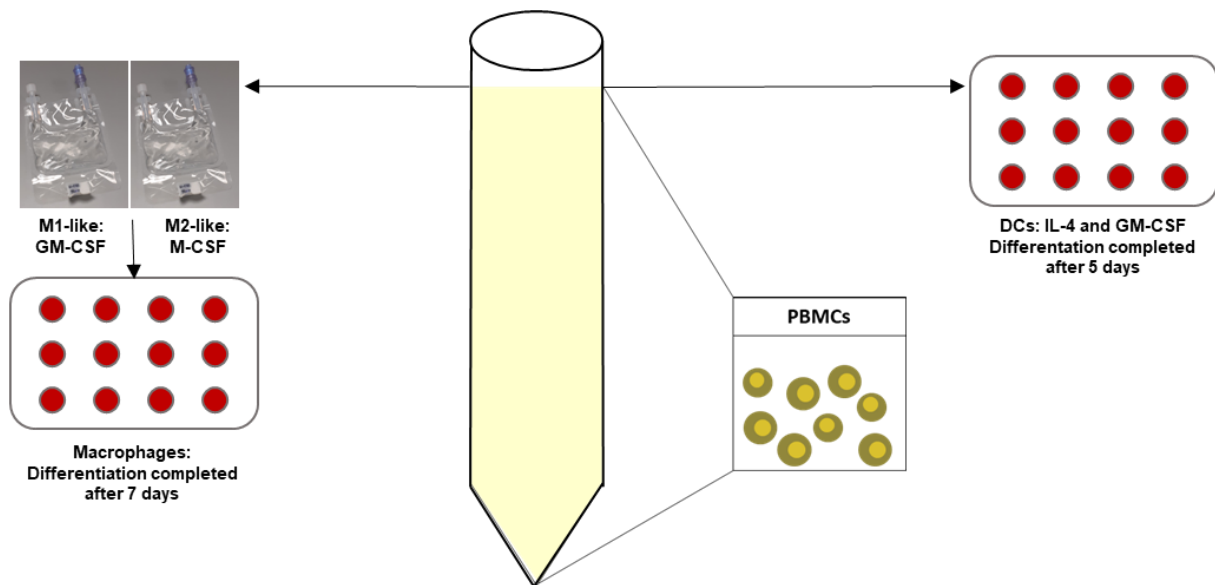


Figure 8: Illustration of the generation of differently polarized macrophages and dendritic cells. Stimulation with GM-CSF and M-CSF, respectively, was only executed on day 1 for generation of M1-like and M2-like macrophages after seven days. GM-CSF and IL-4 were added to the wells on day 1 and day 3 to ensure proper differentiation of monocytes into human DCs after five days.

3.1.9. Isolation of CD8⁺ T cells obtained from OT-1 mice

To make use of CD8⁺ T cells, specifically detecting SIINFEKL in the context of H-2K^b for *in vitro* experiments, OT-1 mice were killed and splenectomised. Then, the explanted spleen was mechanically crushed and filtered twice, first through a 100 µm and hereafter through a 30 µm cell strainer. In a total of 40 ml MACS buffer the cells were centrifuged at 4°C and 300 g for 10 minutes. After an erythrocyte lysis for six minutes with erythrocyte lysis buffer, 40 ml of MACS buffer were added and cells were centrifuged under the identical conditions as before. After a third centrifugation, CD8⁺ T cells were isolated from the splenic cell population by using the MojoSort™ Kit produced by Biolegend according to the manufacturer's protocol. Negative selection was performed, meaning that antibodies against various antigens but not against CD8 were used to mark all cells except the cells of interest. All splenocytes were resuspended in MACS buffer until a concentration of 1x10⁸ cells per ml was obtained. Then, 10 µl of biotin-antibody cocktail were added per each 10⁷ cells. After incubation on ice for 15 minutes and careful vortexing, 10 µl of streptavidin nanobeads were added. After incubating for another 15 minutes 2.5 ml MACS buffer were added to the suspension. Thereafter, the tube containing the cell suspension was placed into a kit-specific magnet for 5 minutes. Then, the liquid was

poured out of the tube with the cells in it being collected most carefully. A second separation, repeating the outlined steps was performed based on the cell count after the first separation. After the magnetic separation, a sample was taken for performing flow cytometric analyses determining CD8⁺ T cell purity (**see chapter 3.2.1**).

3.1.10 Coculture of CD8⁺ T cells with antigen-pulsed DC2.4 cells and assessment of T cell activation markers

The isolated CD8⁺ T cells were counted and added to murine DC2.4 cells to start the coculture. The day before, DC2.4 cells had been seeded into flat-bottom 12-well plates. Five hours before starting the coculture DC2.4 cells were left untreated or stimulated with CNPs or soluble SI-INFEKL peptide (**see chapter 3.1.5**). For initiating the coculture, DC2.4 cells were washed twice with 500 μ l PBS per well before gently detaching them with a cell scraper and centrifuging them for 5 minutes at 300 g. Then, probes of the different DC2.4 cell samples were taken to determine MHC-I mediated presentation of SIINFEKL with flow cytometry (**see chapter 3.2.1 and supplementary figure 1**). Remaining cells were counted and 7.5×10^4 cells per well seeded into flat-bottom 96-well plates. After DC2.4 cells had properly adhered, 2.5×10^5 CD8⁺ T cells were added to each well resulting in a DC: CD8⁺ T cell ratio of 1:3,3. The coculture was stimulated with 50 ng/ml and in later experiments with 150 ng/ml of murine IL-2, a procedure that was repeated after 48 hours. 72 hours after starting the coculture, CD8⁺ T cells were either used for killing assays (**see chapter 3.1.11**) or activation marker expression on CD8⁺ T cells was assessed via flow cytometry (**see chapter 3.2.1**).

3.1.11 Coculturing PancOVA/Panc02 cells with CD8⁺ T cells and subsequent killing assay

After coculture with differently stimulated DCs (**see chapter 3.1.10**), CD8⁺ T cells were used to perform killing assays with PancOVA and Panc02 cells. For this purpose, CD8⁺ T cells were transferred into flat bottom 96-well plates in which PancOVA and Panc02 cells, respectively, had been seeded the day before at a density of 1×10^3 cells per well. 2.5×10^5 CD8⁺ T cells were added to the pancreatic tumor cells. (**Figure 9**). After 24 hours in the incubator or for live cell imaging purposes in the Lionheart™ FX Automated Microscope under identical conditions

with 5% CO₂ and 37°C, killing of the tumor cells was evaluated with the Lionheart™ FX Automated Microscope (see chapter 3.2.4). For this experiment, only CD8⁺ T cells that were stimulated twice with 150 ng/ml mL-2 were used.

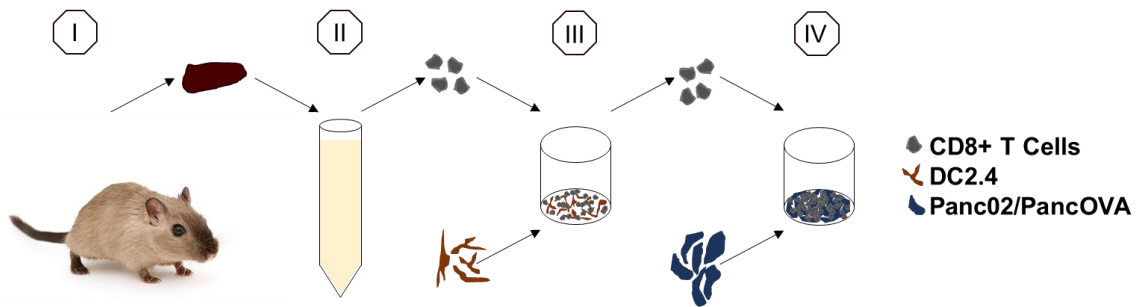


Figure 9: Schematic overview of the CD8⁺ T cell related working steps and the performed coculture assays. After executing splenectomy in OT-1 mice (I), CD8⁺ T cells were isolated (II) and cocultured with stimulated DC2.4 cells for 72 hours (III). Hereafter, activation markers expressed on CD8⁺ T cells were assessed, or CD8⁺ T cells were cocultured for 24 hours with Panc02 or PancOVA cells to assess tumor cell killing (IV).

3.2 Immunobiological methods

3.2.1 Flow cytometry

Flow cytometry is a widespread technique to analyze heterogeneous cell populations on a single-cell basis regarding their size, granularity or the expression of proteins detected either on the cells' surface membrane or intracellularly. The cells get drawn into the measuring chamber of the flow cytometer via overpressure through a thin capillary and are moved into a line due to constantly flowing sheath liquid making it possible for the device to separately measure each cell. Measurement itself occurs after the cells pass a laser beam, which is leading to scattered light and differently high signal intensities on the respective photomultiplier units, acting as signal detectors (Figure 10). These detectors include the forward scatter (FSC), the side scatter (SSC) and fluorescence detectors measuring fluorescence intensities (FI) which is useful if cells are labelled with fluorescence-conjugated antibodies. The FSC measures the scattered light along the laser direction, thus giving information about the cell diameter, while the SSC measures the scattered light in an angle of 90° thereby revealing information about the cellular granularity. A system of mirrors and multiple detectors enables the device to

register and differentiate between emitted light of different wavelength when cells were stained with antibodies conjugated to fluorescent dyes (123).

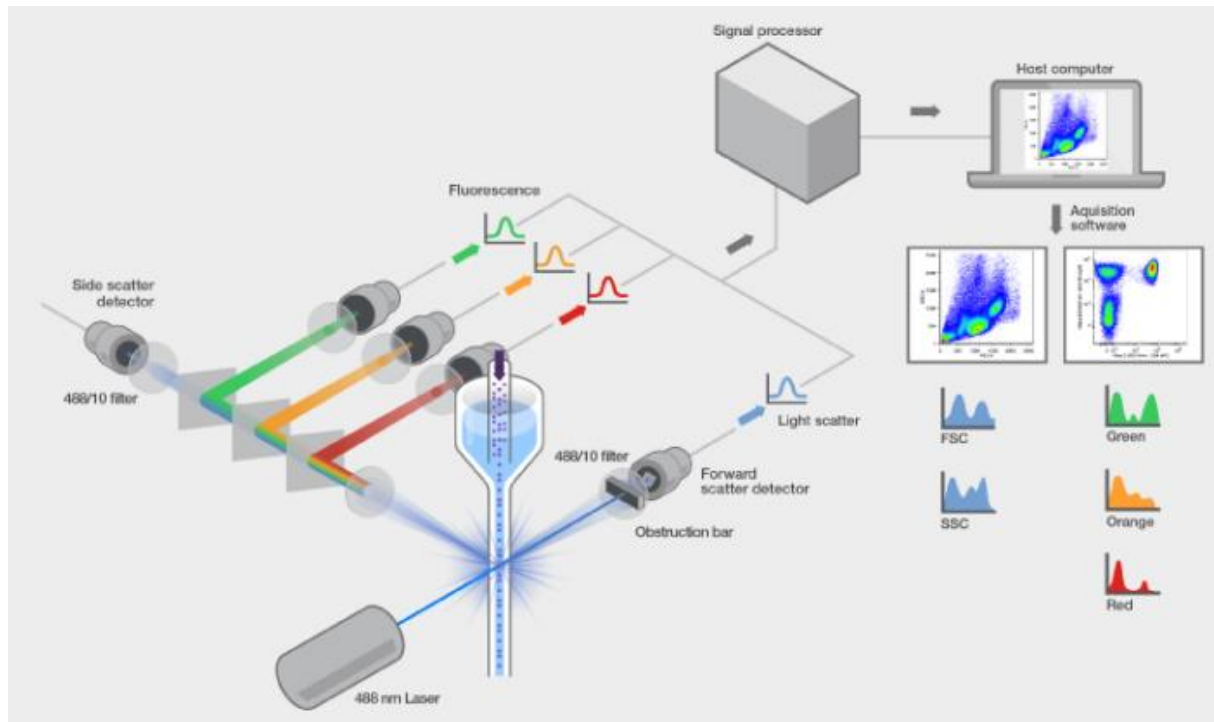


Figure 10: Scheme of a flow cytometer. Figure taken from (124). The employed FACSCalibur had an additional 635 nm red-diode laser with an additional detector implemented.

Flow cytometry was used in this study to determine FITC-CNP uptake, to measure MHC-I mediated SIINFEKL presentation as well as to assess cell phenotype, activation and purity of CD8⁺ T cells. Furthermore, as described before (**see chapter 3.1.5**), after fractionation of PBMCs during monocyte isolation, 100 μ l of each fraction were measured for cell size and granularity. In order to analyze the uptake efficiency of FITC-conjugated CNPs, cells were seeded in 12-well plates 48 hours before measurement (DC2.4 cells, 1.2×10^5 cells per well) or six days before measurement (human DCs (**see chapter 3.1.7**)). After stimulating the cells with CNPs for 24 hours, they were detached from the well plates and washed several times with MACS buffer before preparing measurement. For assessing MHC-I mediated SIINFEKL presentation and also the phenotype of APCs after CNP stimulation, cells were incubated with Fc-blocking reagent, diluted in MACS buffer to a concentration of 1:5 for 10 minutes. This was necessary to prevent unspecific antibody binding after washing and detaching the cells. Then, $1-2 \times 10^5$ cells were stained with 25 μ l staining solution containing fluorochrome-conjugated antibodies

in a V-bottom 96-well plate. Washing steps with ice-cold MACS buffer were executed after detaching the cells from the well plates as well as after treatment with Fc-blocking reagent and twice after staining cells with fluorochrome-conjugated antibodies. Cells were centrifuged for 10 minutes at 300 g after each washing step. For measuring the expression of activation markers on CD8⁺ T cells derived from OT-1 mice and determining their purity after magnetic cell sorting, 50 µl of staining solution were used while the rest of the protocol remained unchanged. All the described working steps were executed either at 4°C or on ice, while particular focus was given to the avoidance of unnecessary light exposure during the process.

3.2.2 ImageStream

Imaging flow cytometry performed with the ImageStream XMark II cytometer was utilized as a precise method to examine FITC-conjugated CNP uptake in various cells and cell lines. Sample preparation was executed as described before (**see chapter 3.2.1**). Cells were washed with PBS, detached with a cell scraper, trypsin or Accutase[®] solution, washed with MACS buffer and - depending on the examined cells - stained with a surface membrane dye. Cells were incubated with staining antibodies for 20 minutes in 50 µl staining solution due to the larger number of cells required for performing these experiments. After two more washing steps with MACS buffer, cells were ready for measurement. Other than determining fluorescence intensities, the ImageStream XMark II cytometer also produced two-dimensional pictures of every cell, thereby allowing to precisely define the cells' membrane with the aid of an analysis mask. As a result, it could be distinguished whether FITC-CNPs were properly internalized or just attached to the outer cellular membrane.

3.2.3 NYONE[®] cell imaging

The NYONE[®] cell imager allowed imaging of cells directly in well plates without needing to detach them and was used to assess cell death of human DCs following CNP stimulation. After human DCs were differentiated and treated with FITC-CNPs for 24 hours, the cell medium was renewed and 1:500 diluted propidium iodide was added. After an incubation time of 15 minutes with strict avoidance of any light at room temperature, measurement of cell morphology and survival was started. Here, the NYONE[®] cell imager generated images and

statistics to accurately demonstrate the effects of different CNPs on the survival and morphology of human DCs.

3.2.4 Imaging with the Lionheart™ FX Automated Microscope

The Lionheart™ FX Automated Microscope enabled us to register cellular activity over the course of time in incubator-like conditions. By employing this method, we tracked CD8⁺ T cell accumulation and activation during coculture with DCs as well as killing of pancreatic tumor cells in the above mentioned cocultures (see chapter 3.1.10 and 3.1.11). During coculture of CD8⁺ T cells and DC2.4 cells, representative images were taken at 20-fold magnification. For assessment of killing of pancreatic tumor cells by CD8⁺ T cells, images were taken at 4-fold magnification and then stitched with the associated Gen5 Data analysis software. From the resulting picture of nearly the entire well, a representative plug of 9000 μm² was selected for quantitative analysis of cellular confluence. The discrimination between cells and cell-free areas was enabled due to differences in phase contrast intensity. For analyzing cellular confluence with the Gen5 software, parameters for setting up the analysis mask were set as follows:

Parameter	Value
Threshold	auto (checked) = 13
Background	light
Split touching objects	checked
Fill holes in the mask	unchecked
Minimal object size	10 μm
Maximal object size	10.000 μm
Include primary edge objects	checked
Analyze entire picture	unchecked
	plug shape = square
	plug size = 3.000 μm x 3.000 μm
Advanced detecting options	
Background flattening	checked
Auto	unchecked

Rolling ball diameter	10 μm
Image smoothing strength	10 cycles
Evaluate background on	0% of lowest pixels
Primary mask	use threshold mask

3.2.5 Caspase 3/7 activity assay

The determination of Caspase 3/7 activity levels provides information about the extent of ongoing apoptosis. Here, using the Caspase-Glo[®] 3/7 assay from Promega, caspase 3/7 activity was investigated in human DCs and macrophages after stimulation with FITC-CNPs in order to quantify possible toxic effects of differently sized CNPs on these cells. Caspase 3/7 activity was checked 24 hours after stimulating DCs, M1-like and M2-like macrophages with FITC-CNPs to obtain the same conditions as used for CNP uptake assays. First, the cell supernatants were transferred into 1.5 ml Eppendorf tubes. Then, cells were carefully detached with a cell scraper in 500 μl PBS per well. The supernatants and the corresponding cells were pooled in an Eppendorf tube which was hereafter centrifuged for 10 minutes at 300 g. Cells were washed with 500 μl PBS and after a second centrifugation under the same conditions eventually resuspended in 500 μl PBS. 25 μl of this suspension were pipetted into a white 96-well microtiter plate along with 25 μl caspase reagent. After an incubation time of 30 minutes at room temperature and in the absence of light, caspase 3/7 activity was determined and quantified using the Tecan Infinite 200 spectrophotometer. The detected bioluminescence is proportional to the caspase 3/7 activity.

3.3 Molecular biological methods

3.3.1 Isolation of nucleic acids

For isolating RNA, the peqGOLD Total RNA Kit from PeqLab was used following the manufacturer's protocol. All working steps were performed at room temperature. Cells were first washed with PBS and then lysed in 300 μl RNA lysis buffer using cell scrapers to detach the cells from the well plates. Afterwards, the lysate was either processed further or stored at -80°C for continuing with the subsequent working steps at a later time. For the former, lysate was transferred into DNA removing columns allowing RNA to pass through while retaining

DNA. The columns were centrifuged for 1 minute at 11000 g before 300 µl of 70% (v/v) ethanol were added to the flow-through. This suspension was transferred into a PerfectBind column that was also centrifuged for 1 minute at 11000 g. Thereafter, the RNA containing column was washed twice first with 500 µl RNA washing buffer I and subsequently with 600 µl RNA washing buffer II. After another centrifugation for 2 minutes at 11000 g, 40 µl RNase-free water were added onto the membrane. In the last step, after incubating the suspension for two minutes and centrifuging it at 8000 g for 1 minute, the eluted RNA was transferred into a 1.5 ml Eppendorf tube. The isolated RNA was stored in a freezer at - 80 °C. To calculate the amount of isolated RNA, probes of every sample were pipetted on NanoQuant plates. For measurement, the Tecan Infinite 200 spectrophotometer was used. The quantification itself is based on the RNA's ability to absorb light in the ultraviolet spectrum. Therefore, the amount of absorbed light can be converted into the amount of nucleic acids making use of the Beer-Lambert law:

$$E = \epsilon \times c \times d$$

This formula equals the attenuation of light (E) with the product of extinction coefficient (ϵ), thickness (d) and concentration (c) of the substrate. A ratio of the wavelengths 260:280 was determined to exclude significant contamination with a desired ratio of around 1.8 to 2.0.

3.3.2 Reverse transcription

For relative quantification of gene expression, the isolated and quantified RNA was transcribed into complementary deoxyribonucleic acid DNA (cDNA). For that purpose, the RevertAid First Strand cDNA Synthesis Kit by Fermentas was used according to the manufacturer's instructions. Between 300 µg and 500 µg of RNA were transcribed by first adding 1 µl Oligo dT primer into the RNA-containing 1.5 ml Eppendorf cup. Then, the volume was adjusted to a total of 11.5 µl with nuclease free water before incubating the mix for 5 minutes at 65 °C. After letting the suspension cool down on ice for a short time, a master mix including reaction buffer, RiboLock RNase inhibitor, deoxynucleoside triphosphate (dNTP) Mix and RevertAid M-MuLV RvT was added (**see table below for the exact volumes of each component**). It was ensured that the suspension was properly mixed before incubating it for 1 hour at 42 °C. The

suspension was finally heated up to 70 °C for 5 minutes before storing the cDNA in a freezer at - 80 °C.

Reagent	Volume per sample
Mastermix for producing complementary DNA (cDNA)	
Reaction buffer (5x)	4 µl
RiboLock RNase inhibitor (20 U/µl)	0.5 µl
10 mM dNTP mix	2 µl
RevertAid M-MuLV RvT (200 U/µl)	1 µl

3.3.3. Quantitative real-time polymerase chain reaction

Quantitative real-time polymerase chain reaction (qPCR) was performed with cDNA (**see chapter 3.3.2**) of DCs to determine phenotypic changes upon CNP stimulation. Initially, cDNA was diluted 1:4 with RNase-free water. For sample preparation, 2.5 µl of the diluted cDNA was pipetted into a white 96-well microtiter plate with each sample being tested twice to achieve more precise results. After this, each well was filled up to a volume of 10 µl with SybrGreen I Mastermix, nuclease free H₂O and the respective primer (**see table below for the exact volumes of each component**). The SybrGreen I Mastermix contains FastStart Taq Polymerase, SYBR Green I dye, dNTPs as well as MgCl₂. In a next step, the microtiter plate was sealed with a translucent foil and centrifuged for 2 minutes at 300 g. The prepared microtiter plate was then inserted into and measured with the LightCycler 480 by Roche. The process of quantitative PCR starts with the initial denaturation of cDNA at 95°C. Then, the sample gets cooled down enabling the respective primers to bind to the single-stranded DNA at their optimal annealing temperature (**see 2.9.1 and 2.9.2**). Next, at the optimal temperature for the Taq DNA polymerase, which is 72°C, DNA gets amplified. This process of DNA denaturation, annealing of primers to the single-stranded DNA and amplification of DNA is constantly being repeated for at least 40 cycles with the temperature being adjusted as described to assure proper denaturation and amplification (**see 2.9.1 and 2.9.2**). In all qPCR experiments, GAPDH was used as housekeeping gene and utilized as a reference for the obtained results of genes of interest. Thus, the respective mean cycle threshold (Ct) values of genes of interest which were

measured in duplicates were compared to the values of GAPDH to calculate the relative gene expression according to the delta-delta Ct method. A melting curve analysis was performed to ensure reaction specificity and exclude any reaction artefacts.

Primers purchased from Eurofins	Primers purchased from Realtime primers	Primers purchased from Biometra
<ul style="list-style-type: none"> ▪ 5 µl Light Cycler SybrGreen I Master ▪ 1 µl primer forward ▪ 1 µl primer reverse ▪ 0.5 µl H₂O 	<ul style="list-style-type: none"> ▪ 5 µl Light Cycler SybrGreen I Master ▪ 1 µl primer ▪ 1.5 µl H₂O 	<ul style="list-style-type: none"> ▪ 5 µl Light Cycler SybrGreen I Master ▪ 0.0375 µl primer forward ▪ 0.0375 µl primer reverse ▪ 2.425 µl H₂O

3.4 Statistical analysis

For statistical analyses, SigmaPlot version 12.5 by Systat was utilized. In a first step, all data were analyzed for normality. For comparison of two sets of data the Student's t-test was applied. One-way analysis of variance (one-way ANOVA) was performed for checking data of multiple, related groups. Data which failed normality testing or equal variance testing was analyzed with the Kruskal-Wallis one-way ANOVA on ranks test. Statistical significance was determined by running the Student-Newman-Keuls or by using Dunn's method. Statistical significance is highlighted, p-values < 0,05 are labelled with an asterisk (*).

3.5 Ethics statement

This research project was carried out in accordance with the World Medical Association's Declaration of Helsinki. Approval was obtained by the ethics committee of the medical faculty at Kiel University (reference number: D490/17). The removal of spleens from OT-1 mice for isolating CD8⁺ T cells was formally declared to the ministry for energy transition, agriculture, environment, nature and digitalization of Schleswig-Holstein (internal test number 1115).

4. Results

4.1 Large chitosan nanoparticles (90/20 and 90/50) but not small ones (90/10) considerably impair viability and morphology of human primary monocytic cells

It has already been demonstrated in previous experiment by our working group that different cell types including human APCs such as DCs, M1- and M2-like macrophages are able to internalize CNPs of various sizes (125). Those uptake assays were conducted with CNPs of three different sizes: 90/10 CNPs with an average diameter of 220 nm, 90/20 (average diameter: 384 nm) and 90/50 CNPs (average diameter: 706 nm). Thus, it was next investigated whether administration of CNPs impacts APCs' cellular viability and/or morphology and whether such effects are related to CNP size. For this purpose, human DCs as well as M1- and M2-like M Φ were stimulated for 24 hours with 100 μ g/ml CNPs of the three mentioned sizes. Hereafter, visible changes in cell density and cell morphology became evident upon light microscopical examination of differently stimulated cells. Especially DCs, but also M Φ pulsed with large CNPs (90/20 and 90/50) presented a loosened cellular layer with less characteristically differentiated cells. Moreover, it was noted that large CNPs seemed to clump together (**Figure 11**). In order to further substantiate these results and to analyze how the reduced cell density could be related to ongoing apoptosis, caspase 3/7 activity was measured after 24 hours of stimulation. Indeed, caspase 3/7 activity in human DCs stimulated with larger, specifically with 90/50 CNPs was drastically elevated. On the other hand, the addition of the smallest CNPs (90/10) to the human primary cells barely went along with an increase in caspase 3/7 activity compared to the untreated control cells (**Figure 12**). In macrophages, differences between the CNP treated samples turned out to be much less pronounced since all treated samples showed markedly elevated caspase 3/7 activity compared to untreated cells and compared to DCs being left untreated or treated with smaller CNPs. Nevertheless, also here 90/10 CNP stimulation led to lower caspase 3/7 activity levels than stimulation with 90/20 or 90/50 CNPs.

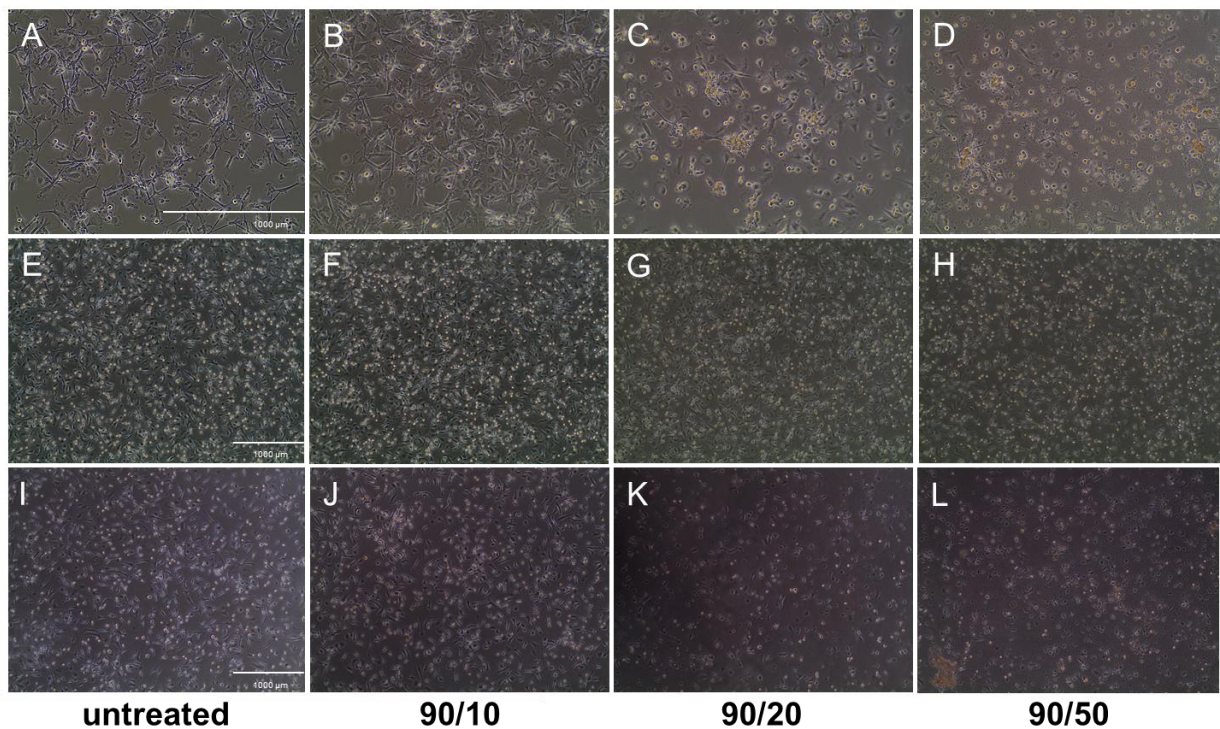


Figure 11: Treatment with large chitosan nanoparticles alters morphology and cellular confluence of human dendritic cells, M1- and M2-like macrophages. Representative images of human DCs (first row; A-D), M1-like macrophages (M Φ) (second row; E-H) and M2-like M Φ (I-L) that were left untreated or were treated for 24 hours with either 90/10, 90/20 or 90/50 CNPs. Brownish colored accumulations (particularly visible in D and L) most likely represent CNPs that had been clumping together during the 24 hours before imaging. Scale bar: 1000 μ m

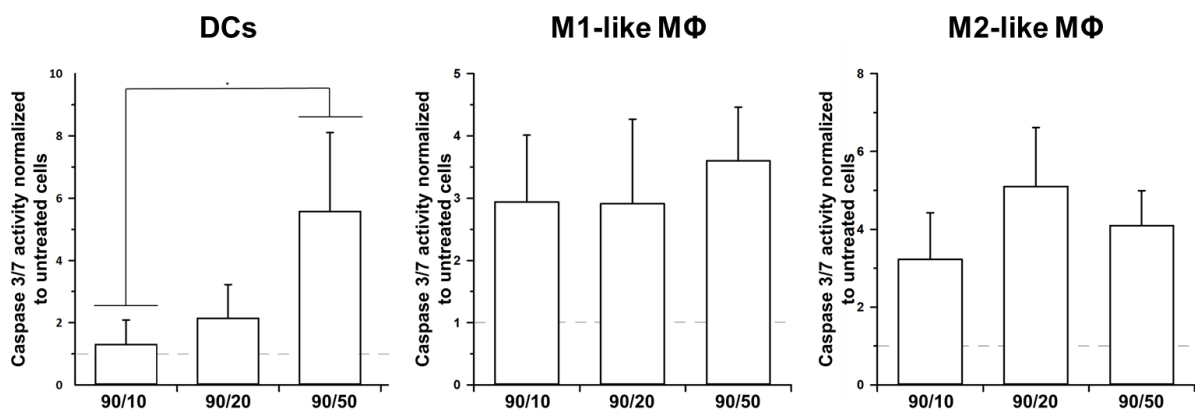


Figure 12: Caspase 3/7 activity level increases after stimulation of human primary monocytic cells with chitosan nanoparticles, in particular with large ones. Human DCs, M1- and M2-like macrophages (M Φ) were stimulated for 24 hours with 90/10, 90/20 or 90/50 CNPs. Data are displayed as n-fold compared to the results in untreated cells. Data for M Φ are shown as mean \pm s.e.m., data for DCs failed the normality test and are shown as median + 75% percentile. Statistical analysis was performed with One-way-ANOVA and subsequent Student-Newman-Keuls-test (M Φ) or Dunn's test (DCs). An asterisk (*) indicates $p < 0.05$; $n = 4$ (DCs), $n = 3$ (M1- and M2-like M Φ).

Since DCs were in the focus of our study, morphology and viability of CNP stimulated human DCs was assessed in more detail by PI staining immediately followed by imaging with the NYOne[®] cell imager. After stimulation with CNPs for 24 hours and PI staining, the cells were examined without having to detach them from the 12-well plates. Based on the pictures (**Figure 13 A**), the NYOne[®]'s analysis software calculated parameters such as cell confluence, PI intensity, which indicated cell death and the percentage of cellularly covered area which was additionally PI positive. In-line with the results of the caspase 3/7 activity assays, reduced cell confluence in wells treated with large CNPs was found, most notably upon treatment with 90/50 CNPs. Moreover, PI positive cell area was larger the bigger the particles were with which the wells had been treated, particularly with respect to the total area covered by DCs (**Figure 13 B**). Furthermore, no considerable differences between samples that were left untreated and those which were stimulated with 90/10 CNPs could be noticed (**Figure 13**).

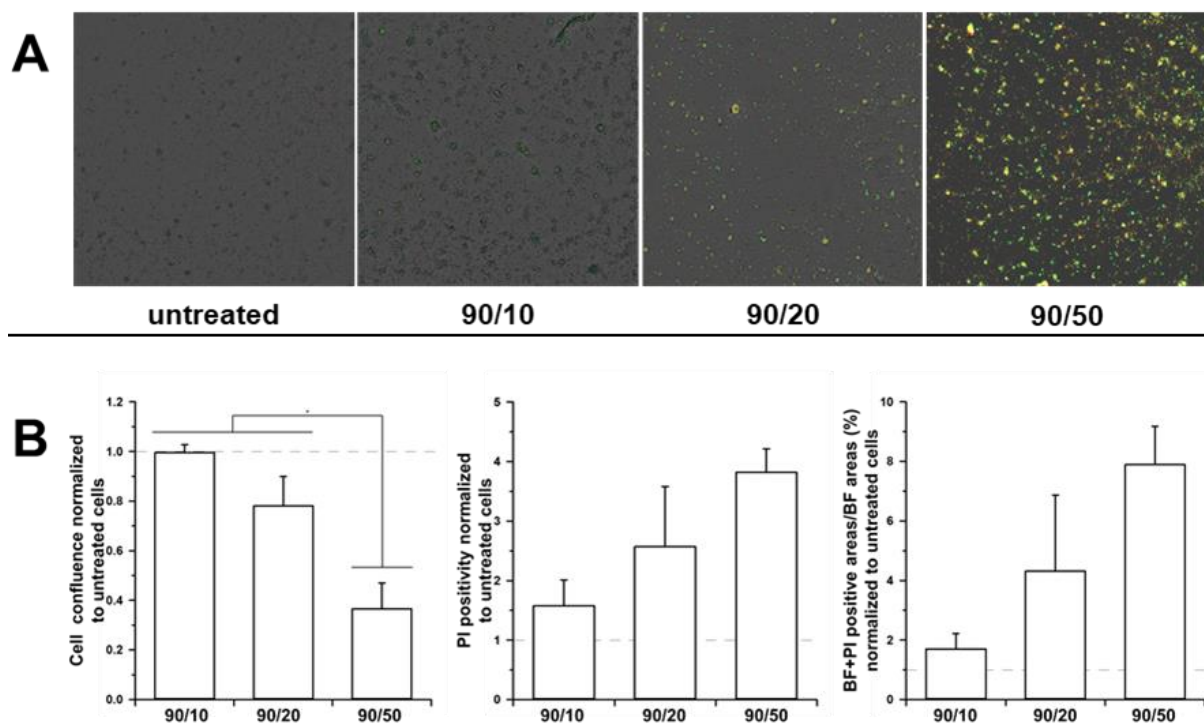


Figure 13: In human dendritic cells, propidium iodide intensity is higher and cell confluence lower, the bigger the diameter of added chitosan nanoparticles. Human DCs were either left untreated or were treated for 24 hours with CNPs of different sizes (90/10, 90/20, 90/50). Representative pictures (A) taken with the NYOne[®] Cell Imager show increased orange PI signal in the samples to which 90/20 and especially 90/50 CNPs were added, while only minimal PI signal is apparent in the untreated well and in cells stimulated with 90/10 CNPs. FITC-conjugated CNPs appear green. Graphs (B) illustrate cell confluence of human DCs, PI intensity as well as a quotient of areas with PI and brightfield signals divided by areas with BF only (n=3). Data are displayed as n-fold compared to the results of untreated cells and are shown as mean

± s.e.m.. Statistical analysis was performed with One-way-ANOVA followed by a Student-Newman-Keuls-test. An asterisk (*) indicates $p < 0.05$. Abbreviations: brightfield (BF), propidium iodide (PI).

Overall, these results indicate that larger CNPs (90/20 and 90/50) promote induction of apoptosis while small CNPs (90/10) do not considerably impair viability of human APCs, in particular of human DCs. Therefore, 90/10 CNPs were chosen for the further experiments.

4.2 Antigen-loaded chitosan nanoparticles are taken up by human and murine dendritic cells

In the next step, it had to be ensured that DCs can effectively internalize CNPs carrying encapsulated antigens. As model antigens, OVA and the OVA-derived peptide SIINFEKL (OVA 257-264) were selected. For uptake assays, CNPs were conjugated with the fluorochrome FITC. Murine DCs of the cell line DC2.4 as well as human DCs were stimulated with FITC-conjugated CNPs (concentration: 100 $\mu\text{g}/\text{ml}$) for 24 hours while untreated cells were used as negative control (not shown in graphs). Hereafter, utilizing the ImageStream XMark II cytometer and the FACScalibur flow cytometer, nanoparticle uptake was examined. Flow cytometry analyses revealed a similar number of FITC-positive cells comparing the two samples treated with either 90/10 SIINFEKL or 90/10 OVA CNPs. The percentage of FITC-positive cells was nearly 100% in human and murine cells treated with 90/10 SIINFEKL CNPs while pulsing cells with 90/10 OVA CNPs also led to nearly 100% FITC-positive murine DCs and only to a slightly lower amount of FITC-positive human DCs (**Figure 14**).

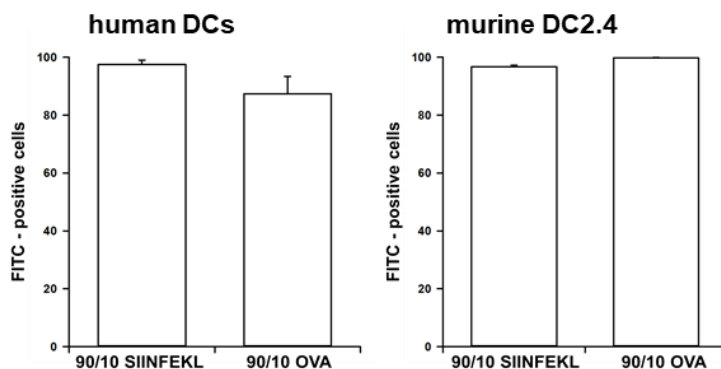


Figure 14: Stimulation with FITC-conjugated chitosan nanoparticles loaded with SIINFEKL or OVA leads to similar percentages of FITC-positive dendritic cells. Human and murine DCs ($n=3$ each) were stimulated for 24 hours with FITC-conjugated, antigen-loaded CNPs and analyzed by flow cytometry. Data are shown as mean \pm s.e.m..

By combining flow cytometry with microscopic imaging, the ImageStream XMark II cytometer analysis allows to distinguish between cells that properly internalized FITC-CNPs and those where FITC-CNPs remained tightly attached to the outside of the cell membrane even after extensive washing (**Figure 15 A**). Therefore, ImageStream based examination is a more precise method for assessing CNP uptake efficiency. For defining cellular borders, membrane staining could optionally be performed. However, no relevant differences were found comparing analyses based on membrane staining with CD11c-APC or brightfield images (unpublished data of this working group). As a result of the more accurate measurement, the number of FITC-positive cells was lower in ISX than in FACS analyses. ISX analysis revealed that 90/10 CNPs were internalized by murine and human DCs but some CNPs seemed to attach to the cellular membrane (**Figure 15 B**). Interestingly, the murine DC2.4 cells showed much higher uptake rates than human DCs (murine DC2.4 cells: 75% versus human DCs: 25%). However, overall uptake of antigen-loaded 90/10 OVA and 90/10 SIINFEKL CNPs in murine and human DCs could be clearly confirmed.

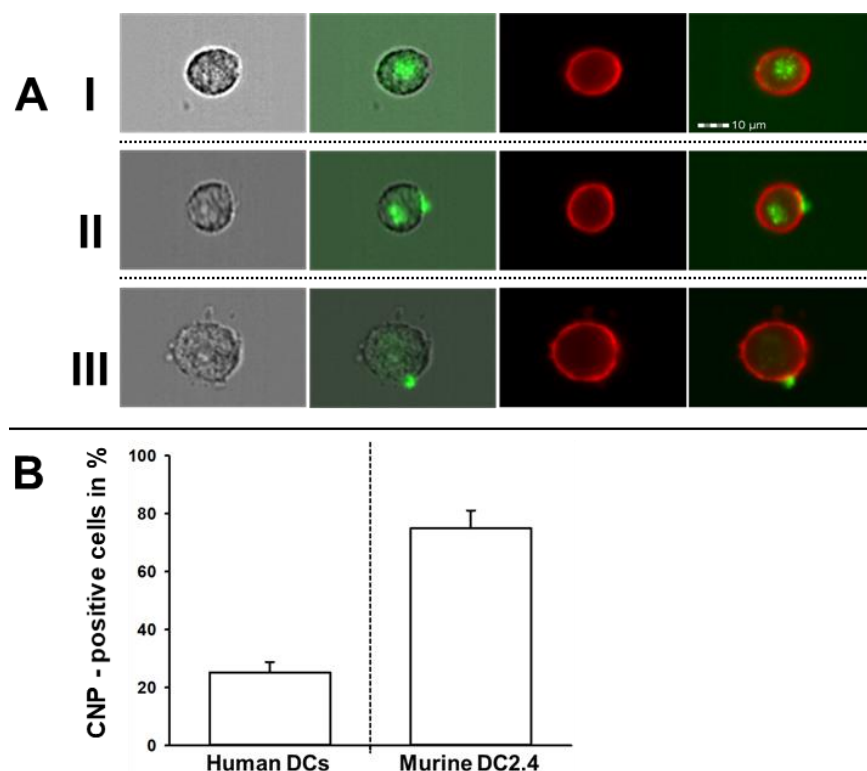


Figure 15: Internalization of ovalbumin-loaded FITC-conjugated chitosan nanoparticles in murine and human DCs is confirmed by ImageStream analyses. Human and murine DCs were stimulated for 24 hours with FITC-conjugated, OVA-loaded CNPs, and then analyzed via imaging flow cytometry with the ImageStream XMark II. (A) The human DCs in I and II have

internalized FITC-labelled nanoparticles as the green fluorescence signal is detectable inside the cellular borders. In cell II, green fluorescence is also present at the outer cell membrane. The human DC presented in III did not internalize FITC-CNPs as the fluorescing material is only attached to the outside of its cell membrane and was therefore identified as a non-internalizing cell. Images display the signal of the following channels from left to right: brightfield, brightfield and FITC, CD11c-APC, FITC and CD11c-APC. The graph below (B) illustrates 90/10 OVA CNP internalization in human and murine DCs each measured in three independent experiments based on cellular borders as defined by brightfield data.

4.3 Antigen-loaded 90/10 chitosan nanoparticles barely affect viability and morphology of human dendritic cells

Having shown that empty CNPs do not harm DCs, we wanted to verify that also antigen-loaded 90/10 CNPs do not impair viability of DCs. For this purpose, effects of 90/10 OVA and 90/10 SIINFEKL CNPs on human DCs were evaluated after 24 hours of CNP stimulation. Morphologically, treatment of 90/10 OVA or 90/10 SIINFEKL did not seem to impair human DCs when comparing with the untreated control cells (**light microscopical images in supplementary figure 2**). In-line with these observations, cell confluence, PI positivity and percentage of PI positive areas were not significantly elevated compared to untreated control cells (**Figure 16 A/B**). Furthermore, caspase 3/7 activity in cells treated with 90/10 OVA or 90/10 SIINFEKL CNPs was not noteworthy increased compared to the untreated control (**Figure 16 B**). These data indicate that also antigen loaded 90/10 CNPs do not impair morphology and viability of human DCs.

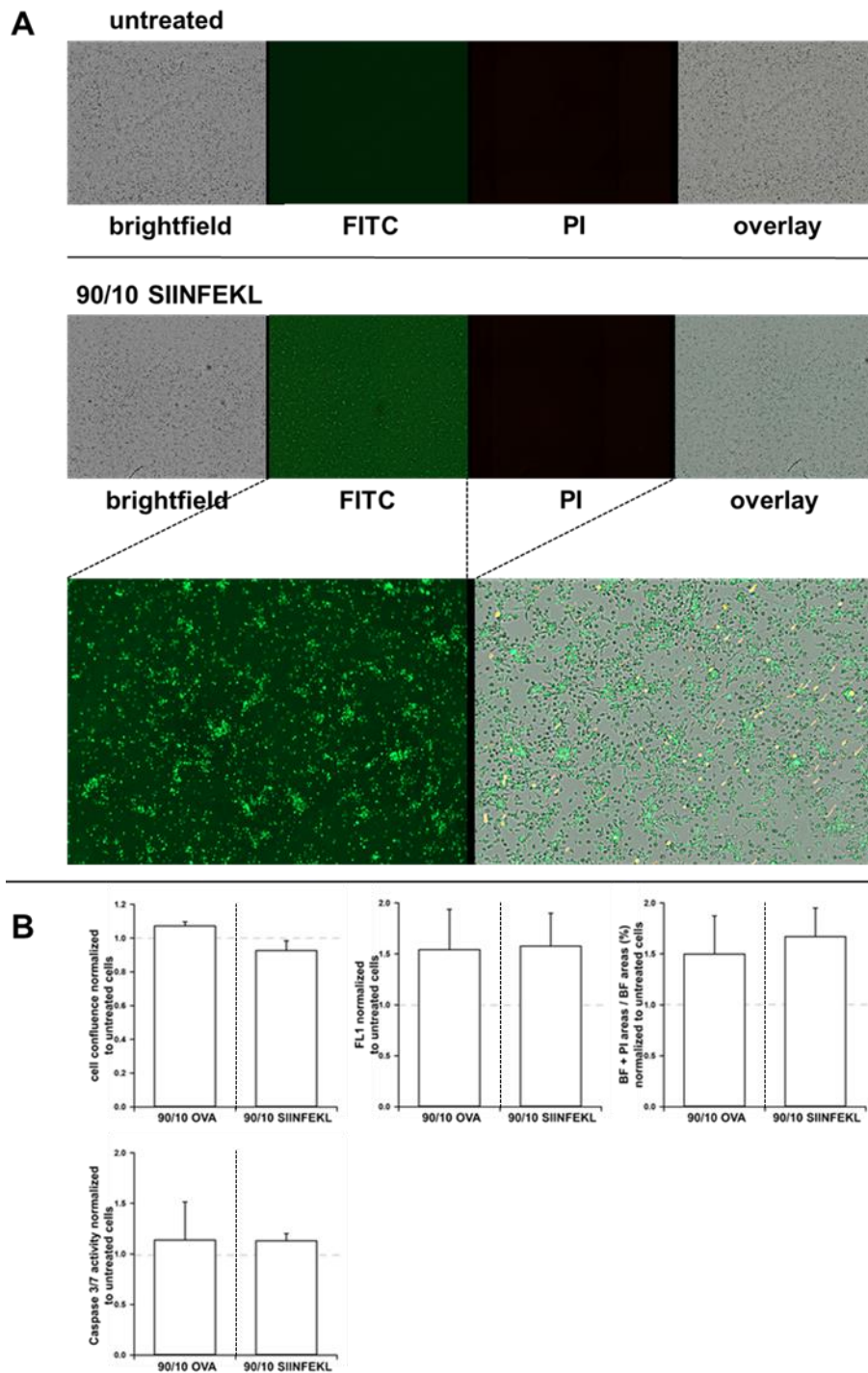


Figure 16: Antigen-loaded 90/10 chitosan nanoparticles do not impair the viability of human dendritic cells. Human DCs were treated for 24 hours with SIINFEKL and OVA- loaded 90/10 CNPs before NYOne® imaging and measurement of caspase 3/7 activity were performed. Representative pictures of untreated and 90/10 SIINFEKL CNP-treated cells (A) demonstrate that there is barely any PI signal detectable in cells stimulated with antigen-loaded 90/10 SIINFEKL CNPs. Green fluorescence indicates the presence of FITC-labelled 90/10 SIINFEKL CNPs in the pictures seen at the bottom row. Graphs (B) display cell confluence, PI positivity and the proportion of cell-covered area that is also PI positive as obtained with the NYOne® imager as well as n-fold caspase 3/7 activity compared to untreated cells for assessing cell viability (N=3). Data are displayed as n-fold compared to the results in untreated cells and are shown as mean

± s.e.m.. Abbreviations: brightfield (BF), fluorescence channel 1/PI channel (FL1), propidium iodide (PI).

4.4 Stimulation with chitosan nanoparticles causes phenotypic changes in human and in murine dendritic cells

4.4.1 Surface marker expression in human dendritic cells is barely affected by treatment with chitosan nanoparticles

To assess effects of unloaded and antigen-loaded 90/10 CNPs on the phenotypic characteristics of human DCs, expression of surface marker molecules involved in effector function or maturation of differentiated DCs was measured in human primary DCs with flow cytometry. Five hours, 24 hours as well as 48 hours after administration of 100 µg/ml CNPs (empty 90/10 CNPs, 90/10 SIINFEKL or 90/10 OVA CNPs) expression levels of PD-L1, CD80, CD86 and HLA-DR were quantified. Compared to empty CNPs, the treatment with antigen-loaded CNPs led to slightly increased expression of the costimulatory molecules CD80 and CD86 (**Figure 17**). Aside from that, the expression of HLA-DR minimally decreased over time in samples stimulated with antigen-loaded CNPs while the opposite effect was registered following treatment with unloaded CNPs. However, these described surface marker expression changes were only small and not statistically significant with the exception of alterations in CD80 and CD86 expression after 48 hours of CNP treatment compared in 90/10 vs. 90/10 OVA and 90/10 SIINFEKL vs. 90/10 OVA samples, respectively. Similar results were obtained after measurement of PD-L1 surface marker expression, with mostly minor changes apart from a statistically significant increase in expression level registered in the 90/10 OVA treated cells after 24 hours compared to the cells after 5 hours of the same CNP treatment and after 24 hours in cells treated with empty 90/10 and 90/10 OVA CNPs, respectively. To summarize, stimulation of human DCs with 90/10 CNPs either unloaded or carrying encapsulated antigens did hardly change expression patterns of surface markers compared to untreated human DCs.

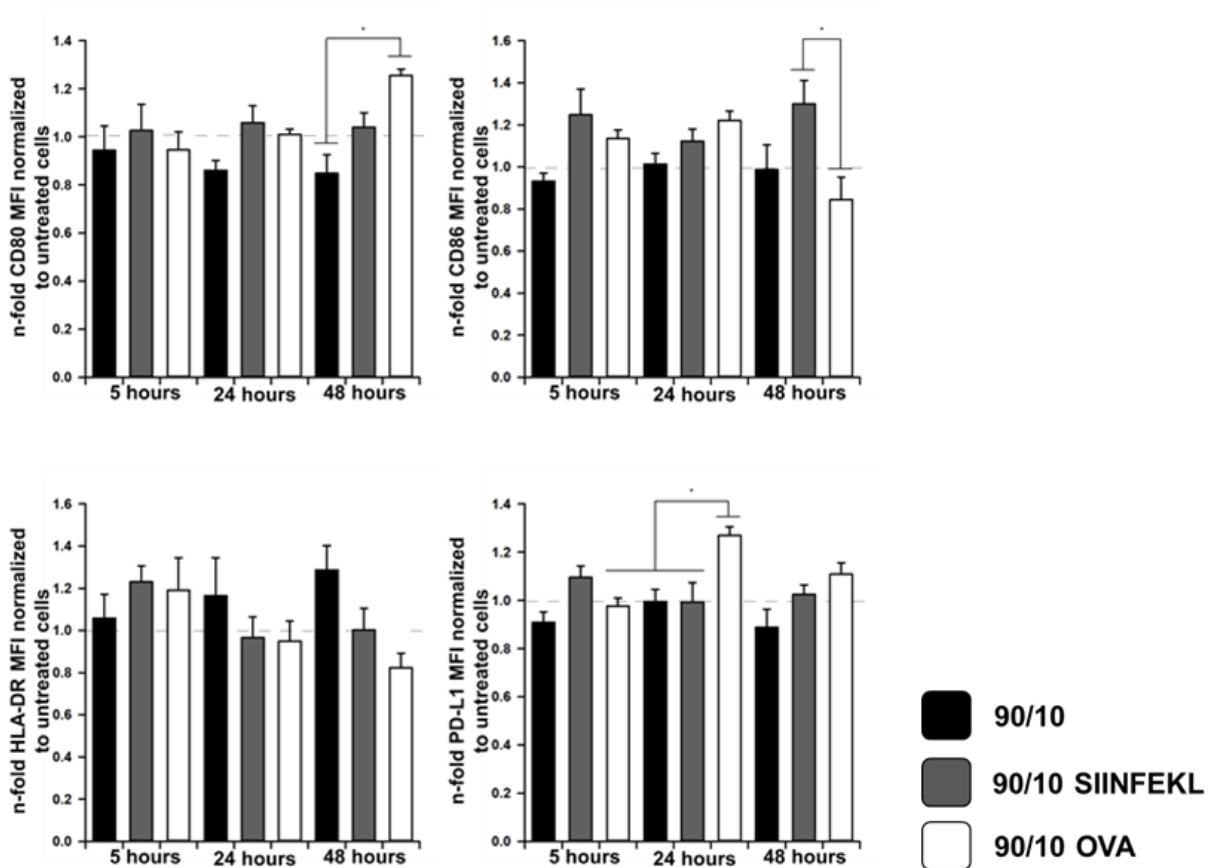


Figure 17: 90/10 chitosan nanoparticles, with or without an encapsulated antigen hardly cause changes in CD80, CD86, HLA-DR and PD-L1 expression on human dendritic cells. Human DCs were left untreated or treated for 5, 24 or 48 hours with the indicated CNPs before expression levels of the four surface markers were analyzed utilizing flow cytometry. MFI of each marker obtained in CNP treated cells was normalized to the measured MFI of the same marker in untreated cells. Data (n=3) are displayed as mean \pm s.e.m.. Statistical analysis was performed with One-way-ANOVA and a subsequent Student-Newman-Keuls-test. An asterisk (*) indicates $p < 0.05$.

4.4.2 RNA analysis of human dendritic cells shows significant proinflammatory phenotypic changes after stimulation with antigen-loaded chitosan nanoparticles

Additionally to the performed experiments assessing surface marker expression, analyses regarding cytokine expression in human DCs were performed in order to find out whether CNP administration leads to phenotypic changes of the expression level of inflammatory mediators. For this purpose, RNA of unstimulated and CNP stimulated human DCs was isolated, converted to cDNA and finally examined by qPCR. Evident and statistically significant differences between the different samples could be noted: While RNA expression levels of the antiinflammatory cytokines IL-10 and TGF- β 1 remained relatively constant besides a detectable TGF- β 1 decrease in 90/10 OVA treated cells after 24 and 48 hours, the RNA expression levels of proinflammatory cytokines clearly varied after the different treatments at the respective timepoints (**Figure 18**). Particularly in cells that were treated with CNPs for only 5 hours, levels of IL-1 β , IL-6 and TNF- α increased up to 100-fold compared to the corresponding expression levels in untreated cells. In general, the administration of 90/10 OVA and 90/10 SIINFEKL CNPs caused more pronounced increasing effects on the expression levels of these proinflammatory cytokines than stimulation with empty 90/10 CNPs. Comparing 90/10 SIINFEKL CNP treated cells with cells treated with 90/10 OVA CNPs, TNF- α expression showed a notably more intense response upon 90/10 SIINFEKL CNP stimulation, whereas the increase of IL-1 β and IL-6 expression was clearer after treatment with 90/10 OVA CNPs. Additionally, it could be noted that these elevations mostly peaked in intensity after 5 hours with the exception of TNF- α whose expression level peaked after 24 hours. Forty-eight hours after stimulation, expression levels had normalized again to levels similar to - or decreased even below - the corresponding levels in the untreated cells. Taken together, these results suggest that antigen-loaded 90/10 CNPs do have a significant effect on human DCs by promoting expression of proinflammatory cytokines within the first 24 hours after stimulation.

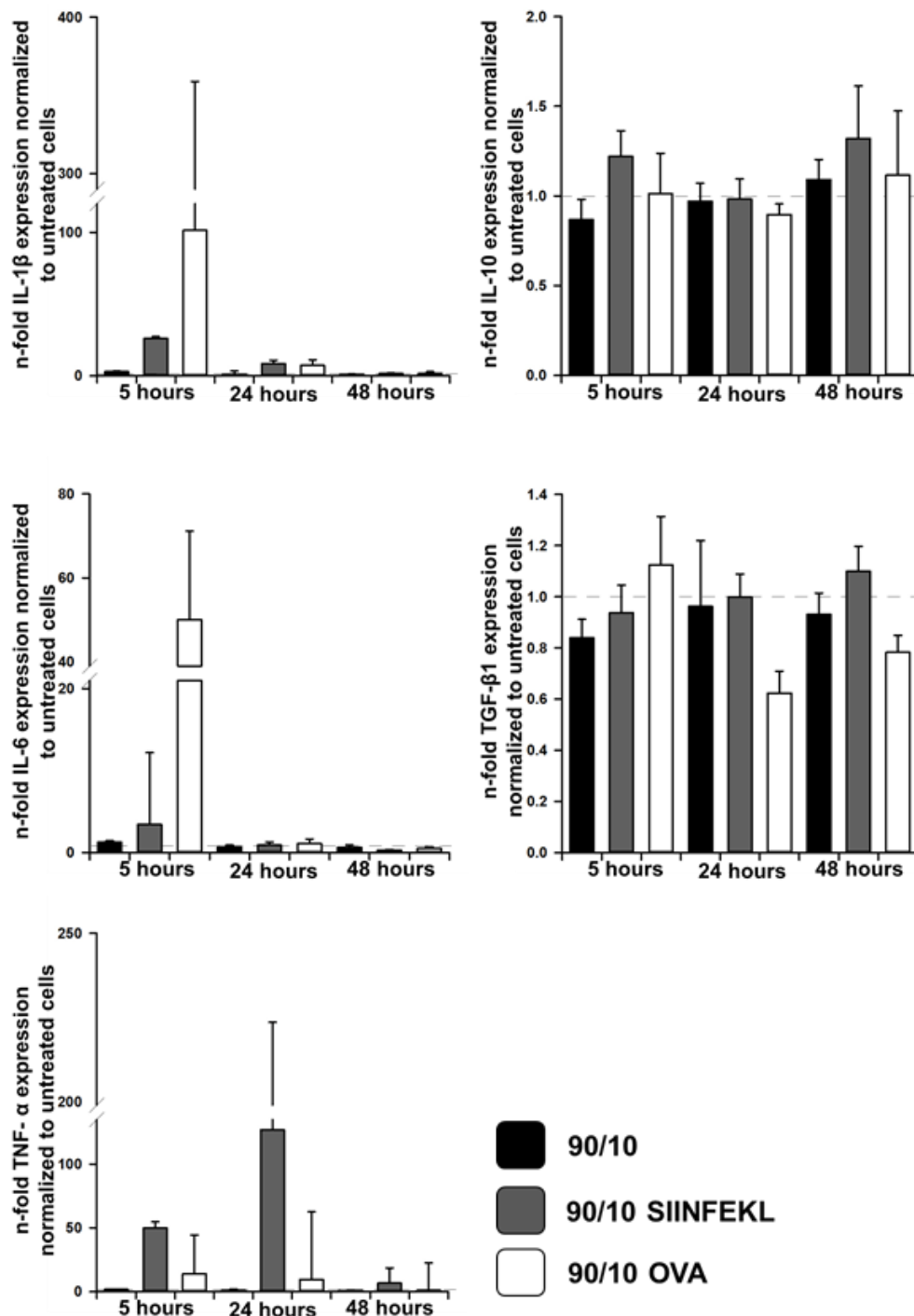


Figure 18: Human dendritic cells exhibit a more proinflammatory phenotype after stimulation with antigen-loaded chitosan nanoparticles. Human DCs were left untreated or were treated for 5, 24 or 48 hours with the respective CNPs before isolating RNA and performing qPCR for subsequently assessing expression of the cytokines IL-1 β , IL-6, IL-10 TGF- β 1, TNF- α . For analyses, expression of genes of interest were normalized to expression of the housekeeping gene GAPDH. Expression levels of treated cells were then normalized to those of untreated cells and are displayed as n-fold gene expression. Data for IL-1 β , IL-6 and TNF- α (n=3) are shown as median \pm 75% percentile since normality tests failed. Data for IL-10 and TGF- β 1 are shown as mean \pm s.e.m. Statistical analysis was performed with One-way-ANOVA and a subsequent Student-Newman-Keuls-test or a Dunn's test for data that failed normality testing.

4.4.3 Murine dendritic cells exhibit a more proinflammatory phenotype after stimulation with antigen-loaded chitosan nanoparticles

The results on RNA level obtained in human DCs led us to investigate how CNPs impact murine DC2.4 cells that were planned for being used in future experiments. Similar to human DCs, antigen-loaded CNPs caused a more pronounced elevation of RNA expression of proinflammatory cytokines (mIL-1 β , mIL-6, mTNF- α) than unloaded CNPs (**Figure 19**). Moreover, compared to untreated cells, the addition of CNPs of either kind led to a more proinflammatory phenotype. Levels of mTNF- α , mIL-6 and to lesser extent mIL-1 β constantly increased over time in cells stimulated with 90/10 SIINFEKL CNPs whereas the expression peak in human DCs was mostly reached after 5 hours of treatment. Even though the increasing effect of antigen-loaded CNPs on expression of proinflammatory cytokines was not as drastic as in human DCs, a more pronounced proinflammatory phenotype could also be registered in murine DC2.4 cells after stimulation with CNPs.

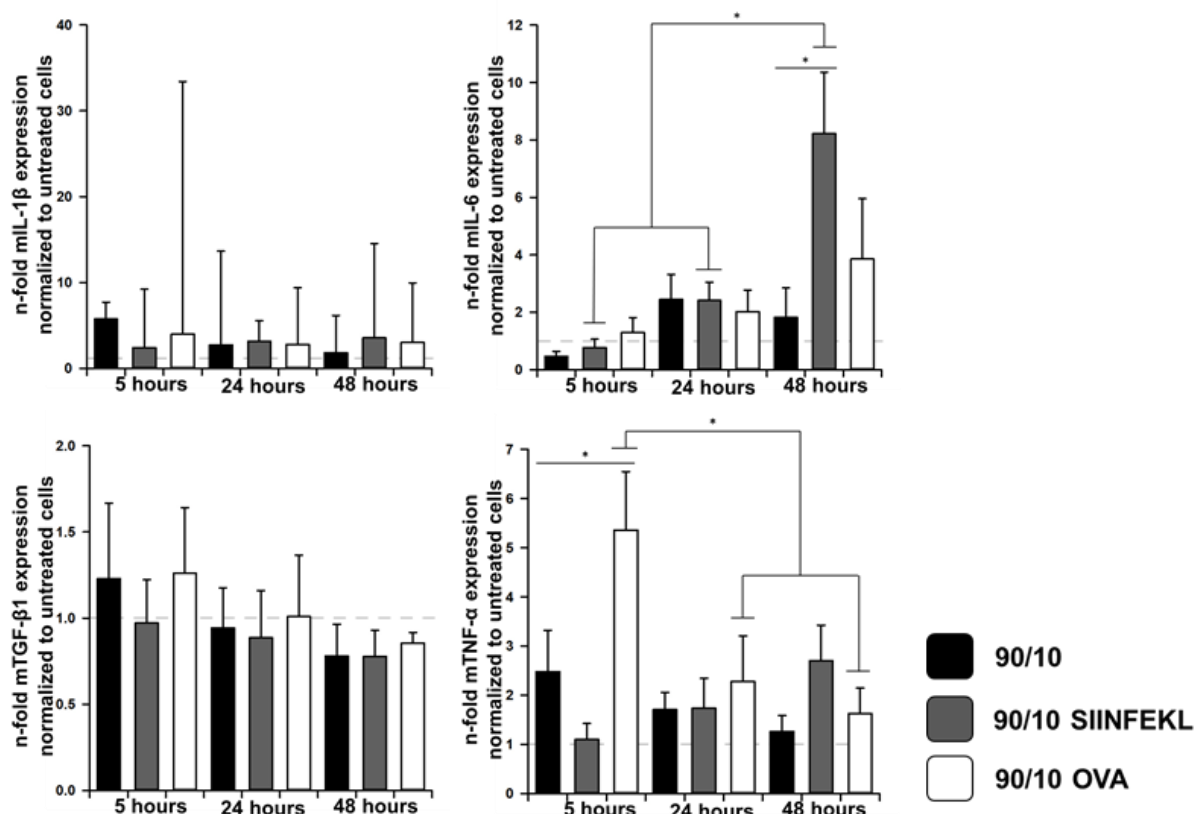


Figure 19: Murine DC2.4 cells display a more proinflammatory phenotype after stimulation with chitosan nanoparticles. Murine DC2.4 cells were left untreated or treated for 5, 24 or 48

hours with the respective CNPs before isolating RNA and performing qPCR for assessing expression of the cytokines mL-1 β , mL-6, mTGF- β 1, mTNF- α . For analyses, expression of genes of interest were normalized to expression of the housekeeping gene GAPDH. Expression levels of treated cells were then normalized to those of untreated cells and are expressed as n-fold gene expression. Data (n=3) for mL-1 β are shown as median \pm 75% percentile since normality tests were failed. Data for the other cytokines (mTGF- β 1, mL-6, mTNF- α) are shown as mean \pm s.e.m.. Statistical analysis was performed with One-way-ANOVA and a subsequent Student-Newman-Keuls-test or Dunn's test for data for mL-1 β . An asterisk (*) indicates p<0.05.

4.5 MHC-I mediated presentation of SIINFEKL can hardly be detected after treatment of DC2.4 cells with 90/10 OVA chitosan nanoparticles

After having evaluated uptake efficiency as well as cell viability and phenotype-related effects of antigen-loaded CNPs, we wanted to clarify whether uptake of these CNPs leads to presentation of the encapsulated antigen via MHC-I by DCs through the process of cross-presentation (53,56,114). For this purpose, murine DC2.4 cells were first stimulated with 100 μ g/ml 90/10 OVA CNPs. Five and 24 hours after CNP stimulation, cells were stained with a PE-conjugated anti-mouse H-2K^b bound to SIINFEKL antibody (clone: 25-D1.16) and analyzed by flow cytometry. Treatment with 90/10 OVA CNPs did only cause a minimal but statistically significant change in MFI compared to the isotype control but only in samples treated for 5 hours. After 24 hours of treatment, no significant change in MFI could be observed (data not shown) (**Figure 20**). Further experiments with DC2.4 cells treated with soluble OVA (concentration: 1 μ g/ml) did also not lead to relevantly increased SIINFEKL presentation by DCs (**Supplementary figure 3**).

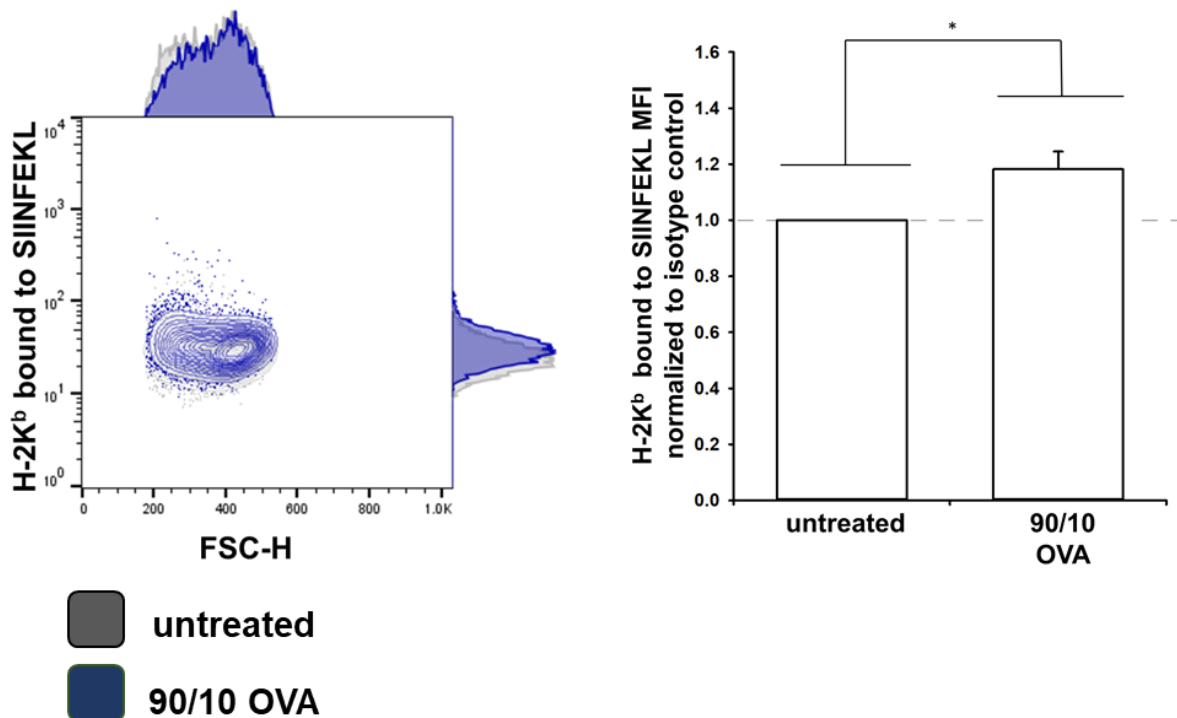


Figure 20: Murine DC2.4 cells hardly present SIINFEKL via MHC-I after treatment with 90/10 OVA chitosan nanoparticles. DC2.4 cells were left untreated or treated with 90/10 OVA CNPs for 5 hours and then analyzed for H-2K^b mediated expression of SIINFEKL. The graph shows MFI determined of the antibody detecting SIINFEKL bound to H-2K^b normalized to the isotype control as determined by flow cytometry (n=4). The displayed dot plot is chosen as a representative image, data on the right side are shown as mean ± s.e.m.. Statistical analysis was performed with One-way-ANOVA on ranks and subsequently with Dunn's method. An asterisk (*) indicates p<0.05.

4.6 90/10 OVA stimulation of DC2.4 cells leads to modest but detectable activation of CD8⁺ T cells

Even though MHC-I mediated SIINFEKL presentation on DC2.4 cells stimulated with 90/10 OVA CNPs was only modest, T cell activation marker expression was assessed on CD8⁺ T cells which had been cocultured with DC2.4 cells pretreated with 90/10 OVA CNPs. CD8⁺ T cells, isolated from OT-1 mice using the MojoSort™ kit by Biolegend, are equipped with a transgenic T cell receptor recognizing SIINFEKL if presented in the context of H-2K^b. Performing negative selection led to isolation of CD8⁺ T cells with a purity of at least 90% (**Figure 21 A**). DC2.4 cells were left untreated or were stimulated with 90/10 OVA CNPs 5 hours before CD8⁺ T cells were added. The results of flow cytometric examination of the cocultivated CD8⁺ T cells showed partial positivity for CD8⁺ T cell activation marker expression which was slightly more

pronounced for CD69 than for CD25 (**Figure 21 B/C**). In two independently performed experiments an upregulation of CD69 and CD25 on CD8⁺ T cells could be detected. A noteworthy number of CD8⁺ T cells could consequently be labelled as double-positive, displaying increased activation marker expression for CD69 as well as for CD25 (**Figure 21 C**).

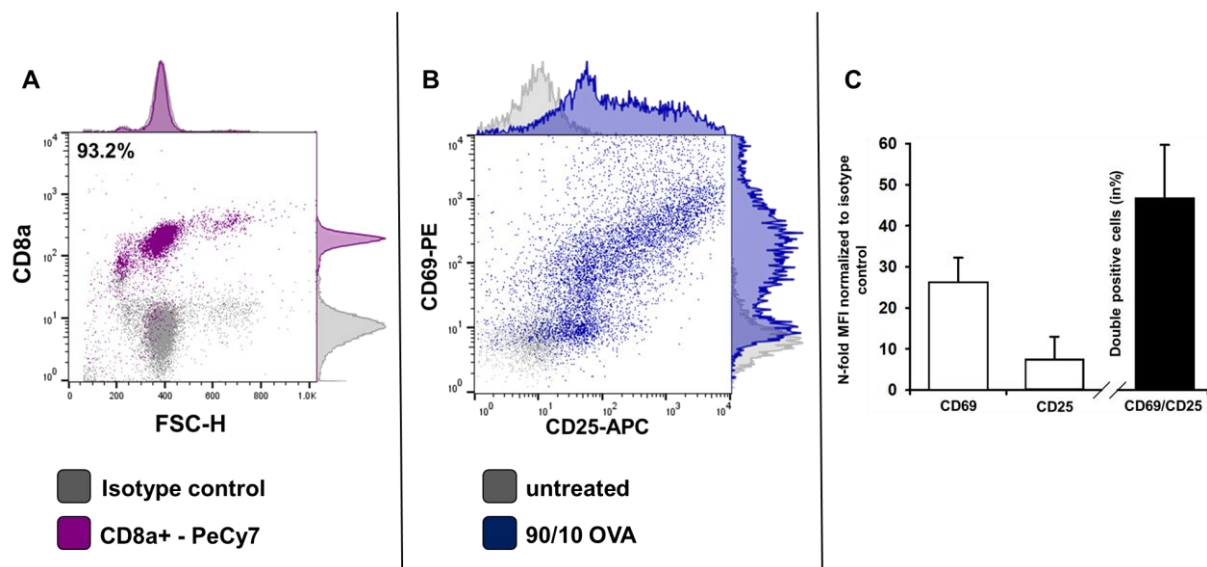


Figure 21: Treatment of DC2.4 cells with 90/10 OVA chitosan nanoparticles leads to activation of CD8⁺ T cells. A representative dot plot (A) shows high purity above 90% after isolation of CD8⁺ T cells from spleens of OT-1 mice. Activation markers CD69 and CD25 after coculture with untreated or 90/10 OVA CNP stimulated DC2.4 cells were assessed by flow cytometry on CD8⁺ T cells. The representative dot plot (B) shows positivity of activation markers CD69 and CD25. Graph (C) shows MFI normalized to the 90/10 OVA treated isotype control and the amount of CD69-CD25 double-positive cells (n=2). Data are shown as mean \pm s.e.m..

4.7 Treatment of DC2.4 cells with 90/10 SIINFEKL leads to pronounced MHC-I mediated SIINFEKL presentation

Having shown that 90/10 OVA CNPs and soluble OVA led only to minor SIINFEKL expression on DC2.4 cells and subsequently mild CD8⁺ T cell activation, 90/10 SIINFEKL CNPs were tested in order to find out whether MHC-I mediated SIINFEKL presentation on DC2.4 cells can be increased. For this purpose, DC2.4 cells were left untreated or treated for 1, 3, 5 and 24 hours, respectively, with 90/10 SIINFEKL CNPs, empty 90/10 CNPs or with soluble SIINFEKL peptide (concentration: 1 μ g/ml) which was used as positive control. Using flow cytometry, a statistically significant increase of the MFI of detectable SIINFEKL bound to H-2K^b in DC2.4 cells treated with 90/10 SIINFEKL CNPs could be noticed compared to the untreated control cells

(Figure 22 A). This increase was most pronounced after 5 hours of CNP treatment (Figure 22 B). However, the measured MFI of the 90/10 SIINFEKL CNP treated cells was still considerably lower than the MFI of DC2.4 cells stimulated with soluble SIINFEKL peptide but significantly higher than in cells stimulated with empty 90/10 CNPs (Figure 22 C and D). Since the utilized antibody is highly specific binding exclusively to H-2K^b molecules that present SIINFEKL, the increase of MFI after treatment of DC2.4 cells with 90/10 SIINFEKL CNPs showed that the encapsulated SIINFEKL peptide had to be liberated and presented by DC2.4 cells via MHC-I. Based on these experiments, a treatment duration of 5 hours was identified as optimal CNP stimulation time for future experiments.

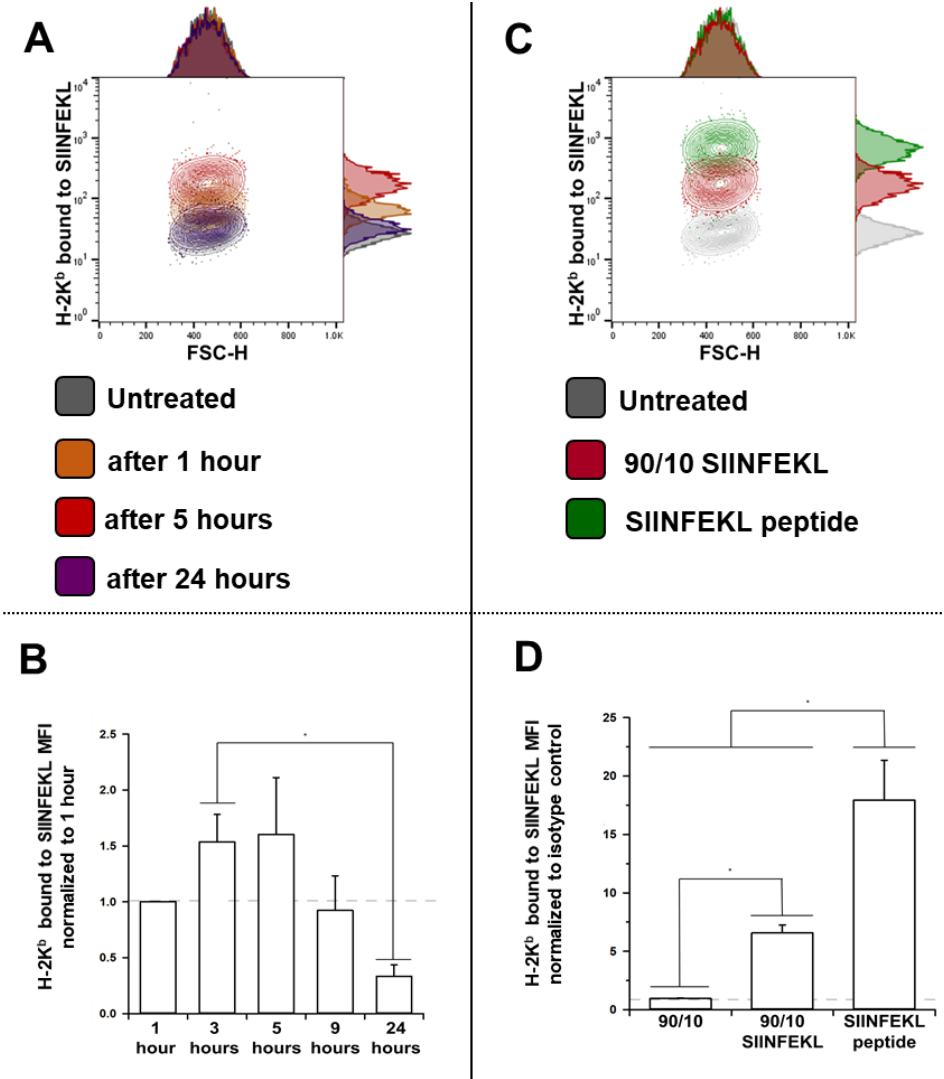


Figure 22: After stimulation with 90/10 SIINFEKL chitosan nanoparticles, DC2.4 cells present SIINFEKL via MHC-I. DC2.4 cells were left untreated or treated with 90/10 SIINFEKL CNPs for the indicated time periods (A and B). DC2.4 cells were left untreated or treated with empty 90/10 CNPs, 90/10 SIINFEKL CNPs or soluble SIINFEKL peptide for 5 hours (C and D). Samples

were stained with an antibody detecting H-2K^b bound to SIINFEKL or with an isotype control antibody and analyzed by flow cytometry. Representative dot plot (A) shows MFI after treatment of DC2.4 cells with 90/10 SIINFEKL CNPs for different periods of time, corresponding to graph (B). Representative dot plot (C) shows the MFI of DC2.4 cells after different treatments, corresponding to graph (D) (n=3 each). Data are shown as mean ± s.e.m.. Statistical analysis was performed with One-way-ANOVA and a subsequent Student-Newman-Keuls-test. An asterisk (*) indicates p<0.05.

4.8 Antigen presentation of DC2.4 cells stimulated with 90/10 SIINFEKL chitosan nanoparticles causes activation of SIINFEKL-specific CD8⁺ T cells

4.8.1 After coculture with 90/10 SIINFEKL treated DC2.4 cells, CD8⁺ T cells expand and upregulate expression of CD25 and CD69

Next, we investigated whether antigen presentation after stimulation of DC2.4 cells with 90/10 SIINFEKL CNPs is sufficient to generate a potent CD8⁺ T cell immune response. Coculture of differently treated DC2.4 cells and CD8⁺ T cells obtained from OT-1 mice was started and morphologic changes of CD8⁺ T cells were analyzed (**Figure 23**). After three days of coculture, CD8⁺ T cells had formed clusters which were the largest in wells that contained DC2.4 cells that had been stimulated with either 90/10 SIINFEKL CNPs or soluble SIINFEKL peptide.

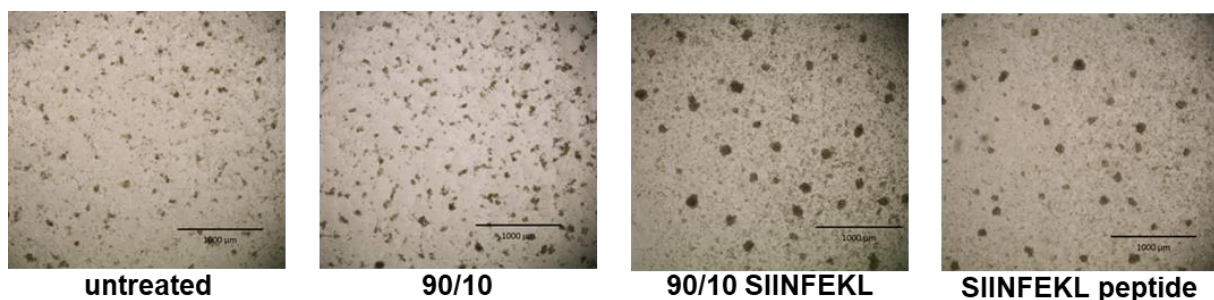


Figure 23: Coculture of CD8⁺ T cells with DC2.4 cells stimulated with 90/10 SIINFEKL chitosan nanoparticles leads to enhanced T cell expansion and clustering. CD8⁺ T cells were cocultured with DC2.4 cells that had been left untreated or treated with either 90/10 CNPs, 90/10 SIINFEKL CNPs or SIINFEKL peptide. Images show CD8⁺ T cells cocultured with DC2.4 cells that had been treated as indicated after 72 hours. CD8⁺ T cell clusters are particularly large in cells treated with 90/10 SIINFEKL CNPs or SIINFEKL peptide. Scalebar: 1000 µm.

In addition, expression of the activation markers CD25 and CD69 was analyzed on CD8⁺ T cells by using flow cytometry. CD8⁺ T cells cocultured with DC2.4 cells, which had been pretreated with 90/10 SIINFEKL CNPs, showed highly elevated MFIs for CD25 and CD69 compared to CD8⁺ T cells that were cocultured with DC2.4 cells that had been left untreated or treated with empty 90/10 CNPs. In comparison to cells after stimulation with soluble SIINFEKL peptide, CD25 and CD69 expression levels of CD8⁺ T cells cocultured with DC2.4 cells that had been stimulated with 90/10 SIINFEKL CNPs were also slightly higher, even though the difference was not statistically significant (**Figure 24**). The visible formation of cellular clusters as well as the increase of CD25 and CD69 expression on the surface of CD8⁺ T cells after coculture of 90/10 SIINFEKL CNP pretreated DC2.4 cells with CD8⁺ T cells suggests that antigen-transport via CNPs with subsequent MHC-I mediated antigen-presentation by DC2.4 cells leads to satisfactory activation of CD8⁺ T cells.

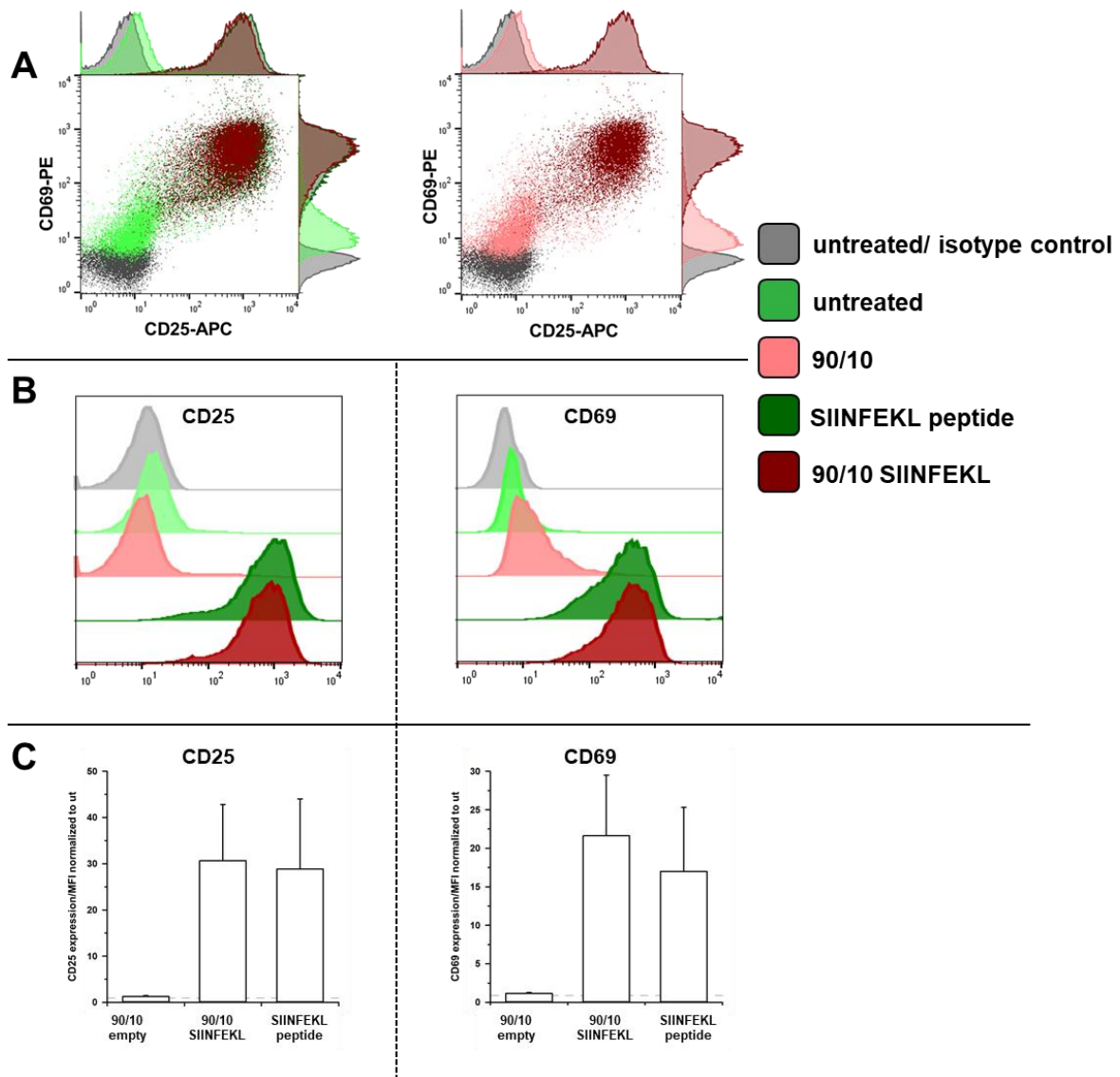


Figure 24: CD8⁺ T cells cocultured with 90/10 SIINFEKL chitosan nanoparticle-stimulated DC2.4 cells exhibit elevated expression of activation markers CD25 and CD69. CD8⁺ T cells cocultured for 72 hours with differently treated DC2.4 cells were assessed for T cell activation marker expression by using flow cytometry. Representative dot plots (A) are shown for the staining experiments. Graphs (B) show MFI of CD25 (left) and CD69 (right) of a representative experiment. Bar charts (C) display MFI of CD25 (left) and CD69 (right) normalized to respective MFI of untreated control cells (n=3). Data are shown as mean \pm s.e.m..

4.8.2 CD8⁺ T cell survival can be improved by increasing mIL-2 concentration

The levels of the measured T cell activation markers CD25 and CD69 were markedly elevated on CD8⁺ T cells after coculturing them with DC2.4 cells pretreated with either soluble SIINFEKL peptide or 90/10 SIINFEKL CNPs. However, since the number of viable CD8⁺ T cells was still too low to conduct further experiments, we tested the effect of a higher mIL-2 concentration. The administered mIL-2 dose was increased from 2 x 50 ng/ml to 2 x 150 ng/ml which clearly

improved cell survival (**Figure 25**). After coculture with DC2.4 cells, slightly but statistically significantly more CD8⁺ T cells were vital after stimulation with 90/10 SIINFEKL CNPs compared to the soluble SIINFEKL peptide. The CD8⁺ T cells markers CD25 and CD69 were again markedly elevated on CD8⁺ T cells cocultured with 90/10 SIINFEKL CNP stimulated DC2.4 cells. Moreover, almost 100% of the examined cells were labelled as positive for CD25 and CD69 confirming that the activation marker expression was not negatively influenced by an increased dosage of mIL-2 (**Figure 26**).

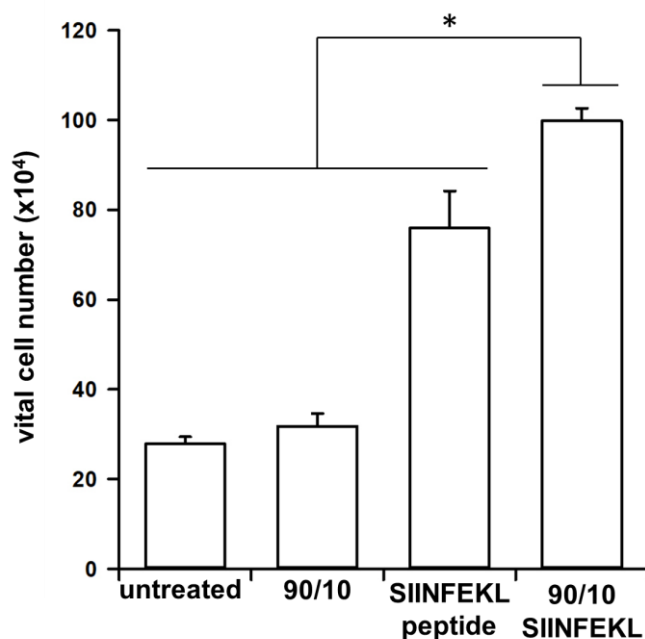


Figure 25: Stimulation of CD8⁺ T cells with 150 ng/ml mIL-2 improves cell survival. CD8⁺ T cells were cocultured with DC2.4 cells that had been left untreated or treated with either 90/10 CNPs, 90/10 SIINFEKL CNPs or SIINFEKL peptide for five hours before starting the coculture. The coculture was stimulated twice with 150 ng/ml mIL-2. After 72 hours, the number of viable cells was determined. Data are shown as mean \pm s.e.m.. Statistical analysis was performed with One-way-ANOVA and a subsequent Student-Newman-Keuls-test. An asterisk (*) indicates $p < 0.05$.

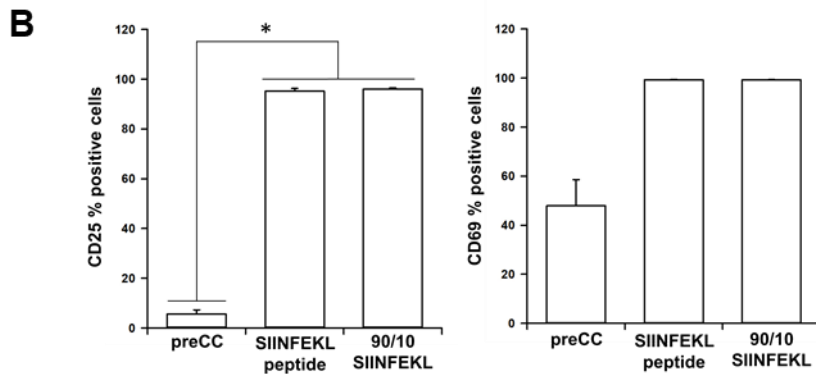
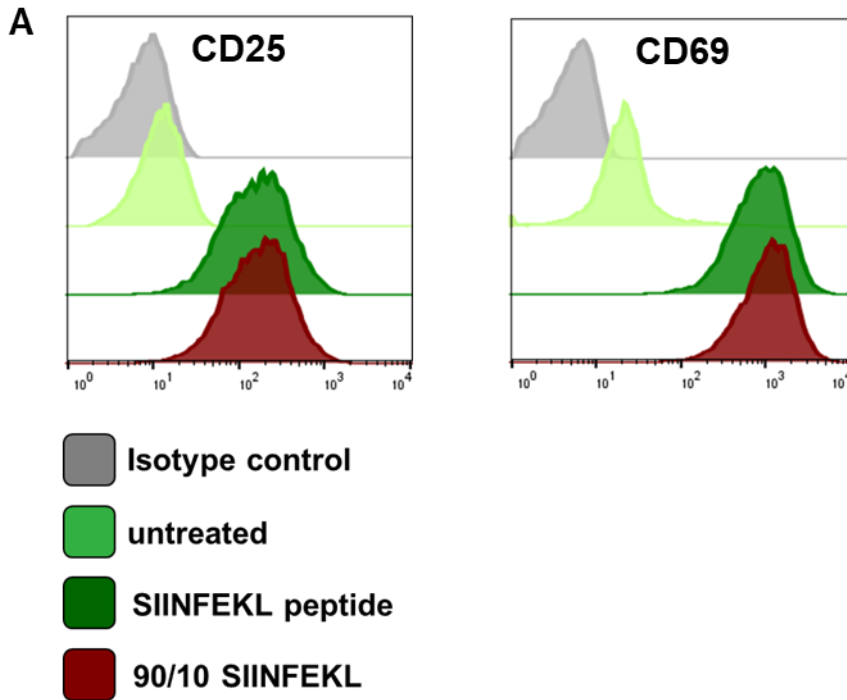


Figure 26: After increasing mL-2 concentration, CD8⁺ T cells cocultured with 90/10 SIINFEKL chitosan nanoparticle-treated DC2.4 cells show CD25 and CD69 positivity. Activation marker expression was analyzed after stimulating the cocultured cells with 150 ng/ml of murine IL-2. (A) shows representative histograms of CD25 and CD69 detection on CD8⁺ T cells after coculture with differently stimulated DC2.4 cells. (B) shows the percentage of positive cells for the respective activation markers (n=3 each). Data are shown as mean \pm s.e.m.. Statistical analysis was performed with One-way-ANOVA and a subsequent Student-Newman-Keuls-test. An asterisk (*) indicates $p < 0.05$. Abbreviation: preCC: CD8⁺ T cells that were analyzed before coculture with DC2.4 cells.

4.9 CD8⁺ T cells cocultured with 90/10 SIINFEKL stimulated DC2.4 cells efficiently kill SIINFEKL expressing PancOVA cells

After having shown that coculture of DC2.4 cells prestimulated with 90/10 SIINFEKL CNPs leads to expansion and activation of CD8⁺ T cells, it was investigated whether these activated CD8⁺ T cells are functionally active. Thus, we examined the ability of CD8⁺ T cells to kill PancOVA cells. PancOVA cells are derived from Panc02 cells which are murine PDAC cells. For generating PancOVA cells, Panc02 cells were transfected with the gene encoding for OVA (257-264) so that PancOVA cells but not Panc02 cells express the sequence SIINFEKL on their surface membrane. CD8⁺ T cells after having been cocultured with differently treated DC2.4 cells were cocultured with PancOVA or Panc02 cells for 24 hours to analyze CD8⁺ T cells mediated PDAC cell killing. While confluence of Panc02 cells was barely impaired by the addition of CD8⁺ T cells, PancOVA cells were clearly harmed resulting in reduced cellular confluence. Whereas confluence of Panc02 cells cocultured with CD8⁺ T cells stimulated with SIINFEKL peptide pretreated DC2.4 cells was 0,78 fold, confluence of PancOVA cells cocultured with identically treated CD8⁺ T cells decreased to 0,32 fold each compared to the respective untreated control. Stimulation of DC2.4 cells with 90/10 SIINFEKL CNPs led to more potent T cell killing activity resulting in the decrease of confluence to 0,73-fold in Panc02 cells and only 0,21-fold in PancOVA cells (**Figure 27**). These data indicate that killing of PancOVA cells was even more pronounced by CD8⁺ T cells following coculture with 90/10 SIINFEKL CNP stimulated DC2.4 cells than after stimulation with the soluble SIINFEKL peptide. Conclusively, these data demonstrate effective killing of PancOVA cells by CD8⁺ T cells which were primed by DC2.4 cells that were pretreated with 90/10 SIINFEKL CNPs. It could be also shown that internalization of 90/10 SIINFEKL CNPs leads to effective MHC-I mediated antigen presentation by DC2.4 cells which activates cocultured CD8⁺ T cells resulting in functionally active CD8⁺ T cells.

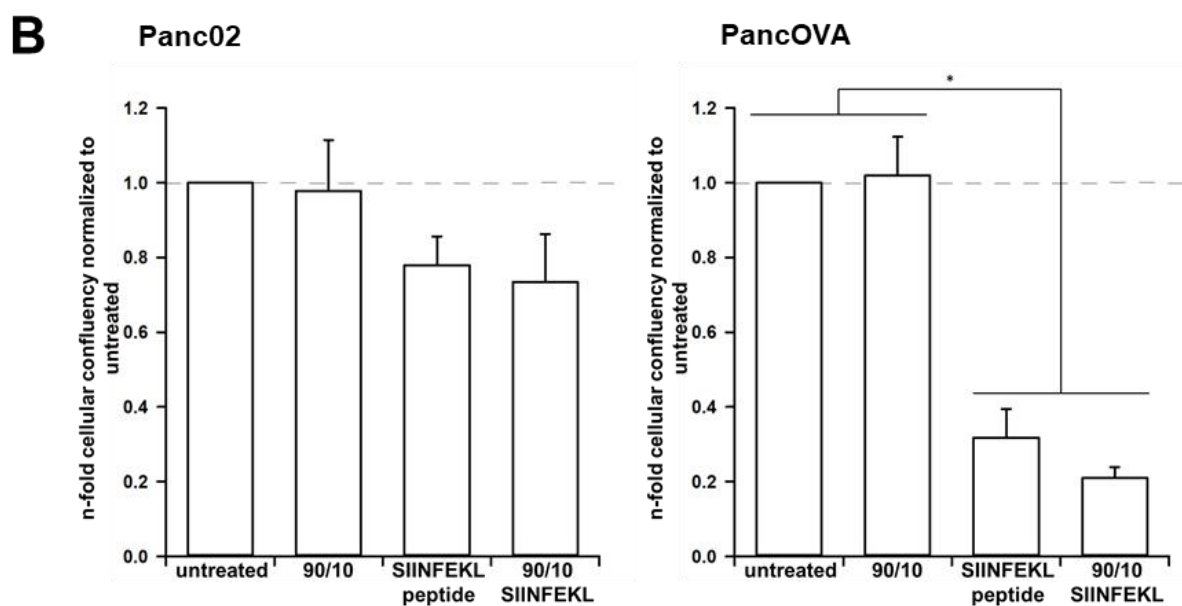
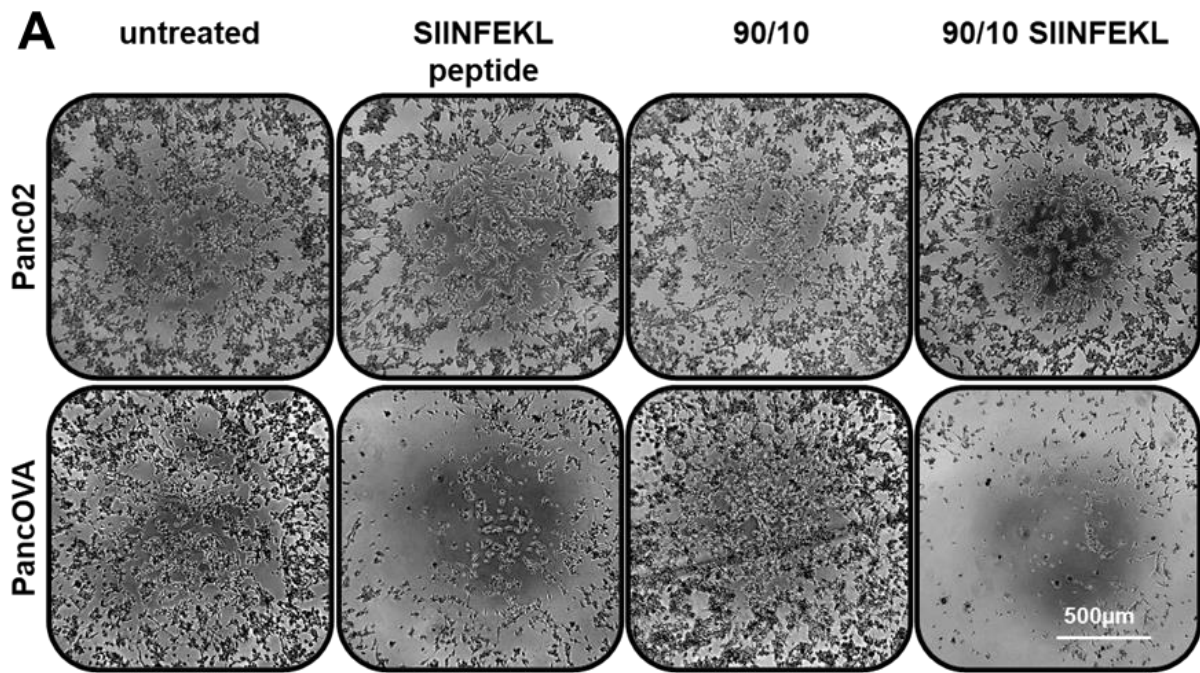


Figure 27: 90/10 SIINFEKL chitosan nanoparticle-stimulated DC2.4 cells activate CD8⁺ T cells being enabled to efficiently kill PancOVA cells. Panc02 or PancOVA cells were cocultured with CD8⁺ T cells taken from coculture with DC2.4 cells that had been left untreated or treated with empty 90/10 CNPs, 90/10 SIINFEKL CNPs or soluble SIINFEKL peptide. After 24 hours CD8⁺ T cells were removed and phase contrast images (A) were taken with the Lionheart™ FX Automated Microscope (Scale bar: 500µm). (B) Cellular confluency was determined as n-fold compared to confluency of Panc02 or PancOVA cells that were cocultured with CD8⁺ T cells after coculture with untreated DC2.4 cells. Data (n=3) are shown as mean ± s.e.m.. Statistical analysis was performed with One-way-ANOVA and a subsequent Student-Newman-Keuls-test. An asterisk (*) indicates p<0.05.

5. Discussion

In the urgent need of finding new therapeutic strategies for treating cancer, anti-tumor vaccines display a promising treatment approach which is currently being assessed for clinical efficacy. The concept of vaccination is successfully performed for prevention from infectious diseases for many years, herewith protecting from tumors closely related to previous infections (50,51). Whereas these conventional, preventive vaccines are usually administered intramuscularly or subcutaneously, non-invasive mucosal vaccination e.g. via the nose could be particularly effective (126) for generating therapeutic anti-tumor effects which are mainly mediated by induced CD8⁺ T cell responses (127), because the mucosa of the respiratory tract is equipped with a variety of immune cells, particularly DCs (128) which are crucial for inducing such immune reactions (53). Using a vaccine with antigens encapsulated in nanoparticles such as CNPs could improve efficacy of anti-tumor vaccine formulations (129). Different nanoparticle carrier substances are being tested but among those, chitosan provides various favorable properties such as low toxicity, good availability, mucoadhesive properties or cheap and easy production (102,104). Additionally, chitosan itself acts as an adjuvant, enhancing the immune reactions induced by peptides that are transported within the nanoparticle structure (130). Moreover, CNPs have already shown promise with regard to the practical capability of eliciting an immune response leading to the proliferation of CD8⁺ T cells (131). Stabilized in a mannitol matrix, a powder suitable for nasal administration can be generated (132). The absence of cytotoxic effects of administered CNPs on the internalizing APCs is fundamental for determining whether further experiments can be executed with CNPs of a certain formulation and size.

5.1 Size of chitosan nanoparticles impacts cellular viability and morphology of human dendritic cells

The experiments with human DCs that were stimulated with unloaded CNPs of different sizes for 24 hours showed that size does in fact matter in terms of CNP-mediated toxicity. The measured parameters - caspase 3/7 activity, morphology and confluence of the DCs as well as PI staining - indicated that 90/10 CNPs with a size of around 220 nm barely affect DCs negatively when comparing with untreated control cells. On the other hand, stimulation with larger 90/20 (average diameter: 384 nm) and 90/50 CNPs (average diameter: 706 nm) significantly

reduced cellular viability and altered cell morphology. Similar results could be observed when M1-like and M2-like M Φ were treated with CNPs with the consequence that only 90/10 CNPs were chosen for further experiments. On the basis of these experiments it can be stated that CNP size is a critical aspect of determining CNPs toxicity as already described (94). However, with the smallest tested CNPs having a size of 220 nm, we could not cover the entire spectrum of common nanoparticle sizes including dimensions of just around 10-20 nm (94). Hence, we do not yet know whether even smaller CNPs of the utilized formulation could have led to even milder cellular impairments. With many studies on the cytotoxicity of nanoparticles having been conducted it became clear that size and concentration of nanoparticles are important determinators of cell viability in *in vitro* assays (133). In-line, larger sized CNPs of our particular formulation led to reduced cell viability. Regarding the concentration, a CNP amount of 100 $\mu\text{g/ml}$ has been shown to be most effective for internalization in previous experiments of the working group. In this context, data from a study conducted with CNPs similar to ours did not reveal increased cytotoxicity with higher CNP concentrations (99). From these experiments it can be concluded that treatment of human DCs with small 90/10 CNPs carrying encapsulated OVA or SIINFEKL administered in a concentration of 100 $\mu\text{g/ml}$ does not lead to strong cytotoxic effects.

5.2 Antigen-loaded 90/10 chitosan nanoparticles are efficiently taken up by dendritic cells with some particles remaining tightly attached to the outer cell membrane

Fundamental for nanoparticle-based tumor vaccines is not only that the nanoparticles do not harm immune cells, but also that they get effectively internalized into DCs. Chitosan as carrier substance for NPs offers multiple advantages because of its biodegradability, biocompatibility, non-toxicity, mucoadhesive capacity and cationic loading (104,134). Hence, CNPs of various formulations are frequently assessed for developing innovative drug delivery systems but also for improving immunotherapeutic methods (99,135,136). For assessing this crucial aspect, un-loaded, FITC-conjugated 90/10, 90/20 and 90/50 CNPs have already been tested with respect to a possible correlation of size and internalization efficacy in human and murine DCs by other members of the research group. Here, no significant correlation between internalization efficacy and CNP size could be revealed. However, other studies provide evidence that for the

purpose of targeting the nasal associated lymphatic tissue (NALT) or the respiratory mucosa in general, a nanoparticle size between 20-200 nm is desirable. This can be explained by the fact that the human respiratory mucus features pores with variable sizes which have to be crossed by nanoparticles (137–139) in order to get internalized by residing immune cells. Furthermore, small nanoparticles (20-200 nm) get taken up primarily by DCs, whereas larger, anionic ones (500-5.000 nm) are internalized primarily by macrophages (139,140). Being around 201 nm (90/10 OVA) and 211 nm (90/10 SIINFEKL) in diameter, the utilized antigen-loaded CNPs are very close to the desired size margin. In this study, antigen-loaded 90/10 CNPs have demonstrated to become internalized by DCs, even though the internalization was seemingly more efficient in murine DC2.4 cells than in human DCs. The relatively low internalization rate found in human DCs might partially be explained by possible insufficient differentiation of a part of the cells. Using light microscopy, the morphology of the utilized primary human DCs was relatively heterogeneous, so that for example not all cells developed the typical dendrites. Interestingly, ImageStream analyses also showed that a significant number of particles did not get internalized in human and murine DCs but instead remained attached to the outer cellular membrane even though cells were conscientiously washed before imaging. One biochemical characteristic of chitosan is that it becomes gel-like after contact with liquids which might be contributing to the sticky CNP agglomerates that were attached to the cells' membrane (141). When comparing the stimulation duration of 24h used in this study with other studies, it is noticeable that the internalization of NPs is usually assessed after a shorter time (99,142,143). Yet, 24 hours after administration of CNPs the highest internalization rate was detected in previous experiments of this research group. Therefore, the same stimulation period was used for this study. Another way of monitoring cell-CNP interactions over time can be live cell imaging. However, having shown internalization via flow cytometry and ImageStream analysis gave us the advantage of examining large numbers of cells at once, ensuring valid results since flow cytometry alone is susceptible for generating a high number of falsely positive-labelled cells and is therefore not sufficient as the only method assessing internalization efficacy (99,143). Still, the exact mechanism by which the CNPs get internalized into APCs remains to be investigated with phagocytosis, micropinocytosis as well as clathrin-mediated endocytosis being proposed as leading cellular uptake mechanisms by different research groups (144).

5.3 SIINFEKL encapsulated in chitosan nanoparticles is liberated and presented by dendritic cells via MHC-I

Aside from taking up exogenous antigens, proper processing and presenting of the internalized antigen is crucial for DCs in order to initiate an immune response (53–57). Our experiments have demonstrated that treatment of murine DC2.4 cells with 90/10 SIINFEKL CNPs led to presentation of SIINFEKL via the MHC class I molecule H-2K^b herewith implying that the other outlined steps – internalization and processing of SIINFEKL inside the DC2.4 cells – had been executed correctly since both are required for achieving successful antigen presentation. The presentation of antigens via MHC-I on DCs enables naïve CD8⁺ T cells to bind to these antigen-presenting MHC-I receptors and subsequently become activated which is pivotal in immune reactions generally and in the concept tumor vaccination, too (145). Currently, we can only speculate about why stimulation with the same CNP size (90/10) carrying encapsulated OVA instead of SIINFEKL only barely led to binding of the antibody that is highly specific for SIINFEKL bound to MHC-I. With the octapeptide SIINFEKL being a part of OVA, uptake of 90/10 OVA CNPs into DC2.4 cells should have theoretically led to a detectable presentation of MHC-I bound SIINFEKL on the DC2.4 cells. In the literature, different techniques for verifying presentation of SIINFEKL after stimulation with NPs are described: While we aimed at directly detecting the MHC-I mediated presentation of SIINFEKL via flow cytometry which is a more exact approach that requires a relatively high concentration of peptide/K^b complexes, other working groups showed peptide presentation indirectly either by demonstrating increased IL-2 concentration after coculturing NP-stimulated DCs or by other activation assays requiring the coculture of NP-stimulated DCs with T cells (143,146–148). Corresponding to our results, in a different study assessing OVA-containing NPs modest results were obtained with flow cytometry when using the SIINFEKL bound to MHC-I antibody to demonstrate SIINFEKL presentation (143). However, when coculturing the NP-stimulated DCs with T cells, a significantly higher IL-2 concentration could be observed after 18 hours as a consequence of OVA-NP administration. Therefore, a possible explanation for the modest antibody binding after stimulation with 90/10 OVA CNPs in our study might be that OVA was only processed to the SIINFEKL sequence in small quantities, thus not sufficiently for causing detectable antibody binding. Supportive for this explanation are our results showing that stimulation with soluble OVA did also not lead to stronger binding of the SIINFEKL bound to MHC-I antibody

(Supplementary figure 3). This finding is confirmed by another study which did not measure improved H-2K^b bound to SIINFEKL antibody binding (clone: 25-D1.16) after stimulation of DC2.4 cells with soluble OVA. In comparison, the 25-D1.16 antibody binding and thus MHC-I mediated presentation of SIINFEKL only slightly increased after stimulation with OVA-loaded NPs but drastically increased after stimulation with SIINFEKL-loaded NPs (142). As we also detected a pronounced binding of 25-D1.16 antibody after stimulation of DC2.4 cells with 90/10 SIINFEKL CNPs, we could demonstrate that our CNP formulation presents a way to efficiently transport antigens into DC2.4 cells where they get cross-presented even if flow cytometry data indicate only modest SIINFEKL presentation via MHC-I molecules after stimulation of DC2.4 cells with 90/10 OVA CNPs. The observation that the vast majority of DC2.4 cells could be labelled as positive with the 25-D1.16 antibody after 5h of stimulation with 90/10 SIINFEKL CNPs demonstrates that 90/10 CNPs present a way to transport an antigen into cells where it can be liberated, processed and presented via MHC-I. Stimulation of DC2.4 cells with 90/10 SIINFEKL CNPs led to significantly increased 25-D1.16 antibody binding, indicating extensive SIINFEKL presentation via MHC-I, an effect which was even more pronounced after stimulation with soluble SIINFEKL peptide. The MHC-I restricted peptide sequence SIINFEKL is known to be able to be loaded directly onto already available MHC-I complexes. Therefore, this difference in antibody binding was not unexpected due to the CNPs precluding this mechanism for the encapsulated SIINFEKL (142,149,150). A limiting factor in the comparison of the results obtained with 90/10 SIINFEKL CNP to the results with soluble SIINFEKL peptide or with other studies is that the amount of antigen – OVA or SIINFEKL – encapsulated into our CNPs could not yet be quantified with certainty. Thus, we did not know whether or not the amount of antigen administered by stimulation with 100 µg/ml 90/10 SIINFEKL CNPs is comparable to 1 µg/ml of SIINFEKL peptide. Noteworthy, stimulation of DC2.4 cells with the three-fold amount of 90/10 SIINFEKL CNPs (= 300 µg/well) which was performed in additional experiments **(Supplementary figure 4)** led to an increase in MHC-I mediated presentation of SIINFEKL. Yet, this increase did not correspond linearly to the triplication of added CNPs and therefore of added antigen. One possible explanation is that the DC2.4 cells could not take up as many CNPs as needed to lead to saturation of all available MHC-I molecules. Even though the amount of antibody binding seen in the positive control when treating DC2.4 cells with free, soluble SIINFEKL could not be reached in the 90/10 SIINFEKL CNP-treated cells, the verification of MHC-I-mediated presentation of SIINFEKL supports the suitability of CNPs as

antigen transporters. These results enabled us to assess the kinetics of MHC-I mediated SIINFEKL presentation on DC2.4 cells resulting from treatment with 90/10 SIINFEKL CNPs via flow cytometry. It has been revealed that the maximal SIINFEKL peptide presentation via MHC-I was reached 5 hours after stimulation of DC2.4 cells. This determined timeframe is in-line with findings of other working groups stating that maximal MHC-I mediated antigen presentation occurs between 2 and 16 hours after treatment with antigen-containing NPs (142,143,150,151). However, the drop in antibody binding and thus SIINFEKL presentation after more than 5 hours of stimulation time in our experiments could not be shown in an extensive study assessing the kinetics of MHC-I/Ovalbumin peptide complexes (147). Here, antigen presentation reached a plateau after a short time with no visible decline in antigen presentation even after 16 hours. Importantly, in this study, murine bone marrow derived DCs were utilized instead of murine DC2.4s in our study.

5.4 Stimulation with antigen-loaded chitosan nanoparticles promotes a proinflammatory phenotype in human and murine dendritic cells

The effect of tumor vaccines relies on activated DCs as mediating initiators of vaccine-induced immune responses (54). Therefore, not only the internalization of CNPs as well as the processing and presentation of the encapsulated peptide but also the direct effects of 90/10 CNPs on the DCs' phenotype were assessed. Overall, our results demonstrate that human and also murine DC2.4 cells exhibit features of a more proinflammatory phenotype after stimulation with 90/10 CNPs. This applies particularly when these 90/10 CNPs were loaded with an antigen as it was the case with 90/10 OVA and 90/10 SIINFEKL CNPs while treatment with chitosan alone in the form of empty 90/10 CNPs led to only minor alterations of the cells' RNA expression level in comparison with untreated control cells. The expression of the proinflammatory cytokines TNF- α , IL-1 β and IL-6 was notably elevated after treating cells with antigen-loaded 90/10 CNPs. On top of that, expression of the antiinflammatory cytokines TGF- β and IL-10 was diminished. Since the CNP structure of 90/10 OVA and 90/10 SIINFEKL CNPs is the same and the respective CNP size is very similar as well, significant differences in RNA expression levels after stimulation with these CNPs can only be explained by the different encapsulated peptide itself leading to different processing and presentation processes. Importantly, the outlined effects were observable 5 and 24 hours but not 48 hours after CNP treatment. Possibly, a

certain level of cytokine expression was reached and could not be maintained for longer with no additional stimuli, resulting in a normalization of RNA expression levels coding for the mentioned cytokines. Additional insights into the development of cytokine expression could be obtained by supernatant analyses. A limitation of our experimental design is that we used untreated cells as negative control and also cells treated with chitosan but without antigen, however, we did not examine cells treated with the respective soluble antigens, OVA and/or SIINFEKL alone without chitosan. Therefore, the modest change in cytokine expression levels after DC stimulation with empty 90/10 CNPs is difficult to interpret. In general, chitosan is said to have properties of an immunostimulatory adjuvant (107,130) and in other studies in which chitosan was used as differentiation stimulus it promoted a proinflammatory phenotype in DCs (152,153). In our experimental setting, human DCs and DC2.4 cells were already cultured and differentiated before being treated with CNPs for a comparably short period of time. Perhaps, the timespan during which DCs and DC2.4 cells were exposed to chitosan has not been sufficient to lead to detectable phenotypic changes. Another possible explanation for the lack of significant phenotypic changes in our experiments with empty 90/10 CNPs might be that the potency of chitosan as stimulus is adequately high for promoting a proinflammatory phenotype if exposure occurs immediately after seeding but is not sufficient to alter already differentiated cells. Conclusively, while treatment with 90/10 OVA and 90/10 SIINFEKL CNPs led to a more proinflammatory phenotype, the role of chitosan itself could not clearly be determined by our experiments. Further investigations including the stimulation of DCs with antigen-loaded CNPs, free antigen and empty CNPs to assess the cellular phenotype after shorter and longer periods of treatment could potentially clarify chitosan's impact. Nonetheless, the presented findings are encouraging, since the more proinflammatory phenotype displayed by 90/10 OVA and 90/10 SIINFEKL CNP-treated DCs as determined by RNA expression analysis could be helpful for the initiation of a strong immune response of a tumor vaccine where the immunosuppressive microenvironment of most cancers poses an obstacle which tumor vaccines have to overcome (34,95). Within this immunosuppressive tumor microenvironment, DCs in particular have been reported to become phenotypically altered towards less immunostimulatory forms with a reduced capacity of stimulating cytotoxic T cells' responses (154).

5.5 Stimulation with 90/10 SIINFEKL chitosan nanoparticles leads to DC2.4 cell-mediated activation of cocultured CD8⁺ T cells

The presented data shows that CD8⁺ T cells obtained from OT-1 mice, cocultured with DC2.4 cells which had been stimulated with SIINFEKL either in its soluble form or encapsulated in 90/10 SIINFEKL CNPs displayed clear elevations of T cell activation marker expression (CD25 and CD69). Furthermore, proliferation of CD8⁺ T cells in a characteristic cluster-like morphology was observed. Interestingly, the activation marker expression levels and number of viable CD8⁺ T cells was even higher after coculture with 90/10 SIINFEKL CNP-treated DCs than after stimulation with soluble SIINFEKL peptide. A possible explanation could be that the CNP structure additionally augmented DC function and thus CD8⁺ T cell activation. This would support the suitability of chitosan-based nanoparticle structures in the context of tumor vaccines which had been demonstrated in various previous studies (99,129). In contrast, CD8⁺ T cells that were cocultured with 90/10 OVA CNP-stimulated DC2.4 cells did not proliferate as much, which is in-line with the obtained results demonstrating modest MHC-I mediated presentation of SIINFEKL on DC2.4 cells. Still, effects on activation marker expression levels of CD8⁺ T cells were visible showing an increase particularly in expression of CD69. These results are thus matching findings from other working groups that demonstrated an effect of OVA-loaded NPs on T cell level but did not register a drastic increase in binding of MHC-I bound to SIINFEKL antibody in flow cytometry analyses of OVA-NP stimulated APCs (142,143). By demonstrating that stimulation of DC2.4 cells with 90/10 SIINFEKL CNPs leads to a drastic increase in expression of CD25 and CD69 on cocultured, OT-1 mice derived CD8⁺ T cells we could show their proper activation as also demonstrated in other studies using these markers (155). Proliferation of CD8⁺ T cells was assessed by monitoring formation of CD8⁺ T cell clusters in contrast to a different study using CFSE labelling and subsequent flow cytometry analyses for quantification (156). Moreover, in the same study, CD8⁺ T cells were assessed morphologically on a single-cell basis after staining them with Wright-Giemsa stain herewith carving out characteristic morphologic changes. Han et al. measured activation and proliferation of CD8⁺ T cells in an *in vivo* setting by intraperitoneal or subcutaneous injection of chitosan-based NPs and PLGA-NPs into OT-1 mice and consequent analyses of murine splenocytes with anti-CD8 and anti-IFN γ staining as well as with anti-OVA tetramer staining thus discriminating and quantifying the exact amount of activated cytotoxic CD8⁺ T cells (99,157). Moreover, the demonstrated

activating effect of 90/10 SIINFEKL CNP-stimulated DC2.4 cells on CD8⁺ T cells could have been investigated in more detail by analyzing functional ability of CD8⁺ T cells and proliferation. Possible approaches in this regard could be IFN- γ release assays or measurement of perforin or granzymes as mediators of CD8⁺ T cell induced killing via multiplex analysis of supernatants.

5.6 CD8⁺ T cells activated by coculture with 90/10 SIINFEKL chitosan nanoparticle pre-stimulated DC2.4 cells efficiently kill SIINFEKL expressing tumor cells

For confirming the elicitation of an antigen-specific CD8⁺ T cell response, not only measurement of activation and proliferation is important but also the assessment of CD8⁺ T cell functionality in the form of quantifying CD8⁺ T cell mediated killing of cells expressing a particular antigen on their surface. Thus, the efficient killing of PancOVA cells expressing SIINFEKL but not Panc02 cells by CD8⁺ T cells previously cocultured with DC2.4 cells that had been stimulated with 90/10 SIINFEKL CNPs supports the hypothesis that an effectful antigen-specific anti-tumor response can be induced with our antigen-loaded CNPs of this specific formulation and size. The killing of also Panc02 cells that lack expression of SIINFEKL on their surface might be partially explainable by the high number of cells that was added to the PDAC cells and the potential lack of nutrients in the solution which are particularly needed by the usually rapidly proliferating pancreatic tumor cells. More importantly, we could demonstrate expression of CD80 - but not CD86 - on the pancreatic tumor cell lines which could have contributed to CD8⁺ T cell activation and thus to their killing activity (data not shown). Interestingly, 90/10 SIINFEKL CNP treatment of DC2.4 cells led to slightly more effective killing than treatment with soluble SIINFEKL indicating that encapsulation of antigens into the utilized CNP structure might lead to an enhancing effect on the elicited immune response of CD8⁺ T cells even if the antigen presentation on DC2.4 cells was lower after 90/10 SIINFEKL CNP treatment compared to stimulation with free, soluble SIINFEKL. The therapeutic efficiency of immune responses generated by immunization via antigen-loaded nanoparticles can also be displayed in mouse models as executed by Han et al. who injected OVA-loaded chitosan nanoparticles (99) or DCs, treated *ex vivo* with OVA-PLGA nanoparticles (157) into tumor bearing mice. Tumor growth inhibition after injection of a polymeric nanoparticle-based vaccine was also reported by Luo et al. in another study (97). Since the performed experiments were performed in 2D culture and without the presence of other possible immunosuppressive influences, the executed experiments

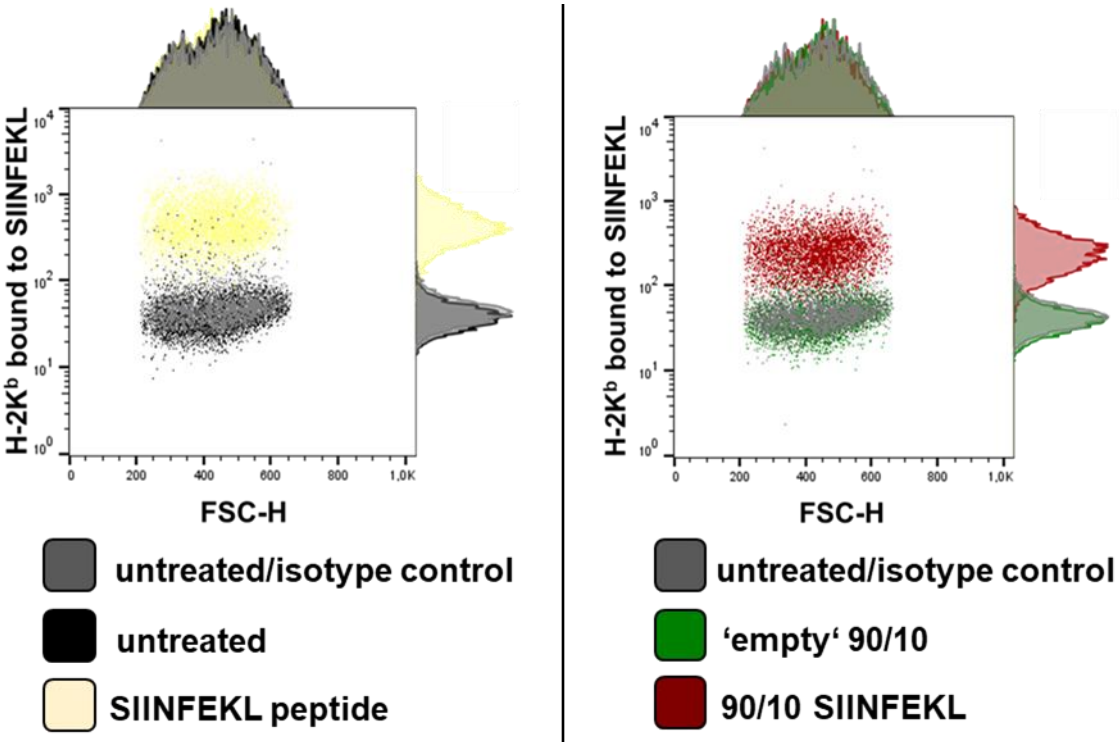
cannot reflect on the *in vivo* tumoral conditions where a multitude of factors contribute to intercellular interactions. Therefore, the encouraging results we obtained, particularly that CD8⁺T cells cocultured with 90/10 SIINFEKL CNP treated DC2.4 cells specifically and effectively killed PancOVA cells can be interpreted as promising findings regarding the suitability of our formulation of CNPs. Thus, the utilization of mouse models to demonstrate the strength of the elicited immune reaction could be a valuable next step in order to further evaluate the potential of the utilized CNPs in the context of tumor vaccination. Furthermore, employing different, clinically relevant antigens instead of model antigens like OVA and SIINFEKL such as the antigen kras which is often mutated in pancreatic cancer would present an opportunity to translate the already obtained knowledge closer to clinical application.

6. Summary

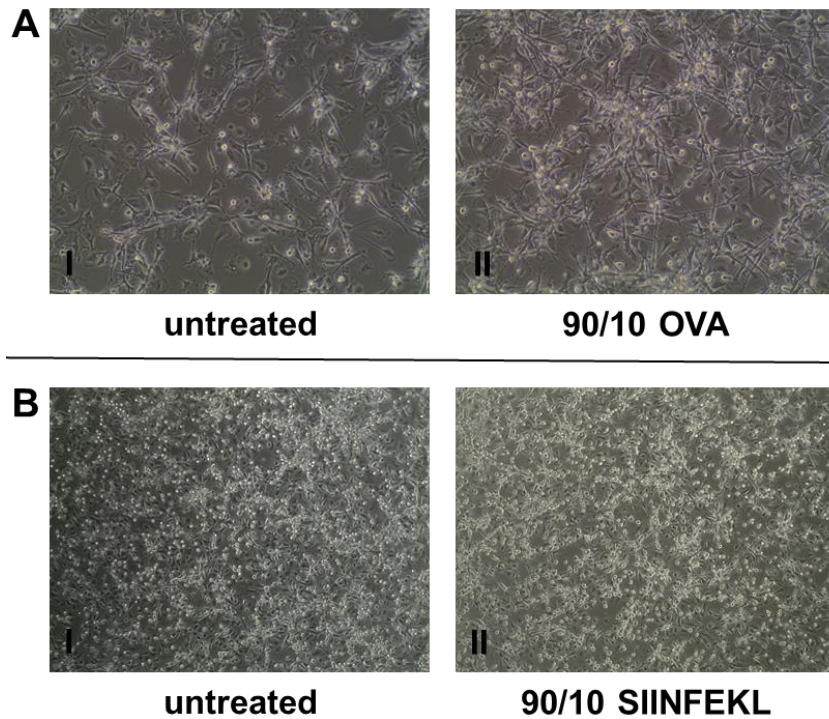
Tumor vaccination is a promising approach for treatment of cancer. Tumor vaccines aim at sensitizing the immune system to tumor-specific antigens and thus stimulate and enhance CD8⁺ T cell immune responses. This immune response's potency can additionally be increased by using a vaccination strategy where nanoparticles act as vehicles enabling more efficient antigen uptake into antigen-presenting cells. The most important cellular subgroup in the outlined context are dendritic cells, among other characteristics due to their ability of efficiently cross-presenting exogenous antigens. With regard on finding fitting materials for generating nanoparticles for tumor vaccination, chitosan has emerged as a promising substance offering favorable biochemical properties such as adjuvant activity and low cytotoxicity. Chitosan nanoparticle-based vaccines can be administered intranasally, which represents a noninvasive way of targeting the immune cells located in the epithelium of the respiratory tract as a first step for eventually eliciting a generalized antigen-specific immune reaction. In this study, the potential of antigen-loaded chitosan nanoparticles as antigen delivery systems for inducing a potent, antigen-specific CD8⁺ T cell response was assessed. Therefore, ovalbumin and the oligopeptide SIINFEKL (ovalbumin 257-264) were used as model antigens. First, uptake of fluorescein isothiocyanate-conjugated antigen-loaded chitosan nanoparticles was verified with flow cytometry and ImageStream analyses. As larger unloaded chitosan nanoparticles (90/20 and 90/50) impaired viability and morphology of human dendritic cells as determined by caspase 3/7 assays and propidium iodide staining, further experiments were conducted with 90/10 chitosan nanoparticles which did not show significant cytotoxic effects on human dendritic cells in both, unloaded or antigen-loaded forms. Moreover, a proinflammatory phenotype could be detected in human dendritic cells and murine DC2.4 cells after stimulation and internalization of antigen-loaded 90/10 chitosan nanoparticles indicated by elevated RNA expression levels of proinflammatory cytokines. Next, MHC-I mediated presentation of SIINFEKL on DC2.4 cells after treatment with SIINFEKL-loaded 90/10 chitosan nanoparticles was demonstrated via flow cytometry whereas treatment with ovalbumin-loaded 90/10 chitosan nanoparticles led only to a modest presentation. Coculturing CD8⁺ T cells isolated from spleens of OT-1 mice with DC2.4 cells that had been treated with antigen-loaded 90/10 chitosan nanoparticles led to an elevation of activation marker expression on CD8⁺ T cells, particularly if the activating DC2.4 cells had been stimulated with SIINFEKL-loaded 90/10 chitosan nanoparticles.

Lastly, the functionality of these OT-1 derived CD8⁺ T cells activated by coculture with DC2.4 cells after pre-stimulation with 90/10 SIINFEKL chitosan nanoparticles was demonstrated by verifying CD8⁺ T cell-mediated antigen-specific lysis of PancOVA cells, pancreatic ductal adenocarcinoma cells expressing SIINFEKL on their cell surface. Overall, the presented data support the suitability of antigen-loaded 90/10 chitosan nanoparticles for tumor vaccination. Verification of internalization into dendritic cells, demonstration of low cytotoxicity and initiation of a more proinflammatory phenotype in dendritic cells, confirmation of MHC-I mediated presentation of the encapsulated antigen and the subsequent activation of functionally active CD8⁺ T cells support this hypothesis. However, further studies are needed to investigate the potential of the utilized chitosan nanoparticles for improving tumor vaccination strategies in *in vivo* studies and with clinically relevant antigens instead of model antigens in order to proceed with the translation of the obtained results closer into clinical application.

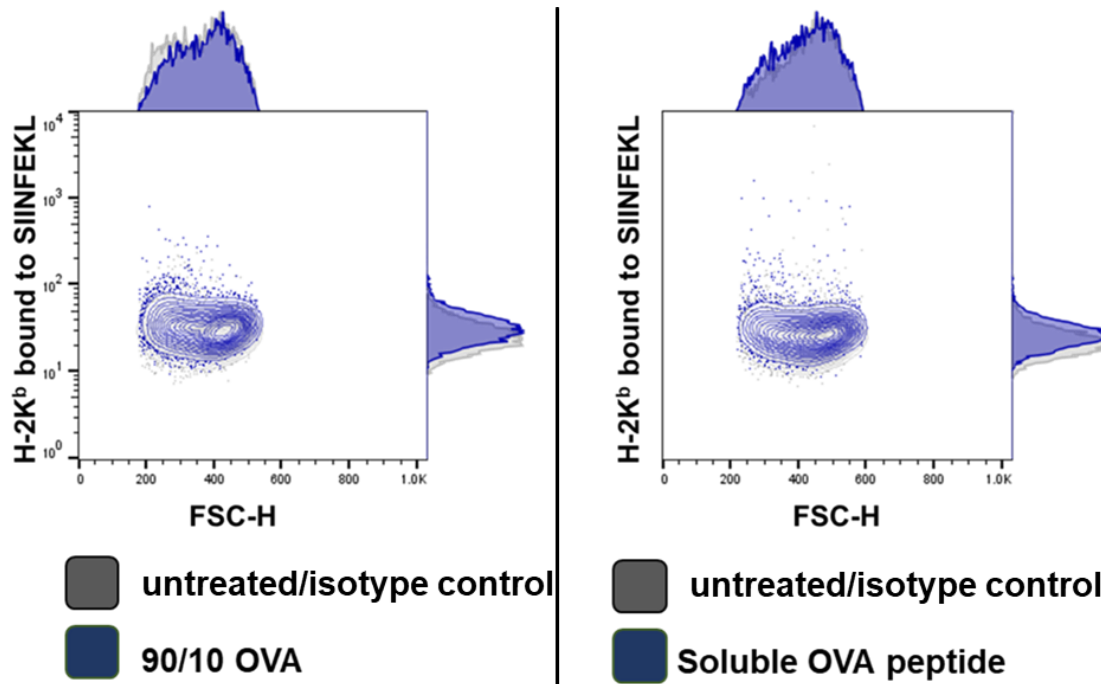
7. Supplementary data



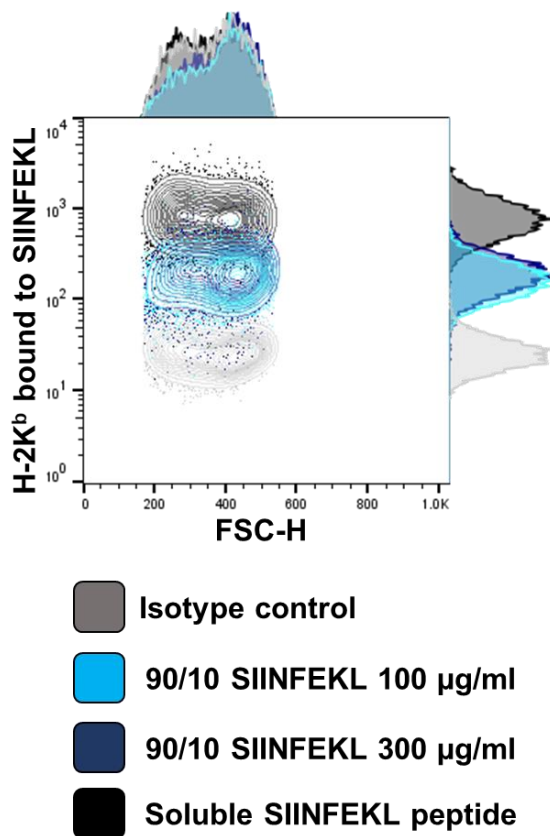
Supplementary figure 1: Prior to coculture of differently treated DC2.4 cells and CD8⁺ T cells, MHC-I mediated presentation of SIINFEKL on DC2.4 cells can be confirmed in cells treated with 90/10 SIINFEKL chitosan nanoparticles or soluble SIINFEKL. After treating DC2.4 cells for 5 hours with soluble SIINFEKL peptide, empty 90/10 CNPs or 90/10 SIINFEKL CNPs or leaving them untreated, cells were analyzed for H-2K^b mediated presentation of SIINFEKL on DC2.4 cells. Dot plots confirm MFI shift compared to the untreated isotype control in DC2.4 cells treated with either soluble SIINFEKL peptide or 90/10 SIINFEKL CNPs whereas MFI of untreated or empty 90/10 CNP stimulated DC2.4 cells remains low.



Supplementary figure 2: Stimulation with 90/10 OVA or 90/10 SIINFEKL chitosan nanoparticles for 24 hours does not negatively impact morphology or confluence of human dendritic cells. Human DCs were treated for 24 hours with 90/10 OVA or 90/10 SIINFEKL CNPs or left untreated as control. Then, images were taken with the EVOS XL light microscope. No impaired cell morphology or reduced cell confluence could be registered as demonstrated with representative images A (untreated vs. 90/10 OVA) and B (untreated vs. 90/10 SIINFEKL). Magnification: 280 x in image set A, 140 x in image set B.



Supplementary figure 3: Stimulation of DC2.4 cells with soluble OVA peptide does not lead to increased 25-D1.16 antibody binding. DC2.4 cells were treated for 5 hours with either 90/10 OVA CNPs or soluble OVA peptide or were left untreated. Cells were then assessed for binding of H-2K^b bound-to SIINFEKL antibody (25-D1.16) via flow cytometry compared to staining with the untreated isotype control. Representative dot plots (n=3) with 90/10 OVA CNPs (and n=2 with soluble OVA peptide) are shown.



Supplementary figure 4: Treatment of DC2.4 cells with increased amount of 90/10 SIINFEKL chitosan nanoparticles only leads to slight increase of H-2K^b mediated SIINFEKL presentation. DC2.4 cells were left untreated or were treated with soluble SIINFEKL, 90/10 SIINFEKL CNPs in the concentration of 100 µg/ml and the three-fold amount of 90/10 SIINFEKL CNPs (100 µg/ml vs. 300 µg/ml). H-2K^b - mediated presentation of SIINFEKL was assessed by flow cytometry and compared to staining with the corresponding isotype control. A representative dot plot of three independent experiments is shown.

8. Bibliography

1. Quaresma M, Coleman MP, Rachet B. 40-year trends in an index of survival for all cancers combined and survival adjusted for age and sex for each cancer in England and Wales, 1971–2011: a population-based study. *The Lancet*. 2015 Mar 28;385(9974):1206–18.
2. Yabroff KR, Lund J, Kepka D, Mariotto A. Economic Burden of Cancer in the US: Estimates, Projections, and Future Research. *Cancer Epidemiol Biomarkers Prev*. 2011 Oct;20(10):2006–14.
3. Beger HG, Rau B, Gansauge F, Leder G, Schwarz M, Poch B. Pancreatic Cancer – Low Survival Rates. *Dtsch Arztebl Int*. 2008 Apr;105(14):255–62.
4. Zappa C, Mousa SA. Non-small cell lung cancer: current treatment and future advances. *Transl Lung Cancer Res*. 2016 Jun;5(3):288–300.
5. Gridelli C, Rossi A, Carbone DP, Guarize J, Karachaliou N, Mok T, et al. Non-small-cell lung cancer. *Nat Rev Dis Primers*. 2015 May 21;1(1):1–16.
6. The top 10 causes of death [Internet]. [cited 2019 May 20]. Available from: <https://www.who.int/news-room/fact-sheets/detail/the-top-10-causes-of-death>
7. Fidler MM, Bray F, Soerjomataram I. The global cancer burden and human development: A review. *Scand J Public Health*. 2018 Feb 1;46(1):27–36.
8. Heron M. Deaths: Leading Causes for 2016. :77.
9. Cancer - Symptoms and causes [Internet]. Mayo Clinic. [cited 2019 Oct 4]. Available from: <https://www.mayoclinic.org/diseases-conditions/cancer/symptoms-causes/syc-20370588>
10. Poirier AE, Ruan Y, Walter SD, Franco EL, Villeneuve PJ, King WD, et al. The future burden of cancer in Canada: Long-term cancer incidence projections 2013–2042. *Cancer Epidemiology*. 2019 Apr;59:199–207.
11. Rahib L, Smith BD, Aizenberg R, Rosenzweig AB, Fleshman JM, Matrisian LM. Projecting Cancer Incidence and Deaths to 2030: The Unexpected Burden of Thyroid, Liver, and Pancreas Cancers in the United States. *Cancer Research*. 2014 Jun 1;74(11):2913–21.
12. Cancer beaten in ‘10 to 20 years,’ says German health minister | DW | 01.02.2019 [Internet]. DW.COM. [cited 2019 May 20]. Available from: <https://www.dw.com/en/cancer-beaten-in-10-to-20-years-says-german-health-minister/a-47320283>
13. Deininger M, Buchdunger E, Druker BJ. The development of imatinib as a therapeutic agent for chronic myeloid leukemia. *Blood*. 2005 Apr 1;105(7):2640–53.
14. Kantarjian H, O’Brien S, Jabbour E, Garcia-Manero G, Quintas-Cardama A, Shan J, et al. Improved survival in chronic myeloid leukemia since the introduction of imatinib therapy: a single-institution historical experience. *Blood*. 2012 Mar 1;119(9):1981–7.
15. Cancer of the Pancreas - Cancer Stat Facts [Internet]. SEER. [cited 2019 Aug 2]. Available from: <https://seer.cancer.gov/statfacts/html/pancreas.html>

16. WHO | Cancer prevention [Internet]. WHO. [cited 2019 Aug 9]. Available from: <http://www.who.int/cancer/prevention/en/>
17. Pinsky PF. Principles of Cancer Screening. *Surg Clin North Am*. 2015 Oct;95(5):953–66.
18. Identifying and Creating the Next Generation of Community-Based Cancer Prevention Studies: Summary of a National Cancer Institute Think Tank [Internet]. [cited 2019 Aug 9]. Available from: <https://www.ncbi.nlm.nih.gov/pmc/articles/PMC5292088/>
19. Livingston EH, Li HC. Breast Cancer Surgery: Less Is More. *JAMA*. 2017 Sep 12;318(10):909–11.
20. Dralle H. Kolorektale Lebermetastasen. *Chirurg*. 2014 Jan 1;85(1):4–5.
21. Sheehan JP, Starke RM, Kano H, Barnett GH, Mathieu D, Chiang V, et al. Gamma Knife radio-surgery for posterior fossa meningiomas: a multicenter study. *Journal of Neurosurgery*. 2015 Jun 1;122(6):1479–89.
22. Yan L, Rosen N, Arteaga C. Targeted cancer therapies. *Chin J Cancer*. 2011 Jan;30(1):1–4.
23. Hanahan D, Weinberg RA. Hallmarks of Cancer: The Next Generation. *Cell*. 2011 Mar;144(5):646–74.
24. Shibuya M. Vascular Endothelial Growth Factor (VEGF) and Its Receptor (VEGFR) Signaling in Angiogenesis. *Genes Cancer*. 2011 Dec;2(12):1097–105.
25. Research C for DE and. Hematology/Oncology (Cancer) Approvals & Safety Notifications. FDA [Internet]. 2019 Aug 8 [cited 2019 Aug 12]; Available from: <http://www.fda.gov/drugs/resources-information-approved-drugs/hematologyoncology-cancer-approvals-safety-notifications>
26. Thomas L. On immunosurveillance in human cancer. *Yale J Biol Med*. 1982;55(3–4):329–33.
27. Chen DS, Mellman I. Oncology Meets Immunology: The Cancer-Immunity Cycle. *Immunity*. 2013 Jul 25;39(1):1–10.
28. Dunn GP, Old LJ, Schreiber RD. The Three Es of Cancer Immunoediting. *Annual Review of Immunology*. 2004;22(1):329–60.
29. Kim R, Emi M, Tanabe K. Cancer immunoediting from immune surveillance to immune escape. *Immunology*. 2007 May;121(1):1–14.
30. Teng MWL, Vesely MD, Duret H, McLaughlin N, Towne JE, Schreiber RD, et al. Opposing roles for IL-23 and IL-12 in maintaining occult cancer in an equilibrium state. *Cancer Res*. 2012 Aug 15;72(16):3987–96.
31. Wu X, Peng M, Huang B, Zhang H, Wang H, Huang B, et al. Immune microenvironment profiles of tumor immune equilibrium and immune escape states of mouse sarcoma. *Cancer Letters*. 2013 Oct 28;340(1):124–33.
32. Müller-Hermelink N, Braumüller H, Pichler B, Wieder T, Mailhammer R, Schaak K, et al. TNFR1 Signaling and IFN- γ Signaling Determine whether T Cells Induce Tumor Dormancy or Promote Multistage Carcinogenesis. *Cancer Cell*. 2008 Jun 10;13(6):507–18.

33. Braumüller H, Wieder T, Brenner E, Aßmann S, Hahn M, Alkhaled M, et al. T-helper-1-cell cytokines drive cancer into senescence. *Nature*. 2013 Feb;494(7437):361–5.
34. Schreiber RD, Old LJ, Smyth MJ. Cancer immunoediting: integrating immunity's roles in cancer suppression and promotion. *Science*. 2011 Mar 25;331(6024):1565–70.
35. Quatromoni JG, Eruslanov E. Tumor-associated macrophages: function, phenotype, and link to prognosis in human lung cancer. *Am J Transl Res*. 2012 Oct 10;4(4):376–89.
36. Cavallo F, De Giovanni C, Nanni P, Forni G, Lollini P-L. 2011: the immune hallmarks of cancer. *Cancer Immunol Immunother*. 2011 Mar;60(3):319–26.
37. Cancer Immunotherapy: The Year in Review and a Look at the Year Ahead - Cancer Research Institute (CRI) [Internet]. [cited 2019 Oct 4]. Available from: <https://www.cancerresearch.org/blog/january-2019/cancer-immunotherapy-2018-review-2019-predict>
38. Feld E, Mitchell TC. Immunotherapy in melanoma. *Immunotherapy*. 2018 Aug 1;10(11):987–98.
39. Buchbinder EI, Desai A. CTLA-4 and PD-1 Pathways. *Am J Clin Oncol*. 2016 Feb;39(1):98–106.
40. Parry RV, Chemnitz JM, Frauwirth KA, Lanfranco AR, Braunstein I, Kobayashi SV, et al. CTLA-4 and PD-1 Receptors Inhibit T-Cell Activation by Distinct Mechanisms. *Mol Cell Biol*. 2005 Nov;25(21):9543–53.
41. Rowshanravan B, Halliday N, Sansom DM. CTLA-4: a moving target in immunotherapy. *Blood*. 2018 Jan 4;131(1):58–67.
42. Yu H, Boyle TA, Zhou C, Rimm DL, Hirsch FR. PD-L1 Expression in Lung Cancer. *Journal of Thoracic Oncology*. 2016 Jul 1;11(7):964–75.
43. Sadelain M. CAR therapy: the CD19 paradigm. *J Clin Invest*. 2015 Sep 1;125(9):3392–400.
44. Almåsbak H, Aarvak T, Vemuri MC. CAR T Cell Therapy: A Game Changer in Cancer Treatment. *J Immunol Res* [Internet]. 2016 [cited 2019 Aug 11];2016. Available from: <https://www.ncbi.nlm.nih.gov/pmc/articles/PMC4889848/>
45. Research C for DE and. FDA expands pembrolizumab indication for first-line treatment of NSCLC (TPS ≥1%). FDA [Internet]. 2019 Nov 4 [cited 2019 Aug 12]; Available from: <http://www.fda.gov/drugs/fda-expands-pembrolizumab-indication-first-line-treatment-nsclc-tps-1>
46. Haslam A, Prasad V. Estimation of the Percentage of US Patients With Cancer Who Are Eligible for and Respond to Checkpoint Inhibitor Immunotherapy Drugs. *JAMA Netw Open*. 2019 May 3;2(5):e192535.
47. Hodi FS, O'Day SJ, McDermott DF, Weber RW, Sosman JA, Haanen JB, et al. Improved Survival with Ipilimumab in Patients with Metastatic Melanoma. *N Engl J Med*. 2010 Aug 19;363(8):711–23.
48. Maude SL, Laetsch TW, Buechner J, Rives S, Boyer M, Bittencourt H, et al. Tisagenlecleucel in Children and Young Adults with B-Cell Lymphoblastic Leukemia. *New England Journal of Medicine*. 2018 Feb 1;378(5):439–48.

49. Magee DE, Hird AE, Klaassen Z, Sridhar SS, Nam RK, Wallis CJD, et al. Adverse event profile for immunotherapy agents compared with chemotherapy in solid organ tumors: a systematic review and meta-analysis of randomized clinical trials. *Annals of Oncology*. 2020 Jan 1;31(1):50–60.
50. Chang M-H, You S-L, Chen C-J, Liu C-J, Lee C-M, Lin S-M, et al. Decreased Incidence of Hepatocellular Carcinoma in Hepatitis B Vaccinees: A 20-Year Follow-up Study. *J Natl Cancer Inst*. 2009 Oct 7;101(19):1348–55.
51. SIGNORELLI C, ODONE A, CIORBA V, CELLA P, AUDISIO RA, LOMBARDI A, et al. Human papillomavirus 9-valent vaccine for cancer prevention: a systematic review of the available evidence. *Epidemiol Infect*. 2017 Jul;145(10):1962–82.
52. Wagner S, Mullins CS, Linnebacher M. Colorectal cancer vaccines: Tumor-associated antigens vs neoantigens. *World J Gastroenterol*. 2018 Dec 28;24(48):5418–32.
53. Palucka K, Banchereau J. Cancer immunotherapy via dendritic cells. *Nat Rev Cancer*. 2012 Mar 22;12(4):265–77.
54. Steinman RM, Banchereau J. Taking dendritic cells into medicine. *Nature*. 2007 Sep;449(7161):419–26.
55. Banchereau J, Steinman RM. Dendritic cells and the control of immunity. *Nature*. 1998 Mar;392(6673):245–52.
56. Rock KL. The ins and outs of cross-presentation. *Nat Immunol*. 2003 Oct;4(10):941–3.
57. Heath WR, Carbone FR. Cross-presentation in viral immunity and self-tolerance. *Nat Rev Immunol*. 2001 Nov;1(2):126–34.
58. Joffre OP, Segura E, Savina A, Amigorena S. Cross-presentation by dendritic cells. *Nature Reviews Immunology*. 2012 Aug;12(8):557–69.
59. Harshyne LA, Zimmer MI, Watkins SC, Barratt-Boyes SM. A Role for Class A Scavenger Receptor in Dendritic Cell Nibbling from Live Cells. *The Journal of Immunology*. 2003 Mar 1;170(5):2302–9.
60. Dhodapkar MV, Dhodapkar KM, Palucka AK. Interactions of tumor cells with dendritic cells: balancing immunity and tolerance. *Cell Death Differ*. 2008 Jan;15(1):39–50.
61. Hildner K, Edelson BT, Purtha WE, Diamond M, Matsushita H, Kohyama M, et al. Batf3 Deficiency Reveals a Critical Role for CD8 α ⁺ Dendritic Cells in Cytotoxic T Cell Immunity. *Science*. 2008 Nov 14;322(5904):1097–100.
62. Butterfield LH. Cancer vaccines. *BMJ [Internet]*. 2015 Apr 22 [cited 2019 Sep 19];350. Available from: <https://www.ncbi.nlm.nih.gov/pmc/articles/PMC4707521/>
63. Bezu L, Kepp O, Cerrato G, Pol J, Fucikova J, Spisek R, et al. Trial watch: Peptide-based vaccines in anticancer therapy. *Oncoimmunology [Internet]*. 2018 Sep 6 [cited 2019 Sep 20];7(12). Available from: <https://www.ncbi.nlm.nih.gov/pmc/articles/PMC6279318/>
64. Li L, Goedegebuure SP, Gillanders WE. Preclinical and clinical development of neoantigen vaccines. *Ann Oncol*. 2017 Dec;28(Suppl 12):xii11–7.

65. Zhang X, Kim S, Hundal J, Herndon JM, Li S, Petti AA, et al. Breast cancer neoantigens can induce CD8+ T-cell responses and antitumor immunity. *Cancer Immunol Res*. 2017 Jul;5(7):516–23.
66. Lawler SE, Speranza M-C, Cho C-F, Chiocca EA. Oncolytic Viruses in Cancer Treatment: A Review. *JAMA Oncol*. 2017 Jun 1;3(6):841–9.
67. Kaufman HL, Kohlhapp FJ, Zloza A. Oncolytic viruses: a new class of immunotherapy drugs. *Nature Reviews Drug Discovery*. 2015 Sep;14(9):642–62.
68. Andtbacka RHI, Kaufman HL, Collichio F, Amatruda T, Senzer N, Chesney J, et al. Talimogene Laherparepvec Improves Durable Response Rate in Patients With Advanced Melanoma. *JCO*. 2015 Jun 22;33(25):2780–8.
69. Research C for BE and. IMLYGIC (talimogene laherparepvec). FDA [Internet]. 2019 May 4 [cited 2019 Sep 22]; Available from: <http://www.fda.gov/vaccines-blood-biologics/cellular-gene-therapy-products/imlygic-talimogene-laherparepvec>
70. Chesney J, Puzanov I, Collichio F, Singh P, Milhem MM, Glaspy J, et al. Randomized, Open-Label Phase II Study Evaluating the Efficacy and Safety of Talimogene Laherparepvec in Combination With Ipilimumab Versus Ipilimumab Alone in Patients With Advanced, Unresectable Melanoma. *J Clin Oncol*. 2018 Jun 10;36(17):1658–67.
71. Pierce RH, Campbell JS, Pai SI, Brody JD, Kohrt HE. In-situ tumor vaccination: Bringing the fight to the tumor. *Hum Vaccin Immunother*. 2015 Jun 9;11(8):1901–9.
72. Brody JD, Ai WZ, Czerwinski DK, Torchia JA, Levy M, Advani RH, et al. In Situ Vaccination With a TLR9 Agonist Induces Systemic Lymphoma Regression: A Phase I/II Study. *J Clin Oncol*. 2010 Oct 1;28(28):4324–32.
73. Cadena A, Cushman TR, Anderson C, Barsoumian HB, Welsh JW, Cortez MA. Radiation and Anti-Cancer Vaccines: A Winning Combination. *Vaccines (Basel)* [Internet]. 2018 Jan 30 [cited 2019 Sep 21];6(1). Available from: <https://www.ncbi.nlm.nih.gov/pmc/articles/PMC5874650/>
74. Liu K, Nussenzweig MC. Origin and development of dendritic cells. *Immunological Reviews*. 2010;234(1):45–54.
75. Hammerich L, Marron TU, Upadhyay R, Svensson-Arvelund J, Dhainaut M, Hussein S, et al. Systemic clinical tumor regressions and potentiation of PD1 blockade with in situ vaccination. *Nat Med*. 2019 May;25(5):814–24.
76. Gulley JL, Mulders P, Albers P, Banchereau J, Bolla M, Pantel K, et al. Perspectives on sipuleucel-T: Its role in the prostate cancer treatment paradigm. *Oncoimmunology* [Internet]. 2015 Dec 10 [cited 2019 Sep 23];5(4). Available from: <https://www.ncbi.nlm.nih.gov/pmc/articles/PMC4839373/>
77. Kantoff PW, Higano CS, Shore ND, Berger ER, Small EJ, Penson DF, et al. Sipuleucel-T Immunotherapy for Castration-Resistant Prostate Cancer [Internet]. <http://dx.doi.org/10.1056/NEJMoa1001294>. 2010 [cited 2019 Sep 24]. Available from: https://www.nejm.org/doi/10.1056/NEJMoa1001294?url_ver=Z39.88-2003&rfr_id=ori%3Arid%3Acrossref.org&rfr_dat=cr_pub%3Dwww.ncbi.nlm.nih.gov

78. Garg AD, Vara Perez M, Schaaf M, Agostinis P, Zitvogel L, Kroemer G, et al. Trial watch: Dendritic cell-based anticancer immunotherapy. *Oncoimmunology* [Internet]. 2017 May 12 [cited 2019 Sep 24];6(7). Available from: <https://www.ncbi.nlm.nih.gov/pmc/articles/PMC5543823/>
79. Carreno BM, Magrini V, Becker-Hapak M, Kaabinejadian S, Hundal J, Petti AA, et al. A dendritic cell vaccine increases the breadth and diversity of melanoma neoantigen-specific T cells. *Science*. 2015 May 15;348(6236):803–8.
80. Wilgenhof S, Corthals J, Heirman C, van Baren N, Lucas S, Kvistborg P, et al. Phase II Study of Autologous Monocyte-Derived mRNA Electroporated Dendritic Cells (TriMixDC-MEL) Plus Ipilimumab in Patients With Pretreated Advanced Melanoma. *JCO*. 2016 Feb 29;34(12):1330–8.
81. Tiriveedhi V, Tucker N, Herndon J, Li L, Sturmoski M, Ellis M, et al. Safety and preliminary evidence of biological efficacy of a mammaglobin-A DNA vaccine in patients with stable metastatic breast cancer. *Clin Cancer Res*. 2014 Dec 1;20(23):5964–75.
82. Schwartzentruber DJ, Lawson DH, Richards JM, Conry RM, Miller DM, Treisman J, et al. gp100 Peptide Vaccine and Interleukin-2 in Patients with Advanced Melanoma. *N Engl J Med*. 2011 Jun 2;364(22):2119–27.
83. Schneble EJ, Berry JS, Trappey FA, Clifton GT, Ponniah S, Mittendorf E, et al. The HER2 peptide nelipepimut-S (E75) vaccine (NeuVax™) in breast cancer patients at risk for recurrence: correlation of immunologic data with clinical response [Internet]. <http://dx.doi.org/10.2217/imt.14.22>. 2014 [cited 2019 Sep 20]. Available from: <https://www.futuremedicine.com/doi/abs/10.2217/imt.14.22>
84. Clifton GT, Mittendorf EA, Peoples GE. Adjuvant HER2/neu peptide cancer vaccines in breast cancer [Internet]. <http://dx.doi.org/10.2217/imt.15.81>. 2015 [cited 2019 Sep 20]. Available from: <https://www.futuremedicine.com/doi/abs/10.2217/imt.15.81>
85. Yuba E, Harada A, Sakanishi Y, Watarai S, Kono K. A liposome-based antigen delivery system using pH-sensitive fusogenic polymers for cancer immunotherapy. *Biomaterials*. 2013 Apr 1;34(12):3042–52.
86. Kranz LM, Diken M, Haas H, Kreiter S, Loquai C, Reuter KC, et al. Systemic RNA delivery to dendritic cells exploits antiviral defence for cancer immunotherapy. *Nature*. 2016 Jun;534(7607):396–401.
87. Rodríguez-Limas WA, Sekar K, Tyo KE. Virus-like particles: the future of microbial factories and cell-free systems as platforms for vaccine development. *Current Opinion in Biotechnology*. 2013 Dec 1;24(6):1089–93.
88. Fan Y, Moon J. Nanoparticle Drug Delivery Systems Designed to Improve Cancer Vaccines and Immunotherapy. *Vaccines*. 2015 Aug 27;3(3):662–85.
89. Neefjes J, Jongsma MLM, Paul P, Bakke O. Towards a systems understanding of MHC class I and MHC class II antigen presentation. *Nat Rev Immunol*. 2011 Dec;11(12):823–36.
90. Shen H, Ackerman AL, Cody V, Giodini A, Hinson ER, Cresswell P, et al. Enhanced and prolonged cross-presentation following endosomal escape of exogenous antigens encapsulated in biodegradable nanoparticles. *Immunology*. 2006 Jan;117(1):78–88.
91. Park Y-M, Lee SJ, Kim YS, Lee MH, Cha GS, Jung ID, et al. Nanoparticle-Based Vaccine Delivery for Cancer Immunotherapy. *Immune Netw*. 2013 Oct;13(5):177–83.

92. Cho N-H, Cheong T-C, Min JH, Wu JH, Lee SJ, Kim D, et al. A multifunctional core–shell nanoparticle for dendritic cell-based cancer immunotherapy. *Nature Nanotech.* 2011 Oct;6(10):675–82.
93. Prasad S, Cody V, Saucier-Sawyer JK, Saltzman WM, Sasaki CT, Edelson RL, et al. Polymer nanoparticles containing tumor lysates as antigen delivery vehicles for dendritic cell-based anti-tumor immunotherapy. *Nanomedicine.* 2011 Feb;7(1):1–10.
94. Shang L, Nienhaus K, Nienhaus GU. Engineered nanoparticles interacting with cells: size matters. *J Nanobiotechnology.* 2014 Feb 3;12:5.
95. Shao K, Singha S, Clemente-Casares X, Tsai S, Yang Y, Santamaria P. Nanoparticle-Based Immunotherapy for Cancer. *ACS Nano.* 2015 Jan 27;9(1):16–30.
96. Uto T, Wang X, Sato K, Haraguchi M, Akagi T, Akashi M, et al. Targeting of Antigen to Dendritic Cells with Poly(-Glutamic Acid) Nanoparticles Induces Antigen-Specific Humoral and Cellular Immunity. *The Journal of Immunology.* 2007 Mar 1;178(5):2979–86.
97. Luo M, Wang H, Wang Z, Cai H, Lu Z, Li Y, et al. A STING-activating nanovaccine for cancer immunotherapy. *Nature Nanotechnology.* 2017 Jul;12(7):648–54.
98. Clercq ED. Degradation of Poly(inosinic acid) · poly(cytidylic acid) [(I)n· (Cn)] by Human Plasma. *European Journal of Biochemistry.* 1979 Jan 1;93(1):165–72.
99. Han HD, Byeon Y, Jang J-H, Jeon HN, Kim GH, Kim MG, et al. In vivo stepwise immunomodulation using chitosan nanoparticles as a platform nanotechnology for cancer immunotherapy. *Scientific Reports [Internet].* 2016 Dec [cited 2019 Mar 22];6(1). Available from: <http://www.nature.com/articles/srep38348>
100. Babu A, Ramesh R. Multifaceted Applications of Chitosan in Cancer Drug Delivery and Therapy. *Mar Drugs [Internet].* 2017 Mar 27 [cited 2019 Sep 29];15(4). Available from: <https://www.ncbi.nlm.nih.gov/pmc/articles/PMC5408242/>
101. Chitosan Uses, Benefits & Side Effects - Drugs.com Herbal Database [Internet]. Drugs.com. [cited 2019 Sep 29]. Available from: <https://www.drugs.com/npc/chitosan.html>
102. Hong S-C, Yoo S-Y, Kim H, Lee J. Chitosan-Based Multifunctional Platforms for Local Delivery of Therapeutics. *Mar Drugs [Internet].* 2017 Mar 1 [cited 2019 Sep 29];15(3). Available from: <https://www.ncbi.nlm.nih.gov/pmc/articles/PMC5367017/>
103. Noh KH, Park YM, Kim HS, Kang TH, Song K-H, Lee Y-H, et al. GM-CSF-loaded chitosan hydrogel as an immunoadjuvant enhances antigen-specific immune responses with reduced toxicity. *BMC Immunology.* 2014 Oct 18;15(1):48.
104. Croisier F, Jérôme C. Chitosan-based biomaterials for tissue engineering. *European Polymer Journal.* 2013 Apr 1;49(4):780–92.
105. Dua* K, Bebawy M, Awasthi R, Tekade RK, Tekade M, Gupta G, et al. Application of Chitosan and its Derivatives in Nanocarrier Based Pulmonary Drug Delivery Systems [Internet]. *Pharmaceutical Nanotechnology.* 2017 [cited 2019 Sep 29]. Available from: <http://www.eurekaselect.com/154750/article>

106. Rao W, Wang H, Han J, Zhao S, Dumbleton J, Agarwal P, et al. Chitosan-Decorated Doxorubicin-Encapsulated Nanoparticle Targets and Eliminates Tumor Reinitiating Cancer Stem-like Cells. *ACS Nano*. 2015 Jun 23;9(6):5725–40.
107. Zaharoff DA, Rogers CJ, Hance KW, Schlom J, Greiner JW. Chitosan solution enhances both humoral and cell-mediated immune responses to subcutaneous vaccination. *Vaccine*. 2007 Mar 1;25(11):2085–94.
108. Bueter CL, Lee CK, Rathinam VAK, Healy GJ, Taron CH, Specht CA, et al. Chitosan but Not Chitin Activates the Inflammasome by a Mechanism Dependent upon Phagocytosis. *J Biol Chem*. 2011 Oct 14;286(41):35447–55.
109. Bernocchi B, Carpentier R, Betbeder D. Nasal nanovaccines. *International Journal of Pharmaceutics*. 2017 Sep 15;530(1):128–38.
110. Apostólico J de S, Lunardelli VAS, Coirada FC, Boscardin SB, Rosa DS. Adjuvants: Classification, Modus Operandi, and Licensing. *J Immunol Res [Internet]*. 2016 [cited 2019 Sep 29];2016. Available from: <https://www.ncbi.nlm.nih.gov/pmc/articles/PMC4870346/>
111. Scherließ R, Mönckedieck M, Young K, Trows S, Buske S, Hook S. First in vivo evaluation of particulate nasal dry powder vaccine formulations containing ovalbumin in mice. *International Journal of Pharmaceutics*. 2015 Feb 20;479(2):408–15.
112. Heidland J. Chitosan Nanoparticles for Mucosal Vaccination – Understanding the Particle Formation Process and Formulation for Nasal Application. 2018 Aug 6 [cited 2021 May 20]; Available from: https://macau.uni-kiel.de/receive/diss_mods_00023571
113. Clarke SRM, Barnden M, Kurts C, Carbone FR, Miller JF, Heath WR. Characterization of the ovalbumin-specific TCR transgenic line OT-I: MHC elements for positive and negative selection. *Immunology and Cell Biology*. 2000 Apr;78(2):110–7.
114. Shen Z, Reznikoff G, Dranoff G, Rock KL. Cloned dendritic cells can present exogenous antigens on both MHC class I and class II molecules. *The Journal of Immunology*. 1997 Mar 15;158(6):2723–30.
115. Corbe TH, Roberts BJ, Leopold WR, Peckham JC, Wilkoff LJ, Griswold DP. Induction and Chemotherapeutic Response of Two Transplantable Ductal Adenocarcinomas of the Pancreas in C57BL/6 Mice. 1984;44:11.
116. Jacobs C, Duewell P, Heckelsmiller K, Wei J, Bauernfeind F, Ellermeier J, et al. An ISCOM vaccine combined with a TLR9 agonist breaks immune evasion mediated by regulatory T cells in an orthotopic model of pancreatic carcinoma. *International Journal of Cancer*. 2011;128(4):897–907.
117. Ellermeier J. Immuntherapie des Pankreaskarzinoms: Mechanismen und Strategien zur Durchbrechung tumorinduzierter Immunsuppression. :74.
118. Scherließ R, Trows S. Novel Formulation Concept for Particulate Uptake of Vaccines via the Nasal Associated Lymphoid Tissue. *Procedia in Vaccinology*. 2011 Jan 1;4:113–9.
119. Geissmann F, Manz MG, Jung S, Sieweke MH, Merad M, Ley K. Development of monocytes, macrophages and dendritic cells. *Science*. 2010 Feb 5;327(5966):656–61.

120. Helm O, Held-Feindt J, Grage-Griebenow E, Reiling N, Ungefroren H, Vogel I, et al. Tumor-associated macrophages exhibit pro- and anti-inflammatory properties by which they impact on pancreatic tumorigenesis. *International Journal of Cancer*. 2014;135(4):843–61.
121. Rahn S. Inflammation associated metabolic rewiring in initiation of pancreatic cancer - master thesis 2015.pdf.
122. Verreck FAW, de Boer T, Langenberg DML, Hoeve MA, Kramer M, Vaisberg E, et al. Human IL-23-producing type 1 macrophages promote but IL-10-producing type 2 macrophages subvert immunity to (myco)bacteria. *Proc Natl Acad Sci U S A*. 2004 Mar 30;101(13):4560–5.
123. BD FACSCalibur Instructions For Use. :238.
124. Flow Cytometry How It Works | Thermo Fisher Scientific - CN [Internet]. [cited 2019 Oct 6]. Available from: <https://www.thermofisher.com/cn/zh/home/life-science/cell-analysis/cell-analysis-learning-center/molecular-probes-school-of-fluorescence/flow-cytometry-basics/flow-cytometry-fundamentals/how-flow-cytometer-works.html>
125. Walter F, Winter E, Rahn S, Heidland J, Meier S, Struzek A-M, et al. Chitosan nanoparticles as antigen vehicles to induce effective tumor specific T cell responses. *PLOS ONE*. 2020 Sep 30;15(9):e0239369.
126. Jaganathan KS, Vyas SP. Strong systemic and mucosal immune responses to surface-modified PLGA microspheres containing recombinant Hepatitis B antigen administered intranasally. *Vaccine*. 2006 May 8;24(19):4201–11.
127. Palucka K, Ueno H, Banchereau J. Recent Developments in Cancer Vaccines. *The Journal of Immunology*. 2011 Feb 1;186(3):1325–31.
128. Blank F, Fytianos K, Seydoux E, Rodriguez-Lorenzo L, Petri-Fink A, von Garnier C, et al. Interaction of biomedical nanoparticles with the pulmonary immune system. *Journal of Nanobiotechnology*. 2017 Jan 9;15(1):6.
129. Shi G-N, Zhang C-N, Xu R, Niu J-F, Song H-J, Zhang X-Y, et al. Enhanced antitumor immunity by targeting dendritic cells with tumor cell lysate-loaded chitosan nanoparticles vaccine. *Biomaterials*. 2017 Jan 1;113:191–202.
130. Smith A, Perelman M, Hinchcliffe M. Chitosan. *Hum Vaccin Immunother*. 2014 Mar 1;10(3):797–807.
131. Koppolu B, Zaharoff DA. The effect of antigen encapsulation in chitosan particles on uptake, activation and presentation by antigen presenting cells. *Biomaterials*. 2013 Mar;34(9):2359–69.
132. Hellfritzsch M, Scherließ R. Mucosal Vaccination via the Respiratory Tract. *Pharmaceutics* [Internet]. 2019 Aug 1 [cited 2020 Nov 10];11(8). Available from: <https://www.ncbi.nlm.nih.gov/pmc/articles/PMC6723941/>
133. Labouta HI, Asgarian N, Rinker K, Cramb DT. Meta-Analysis of Nanoparticle Cytotoxicity via Data-Mining the Literature. *ACS Nano*. 2019 Feb 26;13(2):1583–94.
134. Kamat V, Bodas D, Paknikar K. Chitosan nanoparticles synthesis caught in action using microdroplet reactions. *Scientific Reports*. 2016 Feb 29;6(1):22260.

135. Xiao J, Yu H. Gemcitabine Conjugated Chitosan and Double Antibodies (Abc-GC-Gemcitabine Nanoparticles) Enhanced Cytoplasmic Uptake of Gemcitabine and Inhibit Proliferation and Metastasis In Human SW1990 Pancreatic Cancer Cells. *Med Sci Monit.* 2017 Apr 3;23:1613–20.
136. Arya G, Vandana M, Acharya S, Sahoo SK. Enhanced antiproliferative activity of Herceptin (HER2)-conjugated gemcitabine-loaded chitosan nanoparticle in pancreatic cancer therapy. *Nanomedicine.* 2011 Dec;7(6):859–70.
137. Al-Halifa S, Gauthier L, Arpin D, Bourgault S, Archambault D. Nanoparticle-Based Vaccines Against Respiratory Viruses. *Front Immunol [Internet].* 2019 [cited 2020 Nov 11];10. Available from: <https://www.frontiersin.org/articles/10.3389/fimmu.2019.00022/full>
138. Schuster BS, Suk JS, Woodworth GF, Hanes J. Nanoparticle diffusion in respiratory mucus from humans without lung disease. *Biomaterials.* 2013 Apr;34(13):3439–46.
139. Fries CN, Curvino EJ, Chen J-L, Permar SR, Fouda GG, Collier JH. Advances in nanomaterial vaccine strategies to address infectious diseases impacting global health. *Nature Nanotechnology.* 2020 Aug 17;1–14.
140. Xiang SD, Scholzen A, Minigo G, David C, Apostolopoulos V, Mottram PL, et al. Pathogen recognition and development of particulate vaccines: does size matter? *Methods.* 2006 Sep;40(1):1–9.
141. Brito Baleeiro R, Schweinlin M, Rietscher R, Diedrich A, Czaplewska JA, Metzger M, et al. Nanoparticle-Based Mucosal Vaccines Targeting Tumor-Associated Antigens to Human Dendritic Cells. *Journal of Biomedical Nanotechnology.* 2016 Jul 1;12(7):1527–43.
142. Yan S, Xu K, Li L, Gu W, Rolfe BE, Xu ZP. The Pathways for Layered Double Hydroxide Nanoparticles to Enhance Antigen (Cross)-Presentation on Immune Cells as Adjuvants for Protein Vaccines. *Front Pharmacol [Internet].* 2018 Sep 20 [cited 2019 Mar 22];9. Available from: <https://www.ncbi.nlm.nih.gov/pmc/articles/PMC6158326/>
143. Song C, Noh Y-W, Lim YT. Polymer nanoparticles for cross-presentation of exogenous antigens and enhanced cytotoxic T-lymphocyte immune response. *Int J Nanomedicine.* 2016 Aug 5;11:3753–64.
144. Jia J, Zhang Y, Xin Y, Jiang C, Yan B, Zhai S. Interactions Between Nanoparticles and Dendritic Cells: From the Perspective of Cancer Immunotherapy. *Front Oncol [Internet].* 2018 Sep 25 [cited 2021 Jan 14];8. Available from: <https://www.ncbi.nlm.nih.gov/pmc/articles/PMC6167641/>
145. Palucka K, Banchereau J. Dendritic cell-based cancer therapeutic vaccines. *Immunity.* 2013 Jul 25;39(1):38–48.
146. Lee Y-R, Lee Y-H, Im S-A, Kim K, Lee C-K. Formulation and Characterization of Antigen-loaded PLGA Nanoparticles for Efficient Cross-priming of the Antigen. *Immune Netw.* 2011;11(3):163.
147. Kukutsch NA, Roßner S, Austyn JM, Schuler G, Lutz MB. Formation and Kinetics of MHC Class I-Ovalbumin Peptide Complexes on Immature and Mature Murine Dendritic Cells. *Journal of Investigative Dermatology.* 2000 Sep 1;115(3):449–53.

148. Karttunen J, Sanderson S, Shastri N. Detection of rare antigen-presenting cells by the lacZ T-cell activation assay suggests an expression cloning strategy for T-cell antigens. *Proc Natl Acad Sci U S A*. 1992 Jul 1;89(13):6020–4.
149. Cho S, Dong S, Parent KN, Chen M. Immune-tolerant elastin-like polypeptides (iTEPs) and their application as CTL vaccine carriers. *J Drug Target*. 2016 Apr;24(4):328–39.
150. Carambia A, Gottwick C, Schwinge D, Stein S, Digigow R, Şeleci M, et al. Nanoparticle-mediated targeting of autoantigen peptide to cross-presenting liver sinusoidal endothelial cells protects from CD8 T-cell-driven autoimmune cholangitis. *Immunology* [Internet]. [cited 2021 Jan 30];n/a(n/a). Available from: <https://onlinelibrary.wiley.com/doi/abs/10.1111/imm.13298>
151. Molino NM, Anderson AKL, Nelson EL, Wang S-W. Biomimetic Protein Nanoparticles Facilitate Enhanced Dendritic Cell Activation and Cross-Presentation. *ACS Nano*. 2013 Nov 26;7(11):9743–52.
152. Oliveira MI, Santos SG, Oliveira MJ, Torres AL, Barbosa MA. Chitosan drives anti-inflammatory macrophage polarisation and pro-inflammatory dendritic cell stimulation. *Eur Cell Mater*. 2012 Jul 24;24:136–52; discussion 152-153.
153. Lin Y-C, Lou P-J, Young T-H. Chitosan as an adjuvant-like substrate for dendritic cell culture to enhance antitumor effects. *Biomaterials*. 2014 Oct 1;35(31):8867–75.
154. Di Blasio S, van Wigcheren GF, Becker A, van Duffelen A, Gorris M, Verrijp K, et al. The tumour microenvironment shapes dendritic cell plasticity in a human organotypic melanoma culture. *Nature Communications*. 2020 Jun 2;11(1):2749.
155. Rabenstein H, Behrendt AC, Ellwart JW, Naumann R, Horsch M, Beckers J, et al. Differential Kinetics of Antigen Dependency of CD4+ and CD8+ T Cells. *The Journal of Immunology*. 2014 Apr 15;192(8):3507–17.
156. Luo W-H, Yang Y-W. Activation of Antigen-Specific CD8+ T Cells by Poly-DL-Lactide/Glycolide (PLGA) Nanoparticle-Primed Gr-1high Cells. *Pharm Res*. 2016 Apr 1;33(4):942–55.
157. Han HD, Byeon Y, Kang TH, Jung ID, Lee J-W, Shin BC, et al. Toll-like receptor 3-induced immune response by poly(d,l-lactide-co-glycolide) nanoparticles for dendritic cell-based cancer immunotherapy. *Int J Nanomedicine*. 2016 Nov 2;11:5729–42.

9. Appendix

9.1 Eidesstattliche Erklärung

Hiermit versichere ich, Frederik Walter, an Eides statt, dass

- meine Dissertation, abgesehen von Ratschlägen meiner Doktormutter und meiner sonstigen akademischen Lehrer, sowie Lehrerinnen, nach Form und Inhalt meine eigene Arbeit ist, dass ich keine anderen als die in der Arbeit aufgeführten Hilfsmittel benutzt habe, und dass meine Arbeit bisher, keiner anderen akademischen Stelle als Dissertation vorgelegen hat, weder ganz, noch in Teilen.
- ich nicht mehr als einen erfolglosen Promotionsversuch unternommen habe.
- ich die vorliegende Arbeit selbstständig verfasst habe. Ich habe keine anderen als die angegebenen Quellen benutzt und alle Ausführungen, die anderen Schriften wörtliche oder sinngemäß entnommen wurden, kenntlich gemacht.

Ort, Datum

Frederik Walter

9.2 Publications and poster presentations

Parts of the presented dissertation have already been published here:

Walter F, Winter E, Rahn S, Heidland J, Meier S, Struzek A-M, et al. (2020) Chitosan nanoparticles as antigen vehicles to induce effective tumor specific T cell responses. PLoS ONE 15(9): e0239369. <https://doi.org/10.1371/journal.pone.0239369>

Meier S, **Walter F**, Sebens S and Scherließ R; Poster presentation 'Verification of the suitability of chitosan nanoparticles as potential drug delivery system for immune activation', 3rd European Conference on Pharmaceutics, Biopharmaceutics and Pharmaceutical technology, 25.03 - 26.03.2019, Bologna

Walter F, Winter E, Otto L, Faltinek L, Helm O, Heidland J, Meier S, Wesch D, Lettau M, Rahn S, Scherließ R and Sebens S; Poster presentation 'Tumor Vaccination: Chitosan nanoparticles as antigen vehicles to promote tumor-directed T cell responses', 20th international AEK cancer congress, 27.02. - 01.03.2019, Heidelberg

Winter E, **Walter F**, Lettau M, Heidland J, Rahn S, Scherließ R, Helm O and Sebens S; Poster presentation 'Tumor vaccination: chitosan nanoparticles to improve the antigen uptake by dendritic cells for an enhanced tumor-directed immune response', 5th European Congress of Immunology, 02.09. - 05.09.2018, Amsterdam

Other scientific publication:

Otto L, Rahn S, Daunke T, **Walter F**, Winter E, Möller JL, Rose-John S, Wesch D, Schäfer H, Sebens S. Initiation of Pancreatic Cancer: The Interplay of Hyperglycemia and Macrophages Promotes the Acquisition of Malignancy-Associated Properties in Pancreatic Ductal Epithelial Cells. *International Journal of Molecular Sciences*. 2021; 22(10):5086. <https://doi.org/10.3390/ijms22105086>

9.3 Acknowledgements

– I would like to express my gratitude in my mother tongue –

Gerne möchte ich die Möglichkeit ergreifen, mich bei den Menschen, die mir das Fertigstellen meiner Doktorarbeit ermöglicht haben, zu bedanken.

Zuallererst wäre dies meine Doktormutter, Prof. Susanne Sebens, die mir die Chance gab in ihrer Arbeitsgruppe zu arbeiten, mich stets und aller Widrigkeiten zum Trotz mit Positivität und großem Elan unterstützte, das Projekt eng begleitete und immer ansprechbar war. Merci für die hervorragende Betreuung!

Weiterhin möchte ich mich ganz besonders bei Dr. Sascha Rahn bedanken, der mit beeindruckendem Fachwissen, maximalem Einsatz und begeisternder Geduld in gefühlt jeder Problemsituation in Windeseile einen Lösungsansatz aus dem Ärmel schütteln konnte.

Ich danke den Kollegen und Wegbegleitern in der AG „Inflammatorische Karzinogenese“, Dagmar, Elsa, Johanna, Lauritz, Lilli, Lisa, Luisa, Meike und Nadja mit denen ich definitiv prägende Stunden in und um das Labor herum verbringen durfte.

Außerdem möchte ich mich bei den Mitarbeitern der Immunologie (um Dr. Marcus Lettau, Prof. Daniela Wesch) und Pharmazie (um Prof. Regina Scherließ, Anna-Maria, Judith, Saskia) für die gute Zusammenarbeit und stets freundliche Stimmung bedanken.

Selbstverständlich möchte ich mich bei Luiza bedanken: Für Ihr Verständnis, ihre Aufmunterungen, für ihre Liebe, die mir besonders in frustrierenden Episoden eine fundamentale Stütze war.

Ganz besonders dankbar bin ich meiner Familie, vor allem meinen Eltern Lioba und Franz, die mir von Tag eins an in jeder Lebenslage ermöglicht haben, meine eigenen Wege zu gehen, mich dabei immer unterstützten und die alle meine auf vielfältigste Art und Weise bereichernden Erfahrungen in den letzten Jahren hauptsächlich möglich gemacht haben.

9.4 Curriculum Vitae

Personal data:

Name: Frederik Walter
Date of birth: 16.01.1996
Place of birth: Offenburg
Nationality: German

Education:

2002-2005 Georg Schöner Grundschule Steinach-Welschensteinach
2005-2013 Marta Schanzenbach Gymnasium Gengenbach
2014-2016 University of Tübingen, preclinical part of medical school, first part of the medical state examination
2016-2021 Kiel University, clinical part of medical school, second and third part of the medical state examination
9/2017-2/2018 University of Palermo, Italy, exchange semester supported by ERASMUS
2018-2022 Institut für experimentelle Tumorforschung, Kiel University, doctoral studies supervised by Prof. Susanne Sebens
9/2019-1/2020 Zhejiang University, Hangzhou, People's Republic of China, exchange semester, supported with a grant by Kiel University

Electives during the final clinical year of medical school:

UKSH Campus Kiel – neurology
University Hospital Frankfurt - internal medicine
Cantonal Hospital Aarau, Switzerland - surgery